2011

London penetration depth measurements in Ba(Fe1-xTx)2As2 (T=Co,Ni,Ru,Rh,Pd,Pt,Co+Cu) superconductors

Ryan Todd Gordon
Iowa State University

London penetration depth measurements in $\mathbf{Ba(Fe_{1-x}}T_x\mathbf{)_2As_2}$ (T=Co,Ni,Ru,Rh,Pd,Pt,Co+Cu) superconductors

by

Ryan T. Gordon

A dissertation submitted to the graduate faculty

in partial fulfillment of the requirements for the degree of

DOCTOR OF PHILOSOPHY

Major: Condensed Matter Physics

Program of Study Committee:
Ruslan Prozorov, Major Professor
Paul C. Canfield
Jörg Schmalian
James Cochran
R. William McCallum

Iowa State University

Ames, Iowa

2011

DEDICATION

I would like to dedicate this thesis to my parents Georgeann and the late Gerald R. Gordon and also to my wife Mariko S. Peterson Gordon.

TABLE OF CONTENTS

LIST OF TABLES

LIST OF FIGURES

ACKNOWLEDGEMENTS

I would like to thank all of those people who have helped me during my time spent as a graduate student with the Ames Laboratory and the Physics Department at Iowa State University. In particular, I would like to thank my major professor, Ruslan Prozorov, whose guidance was always valuable. Also, working alongside Makariy Tanatar in the laboratory was very beneficial to me and I am grateful to him for all of his instruction.

For taking the time to attend my preliminary oral exam and my final defense as well as for their constructive criticism, I would like to thank the members of my Program of Study Committee.

To all of those SMLT Group members who I had the pleasure of working with, I would like to extend my thanks for all of their help, both in the laboratory and out.

To all of my family members, I would like to express my thanks for all of their encouragement during these last few years. Especially, I would like to recognize my mother Georgeann and my grandmother Dorothy for all of the help that they have given me.

Lastly, I would like to thank my wife Mari for all of the support that she has given me during our time spent together in Ames.

ABSTRACT

The London penetration depth has been measured in various doping levels of single crystals of $Ba(Fe_{1-x}T_x)_2As_2$ (T=Co,Ni,Ru,Rh,Pd,Pt,Co+Cu) superconductors by utilizing a tunnel diode resonator (TDR) apparatus. All in-plane penetration depth measurements exhibit a power law temperature dependence of the form $\Delta\lambda_{ab}(T) = CT^n$, indicating the existence of low-temperature, normal state quasiparticles all the way down to the lowest measured temperature, which was typically 500 mK. Several different doping concentrations from the $Ba(Fe_{1-x}T_x)_2As_2$ (T=Co,Ni) systems have been measured and the doping dependence of the power law exponent, n, is compared to results from measurements of thermal conductivity and specific heat. In addition, a novel method has been developed to allow for the measurement of the zero temperature value of the in-plane penetration depth, $\lambda_{ab}(0)$, by using TDR frequency shifts. By using this technique, the doping dependence of $\lambda_{ab}(0)$ has been measured in the $Ba(Fe_{1-x}Co_x)_2As_2$ series, which has allowed also for the construction of the doping-dependent superfluid phase stiffness, $\rho_s(T) = [\lambda(0)/\lambda(T)]^2$. By studying the effects of disorder on these superconductors using heavy ion irradiation, it has been determined that the observed power law temperature dependence likely arises from pair-breaking impurity scattering contributions, which is consistent with the proposed $s_{\pm}$-wave symmetry of the superconducting gap in the dirty scattering limit. This hypothesis is supported by the measurement of an exponential temperature dependence of the penetration depth in the intrinsically clean LiFeAs, indicative of a nodeless superconducting gap.

CHAPTER 1. Introduction

The discovery of a new superconducting material can have a tremendous impact on the scientific community. When cooled below a critical temperature, T_c, these materials conduct electricity without any losses in addition to other technologically desirable and interesting magnetic properties. In February of 2008, such a discovery was realized by the report of superconductivity as high as 26 K in $LaFeAsO_{1-x}F_x$ along with other unusual physical properties [Kamihara et al. (2008)]. This compound is just a member of one class from a family of superconductors known as the iron pnictides or more generally the iron-based superconductors. An astonishing amount of effort has been put forth thus far by both experimental and theoretical physicists to understand the fundamentals of superconductivity in these materials to gain a greater understanding of the phenomenon in general and on a larger scale the hope is to some day design a material with superconductivity at room temperature, which could be an amazing technological achievement. The goal of this work was to gain a better understanding of the physical nature of the superconducting state in the iron-based superconductors through experimental measurements of the London penetration depth.

Although great progress has been made since the initial finding of superconductivity below 4.2 K in Hg by the research team of H. K. Onnes in 1911 [Onnes (1911)], much remains a mystery of this incredible state of matter. It took nearly 50 years after this discovery for a theory to be introduced that could account for interactions at the microscopic level to aid in the understanding of how superconductivity is even possible in materials like Hg having low transition temperatures. This work is arguably the most successful theory of superconductivity and is commonly referred to as the Bardeen-Cooper-Shrieffer (BCS) theory [Bardeen et al. (1957)]. After the BCS formulation, most people believed that the basic

fundamental principles involved with understanding superconductivity had been developed, perhaps with the exception of unconventional superconductivity in UPt_3 [Sigrist and Ueda (1991)], UBe_{13} [Ott et al. (1983)] and $CePt_2Si_2$ [Hiebl and Rogl (1985)], but a Nobel prize winning discovery in 1986 by IBM researchers G. Bednorz and K. Müller would change all of that [Müller and Bednorz (1987)].

High-temperature superconductivity was discovered in what later became known as the high-T_c cuprates and many of the properties of these materials went against the rules formulated by B. Matthias that he used to discover many new superconductors [Matthias et al. (1963)]. These materials, which exhibit superconductivity far above 100 K, are insulators in their parent state with long range antiferromagnetic order. However, when these materials are doped away from this parent state with either holes or electrons, the antiferromagnetism can be weakened and for specific dopants superconductivity can then emerge for a critical doping concentration. The T_c rises through a maximum and eventually superconductivity is absent as the doping concentration is increased further. They can also be very two-dimensional materials, meaning that in some cases nearly all of the electric charge flows through CuO_2 planes that exist in the lattice structure, which can create a resistivity anisotropy as large as 100 [Ginsberg (1994)]. The temperature-doping phase diagram for the high-T_c cuprates contains some very rich physics, including a strange metallic phase where the electrical resisitivity has an unusual linear temperature dependence that persists over two decades in temperature, a partial gap of unknown origin in the density of states that occurs at temperatures much higher than T_c that is known as the pseudogap [Basov and Timusk (2005)], and the recovery of a Fermi liquid state in the electrical resistivity for doping concentrations near the overdoped edge of the superconducting dome and beyond. Also, the pairing symmetry, which is related to the symmetry of the superconducting order parameter, in the high-T_c cuprates is $d_{x^2-y^2}$-wave [Harlingen (1995)], in contrast to BCS superconductors which have s-wave pairing symmetry. This may be due to a fundamentally different pairing mechanism, with this being strongly linked to phonons in BCS superconductors as confirmed by the isotope effect [Pippard (1953)] and quite possibly spin fluctuations [Monthoux et al. (2007)] in the high-T_c cuprates for which there has not

yet been smoking gun evidence. During the period from 1986 to 2001, over 100,000 scientific papers were published on the cuprates [Buchanan (2001)], so many of the experimental techniques that were developed to study them were already prepared for the discovery of high-T_c superconductivity in the iron-based superconductors [Kamihara et al. (2008)].

The family of iron-based superconductors can be grouped into at least five different classes up to this date. The parent compounds for these classes are the RFeAsO (where R=rare earth, denoted the "1111" system), AEFe$_2Pn_2$ (where AE=alkaline earth and Pn=pnictogen, denoted the "122" system), AFeAs (where A=alkali metal, denoted the "111" system), Fe$_{1+y}$Se (denoted the "11" system) and $Sr_3Sc_2O_5Fe_2As_2$ classes of iron-based superconducting compounds [Hosono (2010); Paglione and Greene (2010); Canfield and Bud'ko (2010); Johnston (2010); Wen and Li (2011)]. These compounds can be doped in various different ways to achieve superconductivity. Structurally, similar to the cuprates, these classes all have planes consisting of Fe and Pn or Ch atoms, but unlike the cuprates these materials likely have a pronounced three-dimensional band structure. In the parent compounds, the iron-based superconductors are poor metals [Canfield and Bud'ko (2010); Ni et al. (2008b); Sefat et al. (2008); Tanatar et al. (2009); Kamihara et al. (2008); Ren et al. (2008)], most of which undergo antiferromagnetic *and* structural phase transitions below room temperature. Although the community has not yet come to a general consensus, it is quite likely that the antiferromagnetism in the iron-based superconductors is of itinerant character [Cvetkovic and Tesanovic (2009)], in contrast to the localized magnetism in the cuprates. Similar to the cuprates, these transitions are suppressed by doping and superconductivity emerges out of this instability and eventually disappears for high enough doping levels. The fact that there are some similarities between the cuprates and the iron-based superconductors prompts one to consider that there may be a common underlying physical principle responsible for their observed properties [Taillefer (2010)]. One popular idea is that both are examples of spin fluctuation mediated superconductors, with $d_{x^2-y^2}$-wave symmetry of the order parameter [Harlingen (1995)] in the cuprates and the recently proposed $s_{\pm}$-wave symmetry in the iron-based superconductors [Mazin et al. (2008); Mazin and Schmalian (2009)].

The structure of the momentum dependent superconducting gap, $\Delta(\mathbf{k})$, is an experimentally accessible quantity that can provide valuable information about the physical interactions responsible for electronic pairing in a superconductor. Uncovering the structure of the order parameter can be a very challenging task experimentally. One way to address this is by piecing together the information obtained from several experimental techniques that are sensitive to $\Delta(\mathbf{k})$, such as penetration depth, thermal conductivity, nuclear magnetic resonance, angle-resolved photoemission spectroscopy and tunneling measurements, just to name a few. The experiment that provided the smoking gun evidence for $d_{x^2-y^2}$-wave symmetry in the cuprates [Harlingen (1995)] took advantage of the phase difference of the superconducting wave function at a corner junction. The results of this experiment were relatively simple to understand because the Fermi surface of the cuprates arises from a single electronic band crossing the Fermi level and a single superconducting gap. This same type of experiment for the iron-based superconductors is complicated by the fact that there are as many as five different bands crossing the Fermi level and it is possible that the phase of the gap changes sign *between* the sheets that comprise the Fermi surface. Because the Fermi surface of the iron-based superconductors is composed of several different sheets having both hole- and electron-like character, it is widely accepted that there are multiple superconducting gaps [Mazin et al. (2008)], which indeed have been observed experimentally [Evtushinsky et al. (2009a); Liu et al. (2009); Ding et al. (2008)]. The existence of multiple superconducting gaps creates additional complications for understanding the role of impurity scattering because there are both inter- and intraband scattering processes that may be important for superconductivity.

The experimental quantity that has been used in this work to study the momentum dependence of the superconducting gap(s), $\Delta_i(\mathbf{k})$, in the iron-based superconductors is the London penetration depth [Prozorov and Giannetta (2006)]. The penetration depth is sensitive to $\Delta_i(\mathbf{k})$ through an integral which is taken over the entire Fermi surface, thus making this measurement technique insensitive to the actual phase of the gap. The apparatus that was used to make the penetration depth measurements is known as a tunnel diode resonator, which made use of a radio frequency oscillating circuit powered by a tunnel diode [VanDegrift (1975a,b)].

The temperature dependence of the penetration depth can show the existence of normal state quasiparticles at low temperatures, which makes it a well suited tool for detecting nodes in the superconducting gap or for observing pair-breaking impurity scattering effects. The normalized superfluid density, $\rho_s(T) = [\lambda(0)/\lambda(T)]^2$, is another important experimental quantity used to analyze temperature dependent penetration depth data. It is especially useful for observing effects associated with multigap superconductivity or anisotropies of the superconducting gap(s) [Kogan et al. (2009)], but it does require $\lambda(0)$, which can be a difficult quantity to measure. Penetration depth measurements have proven to be very useful for studying the order parameter symmetry in superconductors, especially in the high-T_c cuprates where the linear temperature dependence of the penetration depth in very clean single crystals of YBCO was taken as the first piece of strong evidence to suggest line nodes in the superconducting gap [Hardy et al. (1993)].

The class of iron-based superconductors on which the penetration depth measurements to be reported here have focused is $Ba(Fe_{1-x}T_x)_2As_2$ with T being Co, Ni, Ru, Rh Pd, Pt and also co-doping with Co and Cu. One reason why these series were chosen is because large, high quality single crystals can grown [Ni et al. (2008b)]. The parent compound for these materials is a poor metal having a high temperature tetragonal phase with no long range magnetic order and undergoes structural and magnetic transitions around 140 K into a low temperature orthorhombic phase with long range antiferromagnetic order [Rotter et al. (2008); Canfield and Bud'ko (2010)]. Transition metal doping onto the iron site serves to suppress the structural and magnetic transition temperatures and superconductivity emerges after these phases have been weakened. These features can be seen in Fig. 1.1 for the $Ba(Fe_{1-x}T_x)_2As_2$ (T=Co,Ni,Pd,Ru) series.

The variation of the in-plane penetration depth with respect to its zero temperature value, $\Delta\lambda_{ab}(T)$, has been measured at various doping levels in single crystals of $Ba(Fe_{1-x}Co_x)_2As_2$ [Gordon et al. (2009b,a)] and $Ba(Fe_{1-x}Ni_x)_2As_2$ [Martin et al. (2010a)]. Although fewer dopings were studied, $\Delta\lambda_{ab}(T)$ has also been measured for $Ba(Fe_{1-x}Pt_x)_2As_2$, $Ba(Fe_{1-x}Pd_x)_2As_2$ and $Ba(Fe_{1-x}Ru_x)_2As_2$ and $Ba(Fe_{1-x-y}Co_xCu_y)_2As_2$ [Martin et al. (2010b)]. In addition,

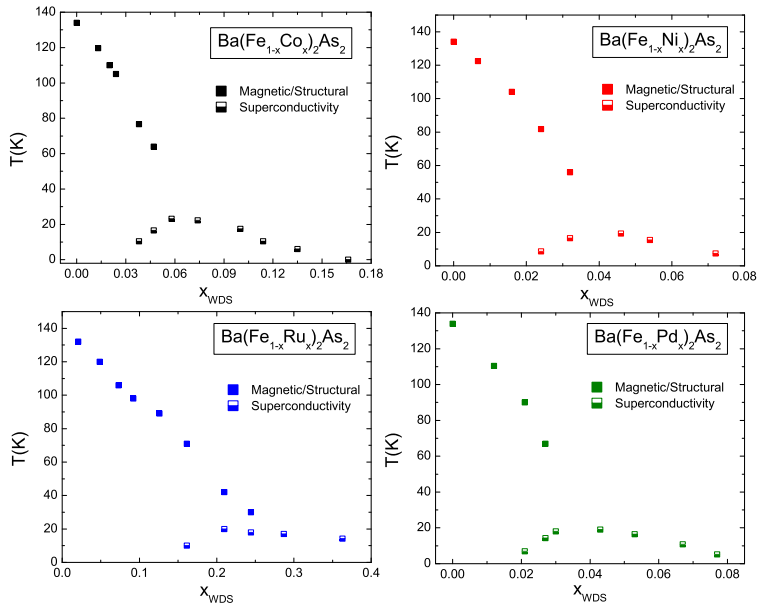

Figure 1.1 Temperature versus doping phase diagram for $Ba(Fe_{1-x}T_x)_2As_2$ (T=Co,Ni,Ru,Pd) as determined from electrical resistivity measurements [Canfield and Bud'ko (2010); Ni et al. (2008b); Thaler et al. (2010); Ni et al. (2010a,b)]. The solid squares show the position of the magnetic and structural phase transitions and the half filled squares show the location of the superconducting transition.

the c-axis component of the penetration depth has been measured for one underdoped and two overdoped concentrations of the $Ba(Fe_{1-x}Ni_x)_2As_2$ series. A procedure has also been developed to measure the absolute value of the in-plane penetration depth, $\lambda_{ab}(T)$, involving an aluminum coating technique for the samples along with the usual tunnel diode frequency shift measurements. This method has been used to measured $\lambda_{ab}(0)$ as a function of doping in the $Ba(Fe_{1-x}Co_x)_2As_2$ series and also to construct the normalized superfluid density, $\rho_s = [\lambda_{ab}(0)/\lambda_{ab}(T)]^2$, in order to study its evolution with doping. Also, the results of an extensive collection of the penetration depth prefactor, β from $\Delta\lambda_{ab}(T) = \beta T^n$, for many different iron-based superconductors is presented [Gordon et al. (2010b)] with a theoretical attempt to explain its dependence on T_c based on pair-breaking impurity scattering arguments [Kogan (2009)]. The following chapters serve to summarize the results of the above mentioned experiments and the inferred properties of the superconducting state in the Ba-based 122 compounds in addition to supplying the necessary information to understand the experimental procedures and penetration depth analyses.

CHAPTER 2. The London penetration depth in superconductors

2.1 The behavior of superconductors in applied magnetic fields: London theory

After the discovery that certain metals, when cooled below a characteristic temperature, T_c, exhibit perfect conductivity [Onnes (1911)], it was found that they also expel applied magnetic fields from their bulk below this temperature, now known as the Meissner effect [Meissner and Ochsenfeld (1933)]. In order to account for these two fascinating electromagnetic properties, F. and H. London proposed a set of equations containing a phenomenological parameter that is now known as the London penetration depth, λ [London (1950); London and London (1935)]. This length scale characterizes the distance over which external electromagnetic fields decay inside of a superconductor and it is one of the two fundamental length scales of these materials, with the other being the coherence length, ξ, which characterizes the distance in real space over which the superconducting wave function varies appreciably [Pippard (1953)]. Experimental measurements of the temperature dependence of the London penetration depth in superconductors can also be used to gain information about the structure of the superconducting gap function, $\Delta(\mathbf{k})$, which is related to the symmetry of the many body interactions that give rise to the electronic pairing.

Historically, the first observation of magnetic field penetration effects that were predicted by the London equations were made by Shoenberg in 1940 [Shoenberg (1940)], where the magnetic susceptibilities of mercury colloids were measured as a function of temperature. The penetration of the magnetic field into each droplet in the colloid decreased the magnitude of the diamagnetic susceptibility of the sample as a whole. Thirteen years later, measurements, performed by A. B. Pippard [Pippard (1953)], of the penetration depths in a series of tin-indium

alloys by microwave techniques were taken as evidence that the electrons in a superconductor have a long range influence on each other. It was in this report that the idea of a superconducting coherence length was first introduced mathematically. These early measurements were useful for giving direction to the field of superconductivity and over the years, penetration depth measurements have contributed greatly to our understanding of the phenomenon.

The behavior exhibited by superconducting materials in applied magnetic fields naturally allows them to be placed into two basic categories: type I and type II superconductors. Below T_c, in the absence of an applied magnetic field, the superconducting free energy, $F_s(T, H = 0)$, is less than the normal state free energy, $F_n(T, H = 0)$. However, there is a critical value of the applied magnetic field, H_c, such that F_n becomes less than F_s and it becomes energetically favorable for the system to revert back to its normal electronic state. This critical field is a function of temperature and its value increases as the temperature of the superconductor is lowered below T_c. The following summary applies only to a demagnetization-free scenario to exclude a complicated discussion of the intermediate state of a type I superconductor.

For a type I superconductor, a single critical field suffices to describe its behavior. Below H_c the applied magnetic field penetrates the material with a screening length of λ and when $H > H_c$, the entire sample becomes normal, corresponding to the limit where $\lambda \to \infty$. However, for type II superconductors there are two associated critical fields: H_{c1} and H_{c2}. For $H > H_{c2}$, the entire sample enters the normal state. For $H < H_{c1}$, the magnetic field penetrates only up to λ and is screened from deep within the bulk. However, for $H_{c1} < H < H_{c2}$, known as the mixed state, in addition to the usual London penetration, magnetic flux also penetrates the sample in the form of vortices, which are normal state regions around which screening supercurrents swirl [Abrikosov (1957)]. These vortices have a characteristic radius on the order of ξ and the magnetic field decays away from them with a screening length of λ. Often the vortices form a periodic lattice in the bulk of the material and have been studied extensively for many different superconductors [Abrikosov (2004)]. The measured penetration depth in the mixed state, λ_{meas}, not only has a Meissner component, λ_L, but also there is a component from the response of the vortex lattice as well, known as the Campbell penetration depth, λ_C.

The relationship between them has the form of $\lambda_{meas}^2 = \lambda_L^2 + \lambda_C^2$ [Prozorov et al. (2009c)].

The ratio of the London penetration depth to the coherence length, $\kappa \equiv \lambda/\xi$, known as the Ginzburg-Landau parameter, allows one to see through a calculation of the surface energy between normal and superconducting regions if a superconductor is classified as type I or type II. For a type I superconductor, $\lambda << \xi$ and the positive surface energy is unfavorable for the formation of vortices in the bulk, whereas for a type II superconductor $\lambda >> \xi$ and the negative surface energy is favorable for the formation of flux vortices. In the original paper outlining this idea [Abrikosov (1957)], Abrikoxov showed that materials with $\kappa > 1/\sqrt{2}$ are type II superconductors and materials with $\kappa < 1/\sqrt{2}$ are type I. Regardless of whether a superconductor is classified as type I or II, information about the superconducting pairing symmetry is inferred in the same way from penetration depth measurements. In this work, all experiments were performed in zero applied *dc* magnetic fields, so all samples remained in the Meissner state.

As previously mentioned, one of the first attempts to describe the electrodynamic behavior of superconductors, namely the loss of electrical resistance below T_c and the Meissner effect, was done by F. and H. London in 1935 [London and London (1935)]. They considered this problem by starting with the essential results of the Drude theory [Drude (1900); Ashcroft and Mermin (1976)] to describe how scattering of electrons from defects can lead to a reduction in the electrical transport:

$$m\frac{d\mathbf{v}}{dt} = e\mathbf{E} - \frac{m\mathbf{v}}{\tau}, \tag{2.1}$$

where m is the mass of the charge carriers, e is the magnitude of each carrier's charge, $\mathbf{v}$ is the average or drift velocity of the charge carriers and τ is the average scattering time between collisions. The first term on the right side of Eqn. 2.1 is the accelerative term describing how an electric field will accelerate charge carriers and the second term accounts for scattering processes decreasing their average acceleration. This leads to a steady state drift velocity given by $\mathbf{v} = e\mathbf{E}\tau/m$ and if there are n conduction electrons per unit volume, we obtain the familiar form of Ohm's law: $\mathbf{J} = ne\mathbf{v} = (ne^2\tau/m)\mathbf{E} = \sigma\mathbf{E}$. The altered form of this result

that the Londons started with, which asserted that a certain density of the charge carriers, n_s, contributes to an accelerative supercurrent that undergoes no scattering, was

$$m\frac{d\mathbf{v}_s}{dt} = e\mathbf{E} \tag{2.2}$$

and this equation leads to an expression for the total supercurrent, $\mathbf{J}_s$, which is governed by the relation

$$\frac{d\mathbf{J}_s}{dt} = \frac{n_s e^2}{m}\mathbf{E} = \frac{c^2}{4\pi\lambda^2}\mathbf{E}. \tag{2.3}$$

Eqn. 2.3 is known as the first London equation and it is important because with the use of Maxwell's equations and further manipulations it leads to $\nabla^2\mathbf{E} = \mathbf{E}/\lambda^2$, which implies that time-varying electric fields are screened out of a superconductor by a supercurrent that will accelerate out to infinity in response to a strictly *dc* electric field. Eqn. 2.3 also implies that time-varying magnetic fields are screened from a superconductor up to a distance of λ.

The second London equation cannot be derived from classical arguments like Eqn. 2.3 was. From the observations made regarding the Meissner effect, the screening of time-*independent* magnetic fields must be accounted for. Let us consider taking the curl of one of the Maxwell equations:

$$\nabla \times (\nabla \times \mathbf{H}) = \frac{4\pi}{c}(\nabla \times \mathbf{J}) \tag{2.4}$$

and making the substitution $\nabla \times \mathbf{J} = -c\mathbf{H}/4\pi\lambda^2$, which leads to

$$\nabla^2\mathbf{H} = \frac{1}{\lambda^2}\mathbf{H} \tag{2.5}$$

where $\lambda^2 = mc^2/4\pi n_s e^2$. Eqn 2.5 is known as the second London equation and implies that time-independent magnetic fields are also screened from the bulk of a superconductor, in agreement with the Meissner effect. The two London equations that were obtained by arguments based on experimental observations are useful, but they lack a microscopic origin for the explanation of the superconducting state. This type of a theory would not come together until 1957 [Bardeen et al. (1957)], many years after the work done by the Londons.

Equation 2.5 is also referred to as the isotropic London equation, which has proven to be unsuccessful for describing superconductors that have significant band mass anisotropies. Anisotropic type II superconductors have been described quite well by a set of Ginzburg-Landau equations, with a phenomenological mass tensor, near H_{c2} [Morris et al. (1972)]. Moving away from H_{c2} this type of analysis is not possible due to these equations becoming non-linear. Near H_{c1} it is helpful to apply the London model [Kogan (1981)], which provides a reasonable approximation at least for large κ superconductors. Although it has low accuracy, this approach nevertheless makes it possible to predict the existence of a transverse magnetic field in a vortex. This justifies the use of the London model, despite the fact that many important aspects, such as temperature dependencies and the origin of the anisotropic superconducting properties, remain beyond the scope of the theory. This approach begins by minimizing the energy given by

$$\epsilon = \int [H^2 + (\lambda_0 \nabla \times \mathbf{H})^2] dV/8\pi, \tag{2.6}$$

which is just the sum of the magnetic and kinetic contributions. For the isotropic case, $\lambda_0^2 \propto M_0$, where M_0 is the mass. The generalization to the anisotropic situation replaces M_0 with the mass tensor in such a way that the kinetic term remains invariant:

$$8\pi\epsilon = \int [H^2 + \lambda^2 m_{ij} (\nabla_i \times \mathbf{H})(\nabla_j \times \mathbf{H})] dV. \tag{2.7}$$

where $\lambda^2 \propto m_{ave}$, with m_{ave} being some mean mass. The components m_{ij} represent the effective masses divided by m_{ave}. The tensor m_{ij} is diagonal if its principal directions are chosen as coordinate axes ($m^0_{xx} = m_1/m_{ave}, m^0_{yy} = m_2/m_{ave}, m^0_{zz} = m_3/m_{ave}$). It is convenient to choose $m^3_{ave} = m_1 m_2 m_3$ so that $\det m_{ij} = 1$. By minimizing this energy, the resulting anisotropic London equations are given by

$$H_i = \lambda^2 m_{kl} \epsilon_{lsi} \epsilon_{ktj} \frac{\partial^2 H_j}{\partial x_s \partial x_t}, \tag{2.8}$$

where ϵ_{ikl} is the Levi-Civita tensor. In the isotropic case by using $m_{ij} = \delta_{ij}$, the usual London equations are recovered from Eqn. 2.8.

In an earlier work, C. J. Gorter and H. B. G. Casimir interpreted the thermodynamics of superconductors in terms of a two fluid model in which a "normal" electronic fluid coexisted with a "condensed" fluid of superconducting electrons [Gorter and Casimir (1934); Gorter (1935)]. Using this model a temperature-dependent form of the penetration depth has been derived through measured temperature dependencies of the specific heat and upper critical field. This form, known as the two-fluid temperature dependence, is given by

$$\lambda(T) \approx \frac{\lambda(0)}{\sqrt{1-(T/T_c)^4}}. \tag{2.9}$$

Although it has no microscopic justification, this form has been used when a simple analytical approximation for $\lambda(T)$ over the full temperature range below T_c was needed. Some successful attempts were made to generalize the Gorter-Casimir result to better fit the results of measurements [Lewis (1956)], but this was before any microscopic theory of superconductivity had been developed. In order to make this equation more practical, the full BCS equations have been solved for s- and two dimensional d-wave superconducting gap symmetries [Poole et al. (2007)], which will be introduced later. The results are

$$\lambda_{s-wave}(T) = \frac{\lambda(0)}{\sqrt{1-(T/T_c)^2}} \tag{2.10}$$

and

$$\lambda_{d-wave}(T) = \frac{\lambda(0)}{1-(T/T_c)^{4/3}}. \tag{2.11}$$

It is important to note here that these equations are quite good approximations over the full temperature range, but they are not accurate at low temperatures.

2.2 Microscopic theory of superconductivity and the connection to λ

In 1957 John Bardeen, Leon Cooper and Robert Schrieffer published a microscopic theory of superconductivity, commonly referred to as the BCS theory, that remains the most successful theory of superconductivity to this day [Bardeen et al. (1957)]. In this work, their goal was to

formulate a theory to describe the unusual experimental observations made on superconductors in terms of the interactions between electrons. The list of main observations that they set out to explain was: (1) a second-order phase transition at T_c, (2) an electronic specific heat varying as exp(-T_0/T) near T=0 K and other evidence for an energy gap for individual particle-like excitations, (3) the Meissner effect, (4) effects associated with infinite conductivity and (5) the dependence of T_c on isotopic mass (isotope effect), $T_c\sqrt{M} = constant$.

The source of the attractive interaction that can result between electrons stems from the motion of the ionic lattice. The repulsive Coulomb interaction between electrons near the Fermi level having opposite spin and momenta is screened by an attractive interaction that exists between electrons and lattice vibrations known as phonons, which results in a net attractive interaction for the pair of electrons, known collectively as a Cooper pair. These bound state electron pairs condense into a ground state where they all share the same wave function, which was provided by the BCS theory. BCS assumed that the total wave function could be built of products of pair wave functions between individual electrons, where the two electrons in the pair have opposite spin and the orbital parts are symmetric, i.e. they are singlet states. Cooper showed that in the presence of a Fermi sea where Pauli exclusion effects are important, two electrons can form such a bound state no matter how weak the attractive interaction is [Cooper (1956)].

For phonon mediated superconductivity, the attractive interaction between electrons of opposite spin and momentum centered about the Fermi energy leads to an energy gap of width $2\Delta(T)$ in the spectrum of single particle excitations, which drastically modifies the electronic density of states. This gap serves as the superconducting order parameter and its momentum dependence is an important, experimentally measurable quantity. Most known phonon mediated superconductors have been assumed to be single gap superconductors, referring to the fact that they possess a single isotropic or weakly anisotropic superconducting gap that exists over the entire Fermi surface in momentum space. In analogy to electronic orbitals, this situation where the gap magnitude is the same in every direction is known as an s-wave superconducting gap function. There is compelling evidence to suggest that some phonon mediated

superconductors, for example MgB_2 [Bouquet et al. (2001a)], $Lu_2Fe_3Si_5$ [Gordon et al. (2008)] and V_3Si [Kogan et al. (2009)], possess two different superconducting gaps that exist on different regions of their Fermi surfaces that both exhibit s-wave symmetry. Many other classic superconductors may well possess multiple superconducting gaps or modest gap anisotropy and these systems should be carefully revisited in future studies.

For the case of a superconductor possessing a single s-wave superconducting gap where impurity scattering is negligible (clean limit), the temperature dependence of the variation in the penetration depth with respect to its zero temperature value can be obtained from the BCS theory [Muhlschlegel (1959)] and found to have the following dependence up to roughly a value of $T_c/3$:

$$\Delta\lambda(T) \approx \lambda(0)\sqrt{\frac{\pi\Delta(0)}{2k_BT}}\exp -\frac{\Delta(0)}{k_BT}. \tag{2.12}$$

This form of the penetration depth is exponentially saturated at very low temperatures, which appears very flat and essentially zero, and this activated temperature dependence is the characteristic signature of a nodeless superconducting gap function from the penetration depth data. Fig. 2.1 shows the in-plane London penetration depth data taken for Nb, a single gap BCS superconductor, using a tunnel diode resonator circuit and the temperature dependence agrees with Eqn. 2.12 quite well. Any deviation from this behavior at low temperatures indicates the presence of low-temperature normal state quasiparticles that can arise from either nodes in the superconducting gap function or from pair-breaking scattering. Magnetic impurity scattering acts as a strong pair-breaking mechanism in s-wave superconductors, but non-magnetic impurities do not alter the low-T behavior of the penetration depth much, which can be understood from Anderson's "theorem" [Anderson (1959)].

For multigap superconductors like MgB_2, $\Delta\lambda(T)$ exhibits the same temperature dependence as in the single gap case, but only up to a temperature of $(T_c/3)(\Delta_{min}/\Delta_{max})$ due to scattering processes associated with the multigap behavior, where Δ_{max} and Δ_{min} are the magnitudes of the largest and smallest gaps, respectively. Fig. 2.1 shows in-plane penetration depth data taken on MgB_2 and indeed one can see that the exponentially saturated region persists up to

a lower temperature than it does for single gap Nb, keeping in mind that the horizontal axis is the reduced temperature, T/T_c.

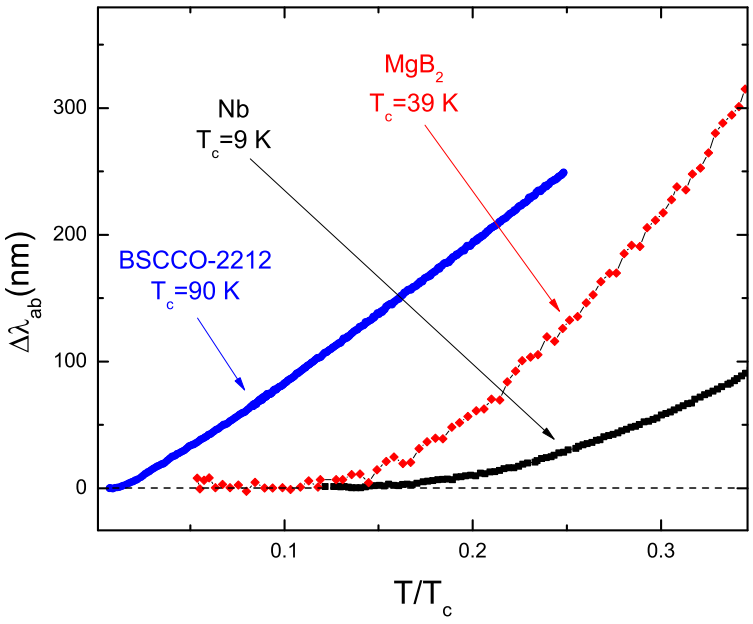

Figure 2.1 The variation with temperature of the in-plane London penetration depth with respect to its zero temperature value, $\Delta\lambda_{ab}(T)$, for three different superconductors: Nb (s-wave), MgB_2 (multi-gap s-wave) and Bi-2212 (d-wave). These data were all taken with a tunnel diode resonator circuit.

There are also some superconductors that have been suggested to be mediated by mechanisms other than phonons. Many believe that one such example is the family of high-T_c cuprates, which are antiferromagnetic insulators in the parent state that when doped with either holes or electrons become superconductors with T_c as high as ≈140 K [Müller and Bednorz (1987)]. These materials can be very two dimensional, where nearly all of the conduction occurs in the CuO_2 planes that exist throughout the structure. The transport anisotropy can be as high as ≈10,000 but as low at 10 for conduction in these planes compared to conduction along the c-axis, which is perpendicular to the CuO_2 planes [Ginsberg (1994)]. Because of the proximity of the superconducting phase in these materials to a magnetic state in the doping phase diagram, it is widely believed that spin fluctuations may play a similar role for pair

mediation to phonons in the case of s-wave superconductors [Monthoux et al. (2007)].

As previously mention, the order parameter symmetry of the cuprates is $d_{x^2-y^2}$-wave. For this type of symmetry, the order parameter changes sign from having a positive amplitude to a negative one on four different points of the Fermi surface. At the points where the gap changes sign its value must go through zero. Any point where the superconducting gap goes to zero with respect to the Fermi surface is known as a node. In the case of $d_{x^2-y^2}$-wave symmetry, lines of nodes that run parallel to the c-axis are present. Due to this unusual momentum dependence of the order parameter and also the proximity of the superconducting phase to an antiferromagetic one, it is widely believed that the mechanism responsible for giving rise to Cooper pairing in the high-T_c cuprates is electronic in origin, quite possibly mediated by spin fluctuations, which could make them fundamentally different than the BCS superconductors that are mediated by phonons. There are other families of superconductors believed to be good candidates for spin fluxuation mediated pairing, with those being the heavy fermion superconductors, the organic Bechgaard salts and the recently discovered iron-based superconductors [Taillefer (2010)].

Nodes in the superconducting gap structure drastically alter the low temperature behavior of any material property which depends on the electronic density of states and therefore they can be detected with the use of several experimental techniques. At absolute zero, the Fermi surface represents the set of highest occupied electronic energy levels in momentum space. At T=0 for an s-wave superconductor in the clean impurity scattering limit, where the coherence length is shorter than the mean free path, this set of energy levels is fully gapped with respect to the unoccupied levels and as the temperature is increased, the unoccupied electronic states which lie just above the occupied ones are populated exponentially fast and this effect gives rise to the activated behavior observed in many of the materials properties, like the penetration depth, spin lattice relaxation rate and ultrasonic attenuation just to name a few. For the case of a superconducting gap function containing nodes, as the temperature is increased, normal quasiparticle states at much lower temperatures are able to become occupied as a result of the zeros in the gap structure. The population of these low energy normal states alters the temperature dependence of all quantities dependent on the electronic density of states and

thus the presence of such a node is experimentally detectable.

In the clean limit, the vertical line of nodes in the superconducting gap function of a $d_{x^2-y^2}$-wave superconductor produce a linear temperature dependence of $\Delta\lambda$, with

$$\Delta\lambda(T) \approx \frac{\lambda(0)2\ln 2}{d\Delta/d\phi|_{\phi\to\phi_{node}}}T \equiv \frac{\lambda(0)2\ln 2}{\alpha\Delta(0)}T, \tag{2.13}$$

where Δ is the momentum dependent superconducting gap and ϕ is the azimuthal angle [Annett et al. (1991)]. This linear dependence in the penetration depth was first observed by the pioneering measurements of the Hardy group using a microwave cavity apparatus to measure single crystals of the cuprate superconductors known as YBCO at the University of British Columbia in 1993 [Hardy et al. (1993)]. From Fig. 2.1, actual tunnel diode resonator measurements confirm that the in-plane penetration depth of the high-T_c cuprate known as BSCCO-2212 exhibits the linear temperature dependence in the low-temperature region, shown in Eqn. 2.13.

In contrast to the s-wave case where non-magnetic impurity scattering does not alter much the low-T behavior of λ, both magnetic *and* non-magnetic scattering effects in a $d_{x^2-y^2}$-wave superconductor change this linear dependence of the penetration depth to a quadratic dependence up to a temperature T^*, which depends on the concentration of impurities in the system [Hirschfeld and Goldenfeld (1993)]. In fact, from Fig. 2.1 the $\Delta\lambda_{ab}(T)$ data for BSCCO-2212 shows a slight upturn near the lowest temperature of the experiment, which is likely due to a small concentration of impurities in the sample. This quadratic temperature dependence was initially observed in the penetration depth of films and impure crystals of high-T_c superconductors before high quality single crystals became available [Hardy et al. (1993)].

With the advent of the ability to make precision measurements of the temperature dependence of the penetration depth in superconductors, these experiments have become very valuable for determining the structure of the momentum dependent superconducting gap. By knowing the gap structure, theoretical models for the pairing mechanism can be tested. The formal connection between the momentum dependence of the superconducting gap, $\Delta(\mathbf{k})$, and the temperature dependence of the penetration depth are given in the following section.

2.3 Calculating $\lambda(T)$ for a general Fermi surface with an arbitrary superconducting gap structure $\Delta(\mathbf{k})$

As it has been indicated from the previous section, by measuring the temperature dependence of the London penetration depth, one can learn about the structure of the superconducting gap in momentum space. It is the goal of this section to provide a formal connection between $\lambda(T)$ and $\Delta(\mathbf{k})$ for a general Fermi surface geometry by following the approach of Chandrasekhar and Einzel [Chandrasekhar and Einzel (1993)].

Recall that in the original effort to understand external field penetration into a superconductor, the Londons arrived at the following form of the penetration depth in relation to other properties of the metal:

$$\lambda^2 = \frac{mc^2}{4\pi n_s e^2}. \tag{2.14}$$

In a real metal, though, it is known that there can be drastic deviations from a spherical Fermi surface, which can in principle lead to mass anisotropies. Differences between the free electron mass and the band mass can lead to large deviations from the penetration depth calculated using Eqn. 2.14 with the free electron mass. The general form of the electronic band mass tensor is

$$m_{im}^{-1} = \frac{\partial^2 \varepsilon_k}{\hbar^2 \partial k_i \partial k_m}. \tag{2.15}$$

The existence of such anisotropic effects has lead to the necessity of using different band masses, m_c and m_{ab}, to be used in attempt to calculate the different components of the penetration depth with respect to the crystalline axes, λ_c and λ_{ab}, respectively.

Another factor that can lead to deviations from the London result in the Free electron case is a variation of the superconducting gap $\Delta(\mathbf{k})$ in momentum space. As it was pointed out in the previous section, vertical line nodes in the gap function can produce a linear temperature dependence in $\lambda(T)$ at low temperatures, which is quite different than the exponential saturation that would arise from a superconducting gap that is isotropic in momentum space.

Measurements that are capable of resolving such differences in the penetration depth are useful for probing the symmetry of the superconducting interactions, but nonetheless one must be able to understand the connection between $\Delta(\mathbf{k})$ and $\lambda(T)$ for the sake of the data analysis.

Due to these deviations, namely anisotropies in the Fermi surface or a superconducting gap magnitude that changes about the Fermi surface in momentum space, the need for a general formalism that can account for such effects is obvious. Such formalism has been provided by the semiclassical approach to calculating all three spatial components of the penetration depth put forth by Chandrasekhar and Einzel [Chandrasekhar and Einzel (1993)].

By considering the response of a superconductor to an externally applied magnetic field, they arrived at the following relationship between the supercurrent density, $\mathbf{J}_s$, and the vector potential, $\mathbf{A}$, of the applied magnetic field:

$$\mathbf{J}_s = e\int(d\nu_k \mathbf{v}_k + d\nu_{-k}\mathbf{v}_{-k}) = -\frac{e^2}{4\pi^3 c}\int d^3k\Big(-\frac{\partial n_k}{\partial \varepsilon_k} + \frac{\partial f(E_k)}{\partial E_k}\Big)(\mathbf{v}_k\mathbf{v}_k)\cdot\mathbf{A} \equiv \mathbb{T}\cdot\mathbf{A}. \quad (2.16)$$

This is just the generalization of the original London equation to a BCS superconductor with a general dispersion relation and at finite temperature T. This allows us to define the symmetric response tensor

$$\mathbb{T} \equiv \frac{e^2}{4\pi^3 c}\int d^3k\Big(-\frac{\partial n_k}{\partial \varepsilon_k} + \frac{\partial f(E_k)}{\partial E_k}\Big)(\mathbf{v}_k\mathbf{v}_k). \quad (2.17)$$

It should be noted that charge conservation is violated in Eqn. 2.16 unless an additional backflow term is added giving

$$\mathbf{J}_s = -\Big(\mathbb{T} - \frac{(\mathbb{T}\cdot\mathbf{q})(\mathbf{q}\cdot\mathbb{T})}{\mathbf{q}\cdot\mathbb{T}\cdot\mathbf{q}}\Big)\cdot\mathbf{A} \quad (2.18)$$

where $\mathbf{q}$ is a wavevector pointing along the direction of the applied magnetic field. The backflow term depends only on the direction of $\mathbf{q}$ and not its magnitude.

Thus, Eqn. 2.17 and Eqn. 2.18 together with the Maxwell equation

$$\nabla\times\mathbf{B} = \frac{4\pi}{c}\mathbf{J}_s \quad (2.19)$$

form the complete solution to the problem of a superconductor at temperature T, with arbitrary $\varepsilon(k)$ and $\Delta(k)$, in an applied magnetic field.

The penetration depth components along a specific direction with respect to the crystalline axes can be computed by using the relationship

$$\lambda_{ii} = \Big(\frac{c}{4\pi T_{ii}}\Big)^{1/2}, i = x, y, z \tag{2.20}$$

and it should be noted that the λ_{ii} are not the components of a vector or a tensor, but rather are the different penetration depths with respect to the crystalline axes. However, the effective mass can be defined by

$$m_{ii} \equiv \frac{ne^2}{cT_{ii}}, \tag{2.21}$$

which gives us the familiar London relation

$$\lambda_{ii} = \Big(\frac{m_{ii}c^2}{4\pi^2}\Big)^{1/2}. \tag{2.22}$$

Consider now the structure of the response tensor, $\mathbb{T}$, shown in Eqn. 2.17. This tensor can be broken into two terms which are usually referred to as the diamagnetic and paramagnetic contributions and are written in form

$$\mathbb{T} = \mathbb{T}_D - \mathbb{T}_P \tag{2.23}$$

with

$$\mathbb{T}_D = \frac{e^2}{4\pi^3 c}\int d^3k\Big(-\frac{\partial n_k}{\partial \varepsilon_k}\Big)(\mathbf{v}_k\mathbf{v}_k) \tag{2.24}$$

and

$$\mathbb{T}_P = \frac{e^2}{4\pi^3 c}\int d^3k\Big(-\frac{\partial f(E_k)}{\partial E_k}\Big)(\mathbf{v}_k\mathbf{v}_k) \tag{2.25}$$

By considering the fact that the derivatives in Eqns. 2.24 and 2.25 are zero unless $|\varepsilon_k - \mu| \lesssim \Delta(k)$ and also that $\Delta(k) \ll \mu$, the value of the tensor $\mathbf{v}_k\mathbf{v}_k$ can be replaced by its value at $\varepsilon_k = \mu$, which is $\mathbf{v}_F\mathbf{v}_F$. For this same reason, we can make the substitution

$$d^3k \rightarrow \frac{dS_F d\varepsilon_k}{\hbar|\mathbf{v}_F|} \tag{2.26}$$

where dS_F is a constant energy surface element and $\mathbf{v}_F$ is the magnitude of the Fermi velocity. These approximations give us

$$\mathbb{T}_D = \frac{e^2}{4\pi^3\hbar c}\oint dS_F \int_0^\infty d\varepsilon_k \Big(-\frac{\partial n_k}{\partial \varepsilon_k}\Big)\frac{\mathbf{v}_F\mathbf{v}_F}{|\mathbf{v}_F|} \cong \frac{e^2}{4\pi^3\hbar c}\oint dS_F \frac{\mathbf{v}_F\mathbf{v}_F}{|\mathbf{v}_F|} \tag{2.27}$$

and

$$\mathbb{T}_P \cong 2\cdot\frac{e^2}{4\pi^3\hbar c}\oint dS_F \frac{\mathbf{v}_F\mathbf{v}_F}{|\mathbf{v}_F|}\int_{\Delta(k)}^\infty dE_k \Big(-\frac{\partial f(E_k)}{\partial E_k}\Big)\frac{E_k}{\sqrt{E_k^2-\Delta^2(k)}}. \tag{2.28}$$

As $T \rightarrow 0$, $\mathbb{T}_P \rightarrow 0$ and as $T \rightarrow T_c$, $\mathbb{T}_P \rightarrow \mathbb{T}_D$. If $\Delta(k)$ is isotropic, the anisotropy of $\mathbb{T}_P$ is temperature-independent and its anisotropy is the same as the anisotropy of $\mathbb{T}_D$. If $\Delta(k)$ is anisotropic, then the anisotropy of $\mathbb{T}_P$ is affected by the anisotropies of both ε_k and $\Delta(k)$, and is temperature-dependent.

In summary, with the formalism provided in this section, the spatial components of the penetration depth, λ_{ii}, can be computed for a general Fermi surface geometry and an arbitrary momentum dependent superconducting gap function, $\Delta(\mathbf{k})$.

2.4 Behavior of the superfluid density for different superconducting pairing symmetries

Consider a superconducting metal with a fixed total density of conduction electrons, n_{total}. Below T_c, some fraction of the electrons in n_{total} will become superconducting, $n_s(T)$, and this fraction will increase as $T \rightarrow 0$. Let the fraction of electrons that remains normal below T_c be $n_n(T)$. In the clean impurity scattering limit, all of the electrons will enter into the

superconducting state, which implies $n_s(T=0) = n_{total}$. For a general temperature $0 < T < T_c$ the relationship

$$n_{total} = n_s(T) + n_n(T) \tag{2.29}$$

holds true for no impurity scattering, with n_{total} being a constant. The normalized superfluid density, $\rho_s(T)$, is the ratio of the concentration of superconducting electrons to the total concentration of available charge and can be related to the penetration depth by

$$\rho_s(T) = \frac{n_s(T)}{n_{total}} = \frac{n_s(T)}{n_s(T=0)} = \frac{\lambda^2(0)}{\lambda^2(T)} = \Big[1 + \frac{\Delta\lambda(T)}{\lambda(0)}\Big]^{-2} \tag{2.30}$$

with the use of the London relation shown in Eqn. 2.14. By using Eqn. 2.20 this can be extended even further:

$$\rho_s(T) = \frac{\lambda_{ii}^2(0)}{\lambda_{ii}^2(T)} = \frac{\mathbb{T}_{ii}(T)}{\mathbb{T}_{ii}(0)}, \tag{2.31}$$

where generally we have

$$\mathbb{T}_{ij} = \frac{e^2}{4\pi^3\hbar c} \oint dS_F \Big[\frac{\mathbf{v}_F^i \mathbf{v}_F^j}{|\mathbf{v}_F|} \Big(1 + 2 \int_{\Delta(\mathbf{k})}^{\infty} \frac{\partial f(E)}{\partial E} \frac{N(E)}{N(0)} dE \Big) \Big]. \tag{2.32}$$

The quantity $\rho_s(T)$ is often used to analyze penetration depth data all the way up to T_c and is useful for accentuating effects related to multigap or anisotropic superconductivity [Prozorov and Giannetta (2006)]. Also, $\rho_s(T)$ can be derived for a given superconducting gap symmetry with the use of the formalism of Chandresekhar and Einzel [Chandrasekhar and Einzel (1993)]. It is very important to emphasize here that in order to properly normalize the superfluid density, one must have the zero temperature value of the London penetration depth, $\lambda(0)$, which can be difficult to determine experimentally.

By using Eqn. 2.31 and 2.32, the superfluid density can be calculated in terms of the superconducting gap, Δ, and the single particle excitation energy with respect to the Fermi level, ε, in a straightforward way for a general Fermi surface geometry. Let us consider two examples to illustrate this. First, consider the case of a two-dimensional cylindrical Fermi

surface, which would be an approximation to the one of the high-T_c cuprates. For this geometry the components of the superfluid density are given by

$$\rho_{aa} = 1 - \frac{1}{2\pi T}\int_0^{2\pi} \sin^2\phi \int_0^{\infty} \cosh^{-2}\Big(\frac{\sqrt{\varepsilon^2+\Delta^2(T,\phi}}{2T}\Big) d\varepsilon d\phi \tag{2.33}$$

and

$$\rho_{bb} = 1 - \frac{1}{2\pi T}\int_0^{2\pi} \cos^2\phi \int_0^{\infty} \cosh^{-2}\Big(\frac{\sqrt{\varepsilon^2+\Delta^2(T,\phi}}{2T}\Big) d\varepsilon d\phi, \tag{2.34}$$

As a second example consider the case of a three dimensional spherical Fermi surface. The superfluid density components are given by

$$\rho_{aa} = 1 - \frac{3}{4\pi T}\int_0^{1}(1-z^2)\int_0^{2\pi} \cos^2(\phi) \int_0^{\infty} \cosh^{-2}\frac{\sqrt{\varepsilon^2+\Delta^2(T,\theta,\phi)}}{2T} d\varepsilon d\phi dz \tag{2.35}$$

and

$$\rho_{bb} = 1 - \frac{3}{4\pi T}\int_0^{1}(1-z^2)\int_0^{2\pi} \cos^2(\phi) \int_0^{\infty} \cosh^{-2}\frac{\sqrt{\varepsilon^2+\Delta^2(T,\theta,\phi)}}{2T} d\varepsilon d\phi dz \tag{2.36}$$

For a BCS superconductor, where there exists a single, isotropic superconducting gap about the Fermi surface, the normalized superfluid density in the clean impurity scattering limit can be found by inserting Eqn. 2.12 into Eqn. 2.30, which gives

$$\rho_s = \Big[1 + \frac{\Delta\lambda(T)}{\lambda(0)}\Big]^{-2} \approx \Big[1 - \frac{2\Delta\lambda(T)}{\lambda(0)}\Big] = 1 - \sqrt{\frac{2\pi\Delta(0)}{k_B T}}\exp\left(-\frac{\Delta(0)}{k_B T}\right), \tag{2.37}$$

which can be derived easily with the use of Eqn. 2.12. This function is plotted in Fig. 2.2 as the blue solid line. Impurity scattering effects have not been taken into account in this function, so it represents the normalized superfluid density of a single gap s-wave superconductor in the clean limit of impurity scattering. Nonmagnetic impurity scattering for an s-wave superconductor does not change the low-temperature behavior of the superfluid density, as can be understood within Anderson's theorem for impurity scattering in s-wave superdonductors [Anderson (1959)], but the presence of magnetic impurities does lead to strong deviations from this

case. Notice that the characteristic exponential saturation at low temperatures for an s-wave superconductor that is evident in the penetration depth is also present at low temperatures in the superfluid density by the flat region existing below roughly $T_c/3$.

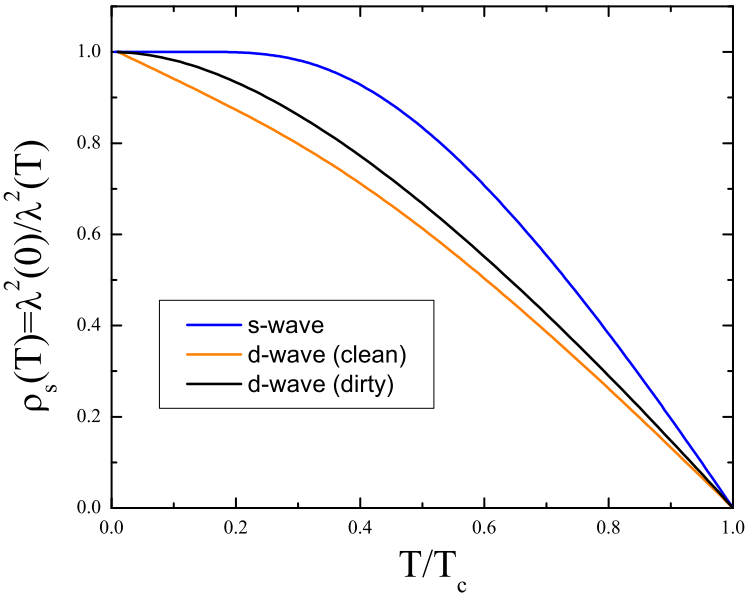

Figure 2.2 Theoretical curves for the normalized superfluid density plotted as a function of reduced temperature for the clean s-wave, clean d-wave and dirty d-wave impurity scattering limits.

For a $d_{x^2-y^2}$-wave superconductor with vertical line nodes in its gap function, as in the high-T_c cuprates [Harlingen (1995)], the normalized superfluid density has the form

$$\rho_s \approx 1 - \frac{2ln2}{\Delta(0)}T, \tag{2.38}$$

which shows the same linear slope with temperature that one finds in the penetration depth data. This is constructed in the same way as Eqn. 2.37 by using Eqn. 2.13. The orange solid line in Fig. 2.2 represents a plot of the normalized superfluid density for a $d_{x^2-y^2}$-wave superconductor in the clean impurity scattering limit. For a $d_{x^2-y^2}$-wave superconductor, both nonmagnetic and magnetic impurities act as pair-breaking scatterers, in contrast to the case of an s-wave superconductor [Anderson (1959)]. The black solid line in Fig. 2.2 represents

the normalized superfluid density for a d-wave superconductor in the dirty impurity scattering limit, where the penetration depth exhibits a characteristic quadratic temperature dependence in the low-temperature region [Hirschfeld and Goldenfeld (1993)].

Together, the penetration depth and the normalized superfluid density offer valuable information about the structure of the gap in a superconductor. The low temperature region of $\lambda(T)$ can show whether or not there are normal state quasiparticles activated by nodes or pair-breaking scattering, while $\rho_s(T)$ can show effects associated with multigap superconductivity or anisotropy of the superconducting gap over the whole temperature range up to T_c. However, it is crucial to know $\lambda(0)$ to properly normalize $\rho_s(T)$ and there are times when it is unavailable experimentally. The uncertainty in knowing $\lambda(0)$ for a superconductor has provided motivation for a technique through which it can be measured by using tunnel diode resonator frequency shifts along with an aluminum coating procedure that is discussed at great length in a different section of this thesis [Gordon et al. (2010a)].

2.5 Multigap superconductivity and the superfluid density

Many superconductors discovered in recent years are multiband materials with complex Fermi surfaces and unconventional order parameters, for example MgB_2 and V_3Si. Not long after the idea that these materials may be well described by a model that takes into account multiple gaps and the associated scattering processes, the α model was introduced and has been widely used to fit specific heat [Bouquet et al. (2001a)] and penetration depth [Bouquet et al. (2001b)] data for alleged multigap superconductors. However, it is now known that this model is not the best one for the job because it takes a shortcut by assigning the BCS temperature dependence to both gaps $\Delta_{1,2}$ in order to fit the total superfluid density $\rho = x\rho_1 + (1-x)\rho_2$. Here, $\rho_{1,2}$ are evaluated by using $\Delta_{1,2} = (\alpha_{1,2}/1.76)\Delta_{BCS}(T)$ with x being the contribution from one of the bands. Although the α model has played an important role for providing convincing evidence for two-gap superconductivity in MgB_2, it is intrinsically inconsistent for describing the actual temperature dependences of the specific heat and superfluid density. The major problem is that one cannot *a priori* assume temperature dependences for the gaps

in the presence of arbitrarily weak interband coupling, which imposes the same T_c for both bands. In the unlikely situation that the interband coupling is zero, both gaps would have BCS temperature dependences, but generally would not have the same T_c, illustrated in Fig. 2.3.

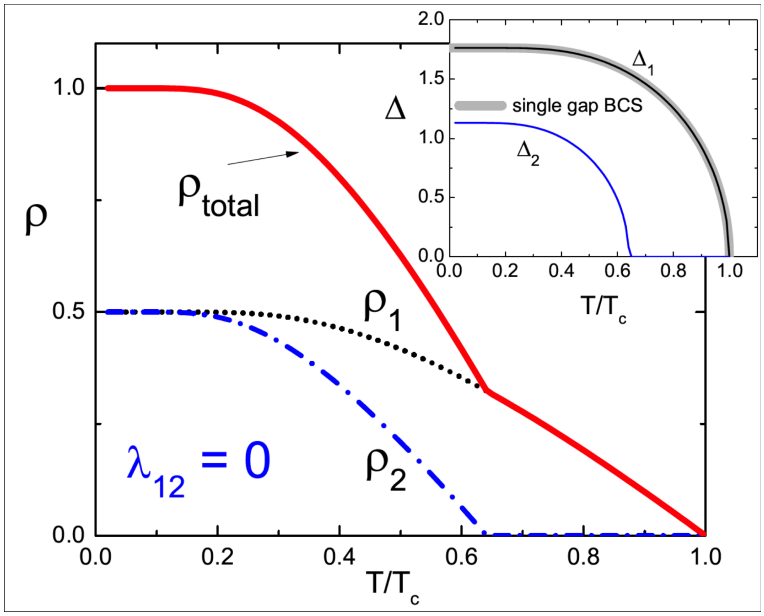

Figure 2.3 Calculated superfluid density and both gaps (inset) vs. reduced temperature for zero interband coupling $\lambda_{12} = 0$. In this calculation, $\lambda_{11} = 0.5$, λ_{22}=0.45, $n_1 = n_2$=0.5 and γ=0.5, where each is defined in the text.

The full blown microscopic approach based on the Eliashberg theory [Golubov and Mazin (1997)] is too cumbersome for analyzing actual experimental data and hence the need for a relatively simple, self-consistent theory accessible to experimentalists is obvious. The weak coupling model provides the framework for such a starting point, which over the years has proven to be very successful for describing superconductivity related phenomena. What follows is based on the "renormalized BCS" model [Nicol and Carbotte (2005)], which incorporates the Eliashberg corrections into the effective coupling constants of the weak-coupling theory. The following approach has been referred to as the "weak-coupling two-band scheme" [Kogan et al. (2009)] and the applicability of the model of the superfluid density and specific heat data is broader than the traditional weak coupling theory. A self-consistent procedure is developed also

by following the procedures outlined in the seminal publications of Ref. [Moskalenko (1959); Suhl et al. (1959)], where the s-wave weak coupling multigap model was originally proposed.

Perhaps the simplest formal weak coupling approach is based on the Eilenberger quasiclassical formulation of superconductivity, which is valid for general Fermi surface geometries and applies when the order parameter is anisotropic [Eilenberger (1968)]. Eilenberger functions f, g for clean materials obey the system

$$0 = 2\Delta g/\hbar - 2\omega f \tag{2.39}$$

$$g^2 = 1 - f^2 \tag{2.40}$$

$$\Delta((k) = 2\pi T N(0) \sum_{\omega>0}^{\omega_D} \Big\langle V(\mathbf{k}, \mathbf{k'}) f(\mathbf{k'}, \omega) \Big\rangle_{\mathbf{k'}}. \tag{2.41}$$

Here, $\mathbf{k}$ is the Fermi momentum, Δ is the gap function, N(0) is the total density of states at the Fermi level per one spin, ω_D is the Debye frequency and the Matsubara frequencies are defined by $\hbar\omega = \pi T(2n+1)$. The quantity in the brackets $\Big\langle ... \Big\rangle$ represents an average taken over the Fermi surface.

Now consider a model material with the gap given by

$$\Delta(\mathbf{k}) = \Delta_{1,2}, \ \mathbf{k} \in F_{1,2}, \tag{2.42}$$

where $F_{1,2}$ are two separate sheets of the Fermi surface. Assume that the gaps are constant on each band. With the density of states on the two sheets given by $N_{1,2}$, the average over the Fermi surface for the quantity X is given by

$$\Big\langle X \Big\rangle = \frac{(X_1 N_1 + X_2 N_2)}{N(0)} = n_1 X_1 + n_2 X_2, \tag{2.43}$$

where $n_{1,2} = N_{1,2}/N(0) = n_1 X_1 + n_2 X_2$, and hence $n_1 + n_2 = 1$.

Equations 2.39 and 2.40 are easily solved, which within the two-band model results in

$$f_\nu = \frac{\Delta_\nu}{\beta_\nu},\ g_\nu = \frac{\hbar\omega}{\beta_\nu},\ \beta_\nu^2 = \Delta_\nu^2 + \hbar^2\omega^2, \tag{2.44}$$

where $\nu = 1, 2$ is the band index.

The self-consistency equation 2.41 takes the form

$$\Delta_\nu = \sum_{\mu=1,2} n_\mu \lambda_{\nu\mu} \Delta_\mu \sum_{\omega}^{\omega_D} \frac{2\pi T}{\beta_\nu} \tag{2.45}$$

where $\lambda_{\nu\mu} = N(0)V(\nu, \mu)$ are the dimensionless effective interaction constants. It is worth noting here that for a given coupling matrix $\lambda_{\mu\nu}$, relative density of states n_ν, and known ω_D, equation 2.66 determines T_c and $\Delta_{1,2}$.

As $T \to T_c$, $\Delta_{1,2} \to 0$ and $\beta \to \hbar\omega$. The sum over ω in equation 2.66 is readily evaluated:

$$S = \sum_{\omega}^{\omega_D} \frac{2\pi T}{\hbar\omega} = ln\frac{2\hbar\omega_D}{T_c \pi e^{-\gamma}} = ln\frac{2\hbar\omega_D}{1.76T_c} \tag{2.46}$$

with γ being the Euler constant. this relation can also be written as

$$1.76T_c = 2\hbar\omega_D e^{-S} \tag{2.47}$$

The system given by the self-consistency relation from equation 2.66 is linear:

$$\Delta_1 = S(n_1\lambda_{11}\Delta_1 + n_2\lambda_{12}\Delta_2) \tag{2.48}$$

$$\Delta_2 = S(n_1\lambda_{12}\Delta_1 + n_2\lambda_{22}\Delta_2). \tag{2.49}$$

It has nontrivial solutions $\Delta_{1,2}$ if its determinant is zero:

$$S^2 n_1 n_2 \eta - S(n_1\lambda_{11} + n_2\lambda_{22}) + 1 = 0, \tag{2.50}$$

where $\eta = \lambda_{11}\lambda_{22} - \lambda_{12}^2$. The roots of this equation are

$$S = \frac{n_1\lambda_{11} + n_2\lambda_{22} \pm \sqrt{(n_1\lambda_{11} + n_2\lambda_{22})^2 - 4n_1 n_2 \eta}}{2n_1 n_2 \eta} \tag{2.51}$$

which can be written as

$$S = \frac{n_1\lambda_{11} + n_2\lambda_{22} \pm \sqrt{(n1\lambda_{11} - n_2\lambda_{22})^2 + 4n_1n_2\lambda_{12}^2}}{2n_1n_2\eta}. \tag{2.52}$$

Denoting the properly chosen root as $S = 1/\lambda'$ we have:

$$1.76T_c = 2\hbar\omega_D \exp -1/\lambda' \tag{2.53}$$

One can easily check that for all λs equal, this yields the standard BCS result. Among various possibilities, let us mention here the case $\eta = \lambda_{11}\lambda + 22 - \lambda_{12}^2 = 0$, for which

$$\lambda' = n_1\lambda_{11} + n_2\lambda_{22} = \Big\langle \lambda \Big\rangle. \tag{2.54}$$

This case corresponds to a popular model with factorizable coupling potential $V(\mathbf{k}, \mathbf{k'}) = V_0\Omega(\mathbf{k})\Omega(\mathbf{k'})$.

Since the determinant of the system is zero, the two gap equations are equivalent and give near T_c:

$$\frac{\Delta_2}{\Delta_1} = \frac{\lambda' - n_1\lambda_{11}}{n_2\lambda_{12}}. \tag{2.55}$$

When the right-hand side is negative, the Δs are of opposite signs. Within the single band BCS theory, the sign of Δ is a matter of convenience; in fact for one band the self-consistency equation determines only $|\Delta|$. For two bands, Δ_1 and Δ_2 may have opposite signs.

Turning to evaluate $\Delta_\nu(T)$, note that the sum in Eqn. 2.66 is logarithmically divergent. To deal with this, it is useful to employ Eilenberger's idea of replacing $\hbar\omega_D$ with the measurable T_c. These are related by Eqn. 2.53, which can be written as

$$\frac{1}{\lambda'} = \ln\frac{T}{T_c} + \sum_{\omega}^{\omega_D} \frac{2\pi T}{\hbar\omega} \tag{2.56}$$

Now add and subtract the last sum from one in Eqn. 2.66:

$$\Delta_\nu = \sum_\mu n_\mu\lambda_{\nu\mu}\Delta_\nu \Big[\sum_{\omega}^{\omega_D} \Big(\frac{2\pi T}{\beta_\mu} - \frac{2\pi T}{\hbar\omega} \Big) + \sum_{\omega}^{\omega_D} \frac{2\pi T}{\hbar\omega} \Big] \tag{2.57}$$

which can be expressed as

$$\Delta_\nu = \sum_\mu n_\mu \lambda_{\nu\mu} \Delta_\mu \Big[\sum_\omega^\infty \Big(\frac{2\pi T}{\beta_{mu}} - \frac{2\pi T}{\hbar\omega} \Big) + \frac{1}{\lambda'} - \ln \frac{T}{T_c} \Big]. \tag{2.58}$$

The last sum over ω is fast-converging and one can repace ω_D with ∞. Numerically, the upper limit of the summation over n can be set to include a few hundred terms and suffices even for low temperature.

Now, introducing the dimensionless quantity

$$\delta_\nu = \frac{\Delta_\nu}{2\pi T} = \frac{\Delta_\nu}{T_c} \frac{1}{2\pi t}, \tag{2.59}$$

with $t = T/T_c$, so now we can write Eqn, 2.58 as:

$$\delta_\nu = \sum_{\mu=1,2} n_\mu \lambda_{\nu\mu} \delta_\mu \Big(\frac{1}{\lambda'} + \ln \frac{T_c}{T} - A_\mu \Big) \tag{2.60}$$

with

$$A_\mu = \sum_{n=0}^\infty \Big(\frac{1}{n+1/2} - \frac{1}{\sqrt{\delta_\mu^2 + (n+1/2)^2}} \Big). \tag{2.61}$$

For given coupling constant $\lambda_{\nu\mu}$ and densities of states n_ν and therefore obtain the gaps $\Delta_\nu = 2\pi T \delta_\nu(t)$. Two simple examples of these solutions are given in insets to Figs. 2.3 and 2.4

Having formulated the way to evaluate $\Delta(T)$, we turn to the London penetration depth given for a general Fermi surface:

$$(\lambda_L^2)_{ik}^{-1} = \frac{16\pi^2 e^2 N(0) T}{c^2} \sum_\omega \Big\langle \frac{\Delta_0^2}{v}_i v_k \beta^3 \Big\rangle. \tag{2.62}$$

where v_i is the Fermi velocity. We consider here only the case of currents in the ab-plane of a uniaxial or cubic material having two deparate Fermi surface sheets, for which a simple algebra gives for the superfluid density:

$$\rho = \Big(\delta_1^2 \sum_{n=0}^\infty \Big[\delta_1^2 + (n+1/2)^2 \Big]^{-3/2} + a\delta_2^2 \sum \Big[\delta_2^2 + (n+1/2)^2 \Big]^{-3/2} \Big) \Big/ (1+a), \tag{2.63}$$

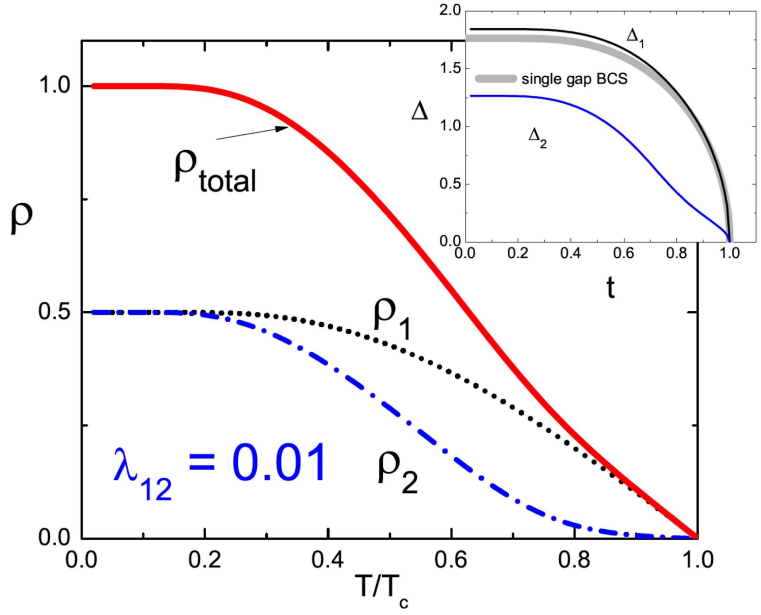

Figure 2.4 Calculated superfluid density and the gaps (inset) vs. reduced temperature. Inset: Calculated with $\lambda_{12} = 0.1$, $\lambda_{11} = 0.5$, $\lambda_{22} = 0.45$, $n_1 = n_2 = 0.5$ and γ=0.5.

with $a = n_2 v_{a2}^2 / n_1 v_{a1}^2$

This equation can be rewritten to mimic the α model as

$$\rho = \gamma\rho_1 + (1-\gamma)\rho_2, \tag{2.64}$$

$$\rho_\nu = \delta_\nu^2 \sum_{n=0}^{\infty} [\delta_\nu^2 + (n+1/2)^2]^{-3/2} \tag{2.65}$$

and

$$\gamma = \frac{n_1 v_{F1}^2}{n_1 v_{F1}^2 + n_2 v_{F2}^2}. \tag{2.66}$$

The formal similarity of the first line here to the α model prompts the name γ model for these results. Note, however, that γ determines the partial contributions from each band and is not just a partial densities of states like n_1 from the α model, which instead involves the band's Fermi velocities.

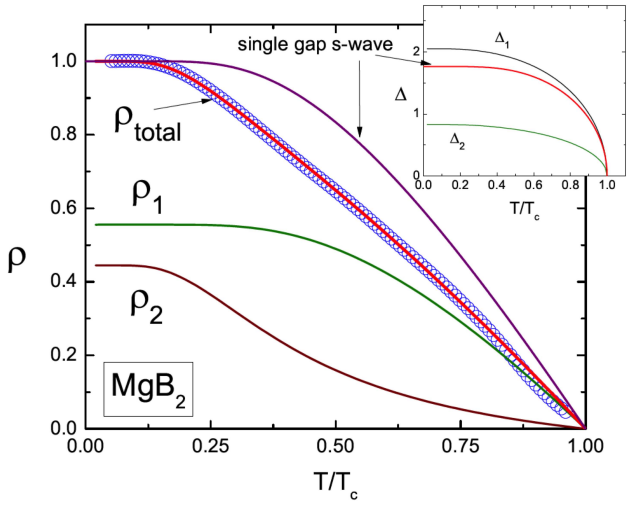

Figure 2.5 The data and fits of the superfluid density for a MgB_2 single crystal and the corresponding temperature-dependent gaps (inset). The fitting parameters were $\lambda_{11} = 0.23$, λ_{22}=0.08, $\lambda_{12} = 0.06$, n_1=0.44 and
$\gamma = 0.56$

Now these results are used to fit the data for the superfluid density obtained in MgB_2 crystals from penetration depth measurements. Fig. 2.6 shows the result of the fitting with three free parameters: λ_{11}, λ_{22} and λ_{12}.

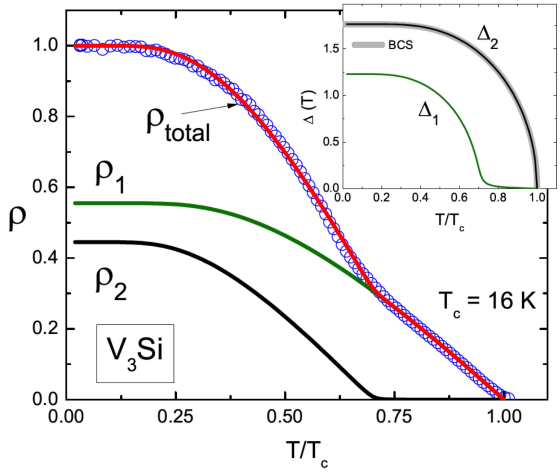

Figure 2.6 The data and fits of the superfluid density for V_3Si single crystal and corresponding temperature dependent gaps (inset). The fitting parameters were: $\lambda_{11} = 0.1$, λ_{22}=0.1, $\lambda_{12} = 1 \times 10^{-5}$, n_1=0.47 and $\gamma = 0.4$.

For V_3Si, we do not have detailed information regarding the band structure, partial densities of states and Fermi velocities on separate sheets of the Fermi surface of this material. Hence, all of these were taken as free parameters in the fitting procedure. The conclusions thus are less reliable for this material than for MgB_2. By mapping onto a two band model, V_3Si results in having two nearly decoupled bands with an extremely weak interband coupling, but still sufficient to give a single T_c. The results and the best fittng parameters are shown in Fig... Note that the long linear tail in $\rho(t)$ as $T \to T_c$ is a direct manifestation of a very small gap, which in this case is Δ_1, in this temperature range.

CHAPTER 3. Principles of a tunnel diode resonator circuit

3.1 Introduction

Due to the great precision with which the frequency of an oscillator can be measured, they have proven to be very useful for making extremely sensitive measurements of material properties. Compared to other popular transducers, for example *ac* bridges, oscillators provide a sensitivity that is a few orders of magnitude higher, but bridge techniques typically have much better accuracy. Bridges usually have a better ability to selectively measure particular physical quantities, while frequency shifts of an oscillating circuit reflect the net effect of all quantities in the circuit which contribute to the shift in the resonance. The ability for oscillators to operate in the radio frequency range makes them more attractive for studying physical processes in solids than *ac* bridges, which typically operate anywhere from the *dc* range to a few kilohertz.

One such oscillator, known as a tunnel diode resonator (TDR) [VanDegrift (1975b,a)], has been carefully optimized for operation at low temperatures, i.e. below about 30 K, by allowing for the detection of changes in its resonance frequency with 0.001 ppm sensitivity and has proven to be an excellent tool for determining the temperature dependence of the London penetration depth in superconductors through its ability to make precision measurements of the *ac* magnetic susceptibility of materials. What follows is a detailed description of exactly how this device has been implemented to make such measurements in our laboratory.

The principle components for understanding the operation of the TDR are an LC tank circuit that is formed by an inductor coil and a capacitor, which has a natural resonance frequency near 10 MHz for our setup, and a tunnel diode, which has a very narrow pn junction that is heavily doped. These special features of the tunnel diode alter its current-voltage (I-V) dependence away from that of a normal diode, most importantly by introducing a region

of negative differential resistance for which an increase in bias voltage leads to a decrease in output current, which is shown in Fig. 3.1. When the bias voltage across the tunnel diode is adjusted to be within this region of the I-V curve, it serves as an *ac* power supply for the LC tank circuit that effectively locks onto its natural resonance frequency by nearly compensating for all of its losses. A sample to be studied is placed at the center of the inductor coil of the tank circuit via a sapphire stage. Any changes in the inductance value of the sense coil brought about from the sample serve to shift the corresponding natural resonance frequency of the tank circuit. By measuring the TDR resonance frequency as a function of the sample temperature, one can in principle extract different material properties, such as thermal expansion, surface impedance, and electric and magnetic susceptibilities.

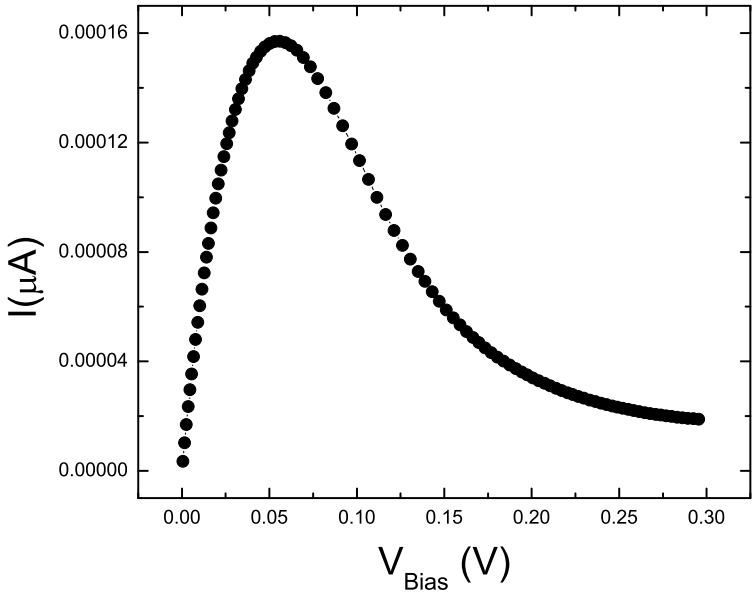

Figure 3.1 I-V curve for an actual tunnel diode measured in the lab. The region of negative differential resistance, where for increasing V there is a decrease in I, allows the diode to act as a power source for the LC tank circuit of the TDR.

Table 3.1 Values of the circuit components used to achieve a noise level of 0.05 Hz along with a 60 turn primary inductor having a 2 mm diameter, a 20 turn tap inductor having a 2 mm diameter and a tunnel diode having a power rating of BD-3.

Component	Value
R_1	1500 Ω
R_2	300 Ω
C_c	22 pF
C_B	0.012 μF
R_p	300 Ω
C (tank)	120 pF

3.2 Optimization for precision measurements

A standard circuit diagram is shown in figure Fig. 3.2, containing all of the TDR circuit components. This design of the TDR circuit has been optimized for use at temperatures below 30 K. This is because the tunnel diode I-V characteristics become nearly temperature independent below this temperature as a consequence of its heavy doping level, which is favorable for stability in the resonance frequency. In general, the TDR resonance is also field dependent, but since measurements of the London penetration depth require that both the circuit and the sample are in zero applied magnetic field, this topic will have no further elaboration here.

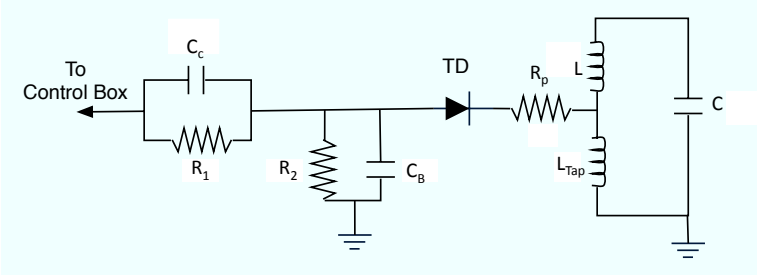

Figure 3.2 A standard TDR circuit diagram [Vannette (2008)].

The *dc* signal that acts to bias the tunnel diode is fed to the circuit through the same coaxial cable that the *ac* signal travels back up through to reach the room temperature electronics used

for analysis. The two resistors R_1 and R_2 together form a voltage divider so that the proper dc bias can be achieved across the tunnel diode. Since R_1 is large it serves as an additional source of rf isolation, while still allowing the dc signal to pass through. The bypass capacitor, C_B, is chosen to be very large so as to act as a short for frequencies in the range of the TDR operating frequency, which is near 10 MHz. The small output coupling capacitor, C_c, allows only a small portion of the ac signal to pass back up the coax to the room temperature electronics. A tap coil, which is chosen to have roughly 1/3 of the inductance of the primary or top portion of the inductor, is used in order to damp away higher harmonics of the resonance frequency. The value of the tapping fraction depends on the impedance of the LC tank circuit at resonance and is generally chosen such that the tap inductance is just beyond the critical value that will allow the tank circuit to resonate. The parasite resistor, R_p, located between the tunnel diode and the LC tank circuit, serves to kill stray oscillations that can be set up between the small capacitance of the diode itself and the tap coil. All of the grounding connections for the circuit were done so by attachment to the circuit chassis, which in turn was routed to a secure Earth ground through the coaxial cable from the top of the cryostat.

The coils used for both the primary and tap inductors were comprised of 40 gauge copper wire that was held together by stycast 1266 epoxy. A small coil winding machine was used to facilitate their construction. The winding process began by inserting a 2 mm diameter drill bit into the winding apparatus to serve as a surface onto which the turns are wound. Next, a thin layer of grease was applied to the outside of the bit so that removing the finished coil could be done more easily. After that, a single turn of very thin mylar was wound around the greased bit that would later be removed from the inside of the finished coil. After the mylar was in place, the winding process was ready to commence. In order to reduce the intrinsic capacitance of the inductors themselves, the copper wire was doubly wound onto the drill bit so each turn in the finished coil was separated from the next by a distance equal to the wire diameter itself. After the winding process was completed, which involved making 60 full turns for the primary coil and 20 full turns for the tap coil, a thin layer of GE varnish was used to coat all of the turns and allowed to dry for 15 minutes. Once dry, one of the doubly wound

turns was removed and the remaining turns on the bit were coated with a very thin layer of stycast 1266 epoxy. After the epoxy cured, the mylar was removed from the inside by pulling on it gently with tweezers.

All circuit components were mounted inside of compartments that were drilled out of the inside of a large piece of gold plated copper known as the circuit block that was mounted to the end of a ^{3}He cryostat. In order to minimize drifts in the resonance frequency that could arise from variations in the temperature of its components, utmost care was taken to ensure that all components were thermally anchored to the circuit block as best as possible. In turn, the temperature of the circuit block itself was controlled by using the proportional-integral-derivative (PID) function of a Lakeshore temperature controller. The voltage divider, consisting of R_1 and R_2, as well as C_c and C_B were all surface mount circuit components that were soldered to a mounting board with an electrically insulating back and the proper electrical pathways were carved into it by using a handheld grinding wheel. This small sheet was firmly mounted to the wall of one of the circuit block compartments so as to achieve the best possible thermalization of the mounted components. A separate compartment leading off of this one housed the tunnel diode and the parasite resistor. This compartment lead to another which housed the capacitor of the tank circuit and the tap coil. The primary coil was located inside of a thin copper tube protruding out of the circuit block to allow for the insertion of the sample, which was mounted to the thin sapphire rod of the sample holder. All components and leads were thermally anchored to the circuit block as best as possible using either direct contact or Apiezon N grease, while avoiding electrical shorts to ground through to the circuit block itself.

The *ac* signal from the LC tank circuit passed up to the room temperature electronics for analysis through the same coaxial cable that delivered the *dc* bias voltage. Once the signal had passed up to the room temperature eletronics it was amplified, mixed to be in the 1-3 kHz region, filtered, amplified again and then counted. Under the best operating conditions, the drift in the measured TDR frequency was roughly $\Delta f \approx$0.05 Hz over the course of several hours, which was achieved for a circuit built using the components specified in Table I. When considering that the resonance frequency of the TDR is $f_0 \approx$ 14 MHz, this translates into

a sensitivity of $\Delta f/f_0 \approx 0.003$ ppm, which implies that the TDR measurement technique is capable of measuring changes in the London penetration depth on the order of 1 Å by applying the standard calibration used to change frequency shifts into length.

3.3 Calibration of the penetration depth from measured TDR frequency shifts

The penetration depth of a superconductor is measured using the TDR by placing a sample, typically being plate-like with a rectangular cross section, onto the end of a sapphire rod and inserting it into the inductor coil of the LC tank circuit. The temperature of the circuit was held as constant as possible, typically to (5 ± 0.001) K, by using the proportional-integral-derivative (PID) control function of a Lakeshore model 340 temperature controller to supply heat to the copper block onto which the circuit components were mounted. The sapphire sample stage was mounted inside of a small copper piece, known as a heater block, with a heater and a thermometer attached to its sides. This allows for the monitoring and controlling of the sample temperature without providing a direct thermal contact between the sample and the TDR circuit. Once inside the coil, a superconducting sample acts to change the resonance frequency of the TDR by directly changing the inductance of the sense coil through its diamagnetic screening of the *ac* magnetic field of the coil, which has a magnitude near 10 mOe.

To see how exactly this shift in inductance caused by the superconductor propagates through to the resonance frequency, let us consider the situation where a sample is placed inside of the coil of a TDR that has an empty coil resonance frequency given by

$$f_0 = \frac{1}{2\pi\sqrt{LC}}, \tag{3.1}$$

where L is the inductance of the empty primary coil and C is the tank capacitance. The diamagnetic response of the superconductor to the applied magnetic field of the primary coil will shift the inductance by some amount, ΔL, which in turn will shift the TDR resonance frequency by some amount, Δf, so then one can write

$$f_0 + \Delta f = \frac{1}{2\pi\sqrt{(L+\Delta L)C}}. \tag{3.2}$$

By using a binomial expansion of the square root and factoring, the result is

$$\frac{\Delta f}{f_0} \approx -\frac{1}{2}\frac{\Delta L}{L}. \tag{3.3}$$

Consider now the case where the primary coil is empty. The value of the applied field from the TDR, H, in this case will be the same throughout the primary coil and the integrated magnetic flux, Φ, can be expressed as

$$\Phi = HV_c, \tag{3.4}$$

where V_c is the volume of the coil. The flux is related to the inductance through the relation

$$L = \frac{d\Phi}{dI}. \tag{3.5}$$

The integrated magnetic flux when the sample is inserted, Φ', has the form

$$\Phi' = H(V_c - V_s) + BV_s, \tag{3.6}$$

where V_s is the volume of the sample and B is the magnetic field inside of the sample. By using $B = H + 4\pi M$, with M being the magnetization of the sample, Eqn. 3.6 takes the form

$$\Phi' = HV_c + 4\pi V_s M. \tag{3.7}$$

The inductance for the case when the sample is inside of the coil, L', now takes the form

$$L' = \frac{d\Phi'}{dI} = \frac{d\Phi'}{dH}\frac{dH}{dI} = \frac{d(HV_c)}{dI} + 4\pi V_s \frac{dM}{dH}\frac{dH}{dI} = L + \Delta L, \tag{3.8}$$

and so now it can be understood that

$$\frac{\Delta L}{L} = \frac{4\pi V_s}{V_c}\chi, \tag{3.9}$$

with χ being the ac magnetic susceptibility of the sample. Finally, an expression relating the susceptibility and the resonance frequency can be written:

$$\frac{\Delta f}{f} \approx -\frac{V_s}{2V_c} 4\pi\chi. \tag{3.10}$$

It is now our goal to understand how the susceptibility can be related to the penetration depth. Generally speaking, the penetration depth is defined as

$$\lambda = \frac{1}{H_0} \int_0^\infty B(x) dx, \tag{3.11}$$

which is only applicable to semi-infinite systems, with H_0 being the field at the interface and $B(x)$ being the field inside of the superconducting half-space. In actual samples, finite size effects and demagnetization, which can really only be defined for a sphere, complicate this problem and we are forced to rely on models relating the susceptibility and the penetration depth that are only applicable to certain geometries. One such model has been developed to relate λ_{ab}, the in-plane penetration depth, to χ, the dynamic magnetic susceptibility, for thin slabs of rectangular cross section with the magnetic field oriented perpendicular to the plane of the slab [Prozorov et al. (2000a)]. The relation

$$-4\pi\chi = \frac{1}{1-N}\Big[1 - \frac{\lambda_{ab}}{R} \tanh\Big(\frac{R}{\lambda_{ab}}\Big)\Big] \tag{3.12}$$

is valid only for the case of a slab with thickness $2d$ in the x-direction, $2w$ in the y-direction and infinite in the z-direction with the field applied along the y-direction, with N being the effective demagnetization factor. An effective dimension R is used to map finite sample dimensions onto this geometry. The most successful solution for rectangular slabs having dimensions $2a$ x $2b$ with $b > a$ and thickness $2d$ has been found by mapping these dimensions onto a disc of radius w and thickness $2d$. This is done by using

$$R \approx \frac{w}{2[1 + [1 + (\frac{2d}{w})^2] \arctan(\frac{w}{2d}) - \frac{2d}{w}]} \tag{3.13}$$

with

$$w = \frac{ab}{a+b} \tag{3.14}$$

For actual samples, $R >> \lambda_{ab}$ and so $\tanh(R/\lambda_{ab}) \rightarrow 1$ and by using Eqns. 3.10 and 3.12 it can be shown straightforwardly that

$$\lambda_{ab}(T) - \lambda_{ab}(T_{min}) = \frac{2V_c R(1-N)}{f_0 V_s}[\Delta f(T_{min}) - \Delta f(T)] \equiv G[\Delta f(T_{min}) - \Delta f(T)] \tag{3.15}$$

where T_{min} is the base temperature for the experiment. The constant of proportionality G can be measured directly by removing the sample from the coil at T_{min} with the use of an extraction mechanism and thus allowing one to exactly measure the empty coil resonance frequency, f_0. Alternatively, G can be determined by using the normal state electromagnetic skin depth

$$\delta = \sqrt{\frac{2\rho}{\mu\omega}}. \tag{3.16}$$

The general expressions relating the frequency shifts of the resonator to the skin depth in the normal state and the penetration depth in the superconducting state for an applied ac magnetic field perpendicular to the c-axis are given by

$$\frac{\Delta f}{f_0} = \frac{V_s}{2V_c}\Big[1 - Re\Big[\frac{\tanh \alpha c}{\alpha c}\Big]\Big] \tag{3.17}$$

and

$$\Delta(1/Q) = \frac{V_s}{V_c} Im\Big[\frac{\tanh \alpha c}{\alpha c}\Big], \tag{3.18}$$

where c is the sample thickness. For a normal metal

$$\alpha = \frac{(1-i)}{\delta} \tag{3.19}$$

and for a superconductor we have

$$\alpha = \frac{1}{\lambda}. \tag{3.20}$$

If we define $\delta f/f_0$ and $\delta(1/Q)$ to be values relative to the values for zero penetration into the sample we have $\delta(1/Q) = \Delta(1/Q)$ and $\delta f/f_0 = \Delta f/f_0 - V_s/2V_c$. In the limit where the skin depth is much less than the sample thickness we have for the normal metal case

$$\frac{\delta f}{f} = -\frac{V_s \delta}{4V_c c} \tag{3.21}$$

and for the superconducting case

$$\frac{\delta f}{f_0} = -\frac{V_s \lambda}{2V_c c}. \tag{3.22}$$

Hence it is enough to know the value of the resistivity at T_c to calibrate the penetration depth by using these relations.

3.4 Measuring the absolute value of $\lambda_{ab}(T)$

The TDR technique described up to this point is able to precisely measure the variation of the London penetration depth with temperature, $\Delta\lambda(T) = \lambda(T) - \lambda(T_{min})$, but not its absolute value, $\lambda(T)$ [Prozorov and Giannetta (2006)]. This can be understood by considering the effect of introducing a superconducting sample into the primary TDR inductor coil. We can imagine that before the sample is introduced, the TDR has some natural resonance frequency f_0, and after the sample is inside f_0 shifts to some value that depends on the properties of the superconductor. The magnitude of this frequency shift is ultimately affected by how the sample perturbs the field of the inductor coil, which is dependent on the ability of the sample to screen the field from the inductor. Since this is a function of the detailed characteristics of the superconductor, e.g. the pairing symmetry, which are usually unknown, calculating the value to which the resonance will shift due to the samples presence is practically impossible.

On the other hand, one might think that it is not necessary to know the absolute value of $\lambda(T)$ because the exact functional form of $\Delta\lambda(T)$ can be calculated for a given order parameter symmetry and this is all that is really needed to analyze the data. This is partly true, but the absolute value of $\lambda(0)$ is required for the proper normalization of the superfluid density, $\rho_s = [\lambda(0)/\lambda(T)]^2$. This quantity is important for studying effects associated with multigap

and/or anisotropic superconductivity and is also related to the phase stiffness of the wave function of the superconducting condensate [Kogan et al. (2009)].

A method for obtaining the absolute value of $\lambda(T)$ must provide an accurate and reliable way to extract a calibration point. Once a calibration point has been established, all other values of λ are automatically known. The procedure for the method used in this work to calibrate λ was initially proposed in Ref. [Prozorov et al. (2000b)]. It is based on the basic idea that if λ is unknown for a given sample, then it can be determined at a single temperature by coating its entire surface with a thin film of a different, conventional superconductor having a much lower T_c and a known value of $\lambda(0)$. The film thickness must be less than the rf skin depth at the TDR operating frequency of $\approx$10 MHz so that once it reaches the normal state, it will be virtually transparent to the *ac* magnetic field of the coil because it will contribute negligibly to the screening of the *ac* electromagnetic field, which a normal metal usually would do in its bulk state.

To understand exactly how this method allows for the determination of the absolute value of the penetration depth of a superconductor, let us consider the case where a bulk superconductor with a given T_c is coated with a thin film of a conventional superconductor having a much lower transition temperature, which we will assume is aluminum. Region 1 corresponds to the film and region 2 is the bulk superconductor. The film thickness will be taken as d_{Al} and the external magnetic field is taken to be in the form of $\vec{H}(\mathbf{r},t) = H_0(\mathbf{r})e^{i\omega t}\hat{y}$, which is parallel to the interface plane between the film and bulk superconductor. The $\hat{x}$-direction is perpendicular to the interface between the film and the bulk superconductor and points toward the interior of the bulk material, which can be seen in Fig. 3.3. Our goal is to evaluate the effective penetration depth into the system consisting of the film and the bulk superconductor in terms of known parameters that will allow us to solve for the unknown penetration depth of the bulk superconductor. The well known London equation

$$\vec{\nabla}^2\vec{H} = \frac{1}{\lambda^2}\vec{H} \tag{3.23}$$

will be taken as being valid inside of both the superconducting film and the bulk superconduc-

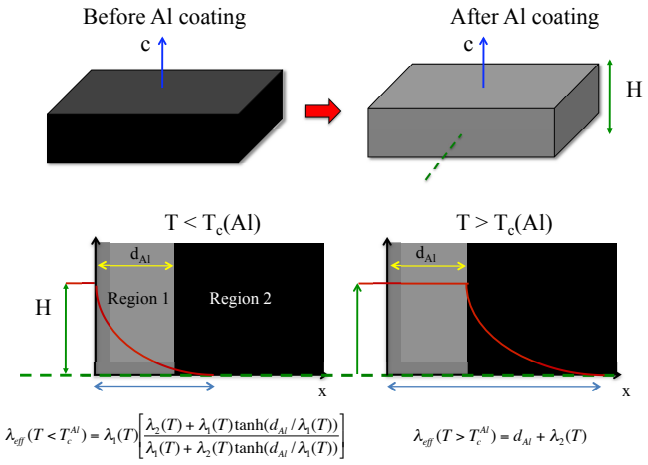

Figure 3.3 Schematic diagram of the sample before and after the aluminum coating procedure.

tor. Therefore, we have the following solutions for the magnetic field inside of regions 1 and 2:

$$\vec{H}_1(x) = [Ae^{\frac{x}{\lambda_1}} + Be^{-\frac{x}{\lambda_1}}]e^{i\omega t}\hat{y} \tag{3.24}$$

$$\vec{H}_2(x) = Ce^{-\frac{x}{\lambda_2}}e^{i\omega t}\hat{y}. \tag{3.25}$$

In addition, the following boundary conditions apply for this setup:

$$\vec{H}_1(x = 0) = H_0\hat{y}, \tag{3.26}$$

$$\vec{H}_1(x = d_{Al}) = \vec{H}_2(x = d_{Al}) \tag{3.27}$$

and

$$\vec{E}_1(x = d_{Al}) = \vec{E}_2(x = d_{Al}). \tag{3.28}$$

To utilize the boundary condition in Eqn. 3.28 we must make use of the relation

$$\vec{\nabla} \times \vec{H} = \vec{J} = \sigma \vec{E}, \tag{3.29}$$

and for superconductors with $T \ll T_c$ we have

$$\vec{J}(\omega) = \frac{\vec{E}(\omega)}{i\omega\mu_0\lambda^2}. \tag{3.30}$$

So the boundary condition in Eqn. 3.28 reduces to

$$\lambda_1^2 \frac{\partial H_1(x = d_{Al})}{\partial x} = \lambda_2^2 \frac{\partial H_2(x = d_{Al})}{\partial x}. \tag{3.31}$$

The equations that result from applying the boundary conditions in Eqns. 3.26, 3.27 and 3.31 to the solutions in Eqns. 3.24 and 3.25 are:

$$A + B = H_0, \tag{3.32}$$

$$Ae^{\frac{d_{Al}}{\lambda_1}} + Be^{-\frac{d_{Al}}{\lambda_1}} = Ce^{-\frac{d_{Al}}{\lambda_2}} \tag{3.33}$$

and

$$Be^{-\frac{d_{Al}}{\lambda_1}} - Ae^{\frac{d_{Al}}{\lambda_1}} = \Big(\frac{\lambda_2}{\lambda_1}\Big)Ce^{-\frac{d_{Al}}{\lambda_2}}. \tag{3.34}$$

Solving for A, B and C using Eqns. 3.32, 3.33 and 3.34 results in:

$$A = H_0\Big[1 - \frac{e^{\frac{d_{Al}}{\lambda_1}}(\frac{\lambda_2}{\lambda_1} + 1)}{2[\cosh\frac{d_{Al}}{\lambda_1} + \frac{\lambda_2}{\lambda_1}\sinh\frac{d_{Al}}{\lambda_1}]}\Big] \tag{3.35}$$

$$B = \frac{H_0 e^{\frac{d_{Al}}{\lambda_1}}(\frac{\lambda_2}{\lambda_1} + 1)}{2[\cosh\frac{d_{Al}}{\lambda_1} + (\frac{\lambda_2}{\lambda_1})\sinh\frac{d_{Al}}{\lambda_1}]}, \tag{3.36}$$

and

$$C = H_0 e^{d_{Al}\{\frac{1}{\lambda_1} + \frac{1}{\lambda_2}\}}\Big(\frac{\cosh\frac{d_{Al}}{\lambda_1} - \sinh\frac{d_{Al}}{\lambda_1}}{\cosh\frac{d_{Al}}{\lambda_1} + (\frac{\lambda_2}{\lambda_1})\sinh\frac{d_{Al}}{\lambda_1}}\Big). \tag{3.37}$$

Having now solved for A, B and C, we have the full solutions of the magnetic fields $H_1(x)$ and $H_2(x)$, which can be used to calculate the effective penetration depth inside of the film and bulk superconductor combination. This is calculated using the definition

$$\lambda_{eff} \equiv \frac{1}{H_0}\int_0^\infty H(x)dx = \frac{1}{H_0}\Big(\int_0^{d_{Al}} H_1(x)dx + \int_{d_{Al}}^\infty H_2(x)dx\Big). \tag{3.38}$$

After some algebra, it can be shown that the resulting value for λ_{eff} is

$$\lambda_{eff} = \lambda_1\Big(\frac{\lambda_2 + \lambda_1 \tanh\frac{d_{Al}}{\lambda_1}}{\lambda_1 + \lambda_2 \tanh\frac{d_{Al}}{\lambda_1}}\Big). \tag{3.39}$$

This result has been used to calibrate experimental penetration depth data on a number of different compounds [Kim et al. (2010b); Gordon et al. (2010a)]. As an example of how this is done, the following analysis is used for a member of the $Ba(Fe_{1-x}Co_x)_2As_2$ series with x=0.074 and $T_c \approx 22.7$ K and no value of $\lambda_{ab}(0)$ that had been reliably determined before the measurement. The process began by selecting the best looking single crystal of this material from a bigger batch that had a plate-like rectangular cross section. A typical basal dimension for such a sample was 0.5-1 mm. Once chosen, $\Delta\lambda_{ab}(T)$ was measured for the sample before it was coated with any superconducting films. This allowed for the determination of useful parameters pertaining to the low temperature functional form of the penetration depth that are unaccessible after the sample has been coated. Once clean data was taken for the uncoated sample, the next step was to coat its entire surface with a thin film of a superconductor having a much lower T_c and a known value of $\lambda(0)$. For this study, aluminum was chosen as the material for the superconducting film, which has $T_c^{Al} \approx 1.2$ K, $\lambda(0) \approx 500 \pm 100$ Å and was deposited with a thickness of $d_{Al} = 1000 \pm 100$ Å. See Fig. 5.1 for an SEM image of the sample after it was coated and a detailed explanation about the coating procedure explained in the text. A typical value for the resistivity of an aluminum film just above T_c is $\rho_{Al} \simeq 10$ $\mu\Omega$-cm. To determine the skin depth for a metal having this resistivity in the presence of an applied field having a frequency $\omega = 2\pi(14$ MHz), corresponding to the TDR frequency, we can use the formula given by Eqn. 3.16 to calculate the normal state electromagnetic skin depth for

aluminum at this frequency, which gives a value of $\delta = 75$ μm. Since $\delta \ggg d_{Al}$, the aluminum film is effectively transparent to the magnetic field of the TDR coil.

Fig. 3.4 shows the temperature dependence of the variation of the London penetration depth for the $Ba(Fe_{0.926}Co_{0.074})_2As_2$ compound for the magnetic excitation field of the TDR coil oriented so that it was parallel to the crystallographic c-axis of the sample and supercurrents flowed only in the ab-plane, $\Delta\lambda_{ab}(T)$. For the $Ba(Fe_{1-x}Co_x)_2As_2$ series, it has been well established by several techniques [Gordon et al. (2009b,a, 2010b)] that the low temperature region of the London penetration depth exhibits a power law temperature dependence, $\Delta\lambda_{ab}(T) = CT^n$, where n is greater than 2. The inset to Fig. 3.4 shows a zoomed in view of the low temperature region, i.e. below $T_c/3$, for $\Delta\lambda_{ab}(T)$ along with a power law fit shown by the solid red line. Taking high quality data in the low temperature region before the aluminum coating procedure is important because the lowest portion of this region is hidden after the aluminum is deposited and the functional form of the penetration depth in that portion for the bulk superconductor is useful for data analysis. The exact form of the fitting function used was $\Delta\lambda_{ab}(T) = CT^n$, where $C = 2.936$ x 10^{-4} and $n = 2.48$.

The main frame in Fig. 3.5 shows the full superconducting transition before the aluminum coating (black circles) as well as the low temperature data after coating (green triangles). The inset to Fig. 3.5 shows a zoomed-in view of the full aluminum transition, which occurs from $T_{min} \approx 0.5$ K up to $T_c^{Al} \approx 1.2$ K. The quantity identified in the inset of Fig. 3.5 as L= $\Delta\lambda_{eff}(T_c^{Al}) - \Delta\lambda_{eff}(T_{min})$ is useful for calibrating the absolute value of the penetration depth.

Let us now consider the quantity L= $\Delta\lambda_{eff}(T_c^{Al}) - \Delta\lambda_{eff}(T_{min})$, which is identified in the inset of Fig. 3.5. We have

$$L = \Delta\lambda_{eff}(T_c^{Al}) - \Delta\lambda_{eff}(T_{min}) = \lambda_{eff}(T_c^{Al}) - \lambda_{eff}(T_{min}), \tag{3.40}$$

where λ_{eff} is given by Eqn. 3.39, which in terms of the present parameters defined takes the form of

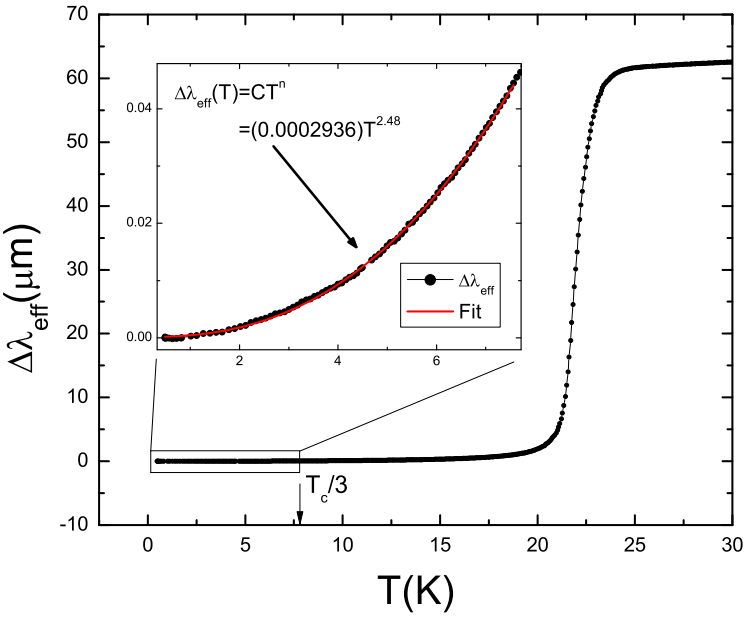

Figure 3.4 TDR measurements of $\Delta\lambda_{ab}(T)$ for a $Ba(Fe_{1-x}Co_x)_2As_2$ compound with x=0.074 before it was coated with an aluminum film for the absolute calibration of the London penetration depth. The inset shows a zoomed-in view of the low-temperature region, i.e. below $T_c/3$, and the red line is a power law fit.

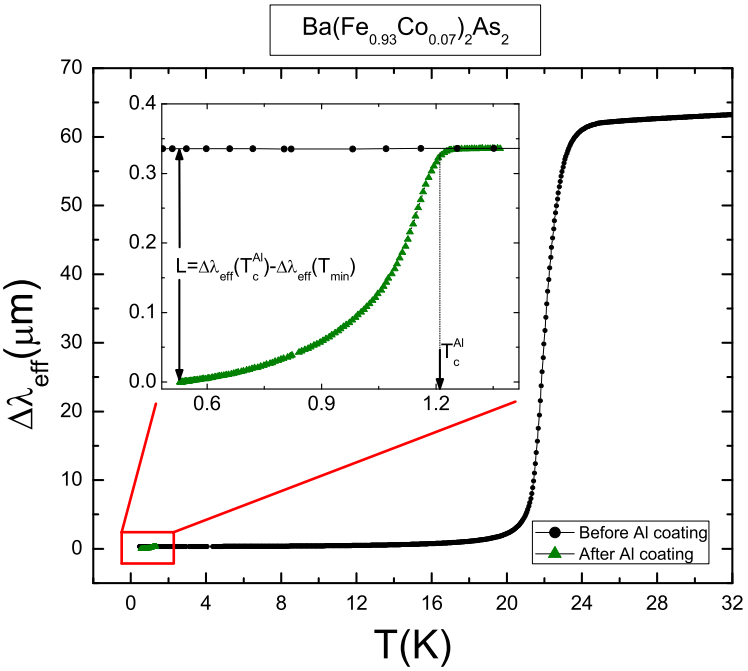

Figure 3.5 $\Delta\lambda_{ab}(T)$ before and after the same compound shown in Fig. 3.4 was coated with an aluminum film.

$$\lambda_{eff}(T) = \lambda_{Al}(T)\Big(\frac{\lambda_{ab}(T) + \lambda_{Al}(T)\tanh\frac{d_{Al}}{\lambda_{Al}(T)}}{\lambda_{Al}(T) + \lambda_{ab}(T)\tanh\frac{d_{Al}}{\lambda_{Al}(T)}}\Big), \tag{3.41}$$

with $\lambda_{Al}(T)$ being the penetration depth of only the aluminum, $\lambda_{ab}(T)$ being the ab-plane penetration depth of only the bulk superconductor and d_{Al} being the thickness of the aluminum film. Now let us consider what happens when $T = T_c^{Al}$. Because the aluminum film has gone into the normal state and because d_{Al} is much less than the skin depth of aluminum at 14 MHz, δ, the TDR field penetrates completely through the aluminum film and into the $Ba(Fe_{0.926}Co_{0.074})_2As_2$ up to a thickness of $\lambda_{ab}(T)$, which gives us

$$\lambda_{eff}(T_c^{Al}) = d_{Al} + \lambda_{ab}(T_c^{Al}). \tag{3.42}$$

We know from the measurements on the $Ba(Fe_{0.926}Co_{0.074})_2As_2$ compound before it was coated with aluminum that

$$\Delta\lambda_{ab}(T) = \lambda_{ab}(T) - \lambda_{ab}(0) = CT^n \tag{3.43}$$

so Eqn. 3.42 becomes

$$\lambda_{eff}(T_c^{Al}) = d_{Al} + C(T_c^{Al})^n + \lambda_{ab}(0) \tag{3.44}$$

Consider now what happens when $T = T_{min}$. At this temperature, both the aluminum film and the $Ba(Fe_{0.926}Co_{0.074})_2As_2$ superconductor participate in the screening of the externally applied rf magnetic field from the TDR and the resulting penetration depth is given by the expression in Eqn. 3.41. In order to evaluate λ_{Al}, we can use the BCS [Bardeen et al. (1957); Poole et al. (2007)] estimate for it at $T = T_{min}$, namely

$$\lambda_{Al}^{BCS}(T_{min}) \approx \lambda_{Al}(0)\Big(1 + \sqrt{\frac{\pi\Delta_{Al}(0)}{2k_BT_{min}}}e^{-\frac{\Delta_{Al}(0)}{k_BT_{min}}}\Big) = \lambda_{Al}(0)\Big(1 + \sqrt{\frac{(0.85)\pi T_c^{Al}}{T_{min}}}e^{\frac{-(1.7)T_c^{Al}}{T_{min}}}\Big), \tag{3.45}$$

where the expression for $2\Delta_{Al}(0)/k_BT_c^{Al}$=3.4 Ashcroft and Mermin (1976) was used and $\lambda_{Al}(0) = 500 \pm 100$ Å . Now, using the expression given in Eqn. 3.40 we obtain

$$L = d_{Al}+C(T_c^{Al})^n+\lambda_{ab}(0)-\lambda_{Al}^{BCS}(T_{min})\Big(\frac{C(T_{min})^n + \lambda_{ab}(0) + \lambda_{Al}^{BCS}(T_{min})\tanh\frac{d_{Al}}{\lambda_{Al}^{BCS}(T_{min})}}{\lambda_{Al}^{BCS}(T_{min}) + (C(T_{min})^n + \lambda_{ab}(0))\tanh\frac{d_{Al}}{\lambda_{Al}^{BCS}(T_{min})}}\Big) \tag{3.46}$$

with the only unknown being $\lambda_{ab}(0)$ since the quantity L itself can be measured directly from Fig. 3.5. To solve for $\lambda_{ab}(0)$, we can use the quadratic equation in the form

$$\lambda_{ab}(0) = \frac{-b - \sqrt{b^2 - 4ac}}{2a} \tag{3.47}$$

where the coefficients are given by

$$a = -\tanh\frac{d_{Al}}{\lambda_{Al}(T_{min})} \tag{3.48}$$

$$b = [L - d_{Al} - C(T_c^{Al})^n - C(T_{min})^n]\tanh\frac{d_{Al}}{\lambda_{Al}(T_{min})} \tag{3.49}$$

and

$$c = -a[(L-d_{Al})C(T_{min})^n - C^2(T_c^{Al}T_{min})^n + \lambda_{Al}^2(T_{min})] + \lambda_{Al}(T_{min})[L-d_{Al}-C(T_c^{Al})^n + C(T_{min})^n]. \tag{3.50}$$

For $L \approx 0.333\mu m$, this procedure produces a value of $\lambda_{ab}(0) \approx 270$ nm, which is in quite reasonable agreement with values of $\lambda_{ab}(0)$ that were obtained later using other techniques [Williams et al. (2010); Luan et al. (2010); Nakajima et al. (2010)].

In summary, a new procedure has been developed to measure the zero temperature value of the penetration depth by using the TDR technique, which is useful for the proper normalization of the superfluid density, $\rho_s(T)$. This procedure takes advantage of the calibration point provided by coating the entire surface of the sample under study with a thin film of a conventional superconductor with a lower T_c and a known value of $\lambda(0)$. By using the analysis provided in this section along with the TDR frequency shift data, $\lambda(0)$ can be determined for a superconductor.

CHAPTER 4. Penetration depth measurements in $Ba(Fe_{1-x}T_x)_2As_2$ (T=Co,Ni,Ru,Rh,Pd,Pt,Co+Cu)

4.1 Introduction

After the initial discoveries of superconductivity with $T_c \approx 26$ K in $LaFeAs(O_{1-x}F_x)$ [Kamihara et al. (2008)], which was soon after shown to be as high as 55 K in $SmFeAs(O_{1-x}F_x)$ [Ren et al. (2008)], an intense flurry of activity aimed at understanding the fundamental physics governing this new family of superconductors has been put forth. Up to this date there have been at least five new classes of iron-based superconductors discovered. Due to the availability of mainly the 1111 and 122 classes of these materials at the time of this work, these will be focused on in the following report of experimental results in this section.

The symmetry of the superconducting order parameter (OP) is of crucial importance for determining the pairing mechanism in any superconductor. This was demonstrated by the experimental uncovering of the $d_{x^2-y^2}$-wave symmetry of the OP [Harlingen (1995)] in the high-T_c cuprates, and many comparisons have been made between them and the iron-based superconductors. However, there are several differences between these two families of materials, such as a single band crossing the Fermi level in the cuprates versus multiple bands crossing in the iron-based superconductors, the cuprates are very two-dimensional materials whereas the iron-based superconductors are likely three-dimensional, the cuprates have a single superconducting gap while the iron-based superconductors likely have multiple ones and the parent compounds of the cuprates are anitferromagnetic insulators compared to the poor metallic parent state of the iron-based superconductors. Perhaps the main reason for this juxtaposition is that the parent state of both exhibit some type of antiferromagnetic ordering at finite temperature that is suppressed as the system is doped away and superconductivity emerges out of

this instability of the magnetic phase for some critical doping concentration [Taillefer (2010)]. It is only natural to suggest that there may be an underlying physical principle which is common to both families, namely that the superconducting pairing mechanism is strongly linked to spin fluctuations, analagous to the role played by phonons in BCS superconductors. Since their discovery, conflicting experimental reports have lead to confusion about the actual OP structure in the iron-based superconductors, which may be due to the unconventional nature of many of their superconducting properties.

As for the 1111 system, point-contact Andreev-reflection (PCAR) spectroscopy experiments have reported the existence of two distinct superconducting gaps in $NdFeAs(O_{0.9}F_{0.1})$ [Samuely et al. (2009)] and $SmFeAs(O_{0.85}F_{0.15})$ [Wang et al. (2009)], with evidence for a pseudogap above T_c as well as a zero bias conductance peak, which has been interpreted as evidence for an OP that changes sign between Fermi surface sheets. However, other PCAR measurements in the $SmFeAs(O_{0.9}F_{0.1})$ compound have shown evidence for a single superconducting gap that exhibits a BCS temperature dependence [Chen et al. (2008)].

Nuclear magnetic resonance (NMR) measurements have indicated the lack of a coherence peak in the spin lattice relaxation rate of the 1111 system and a T^3 power law behavior at low temperatures, interpreted as either a nodal superconducting gap or the presence of strong impurity scattering [Grafe et al. (2008); Nakai et al. (2008)]. On the other hand optical spectroscopy measurements have reported the observation of a coherence peak just below T_c in the 122 system and it has been proposed that these two different techniques see different results because they may be coupling over different length scales of the Fermi surface [Aguilar et al. (2010)].

Angle-resolved photoemission spectroscopy (ARPES) experiments in the $NdFeAs(O_{0.9}F_{0.1})$ [Liu et al. (2008); Kondo et al. (2008)] and $NdFeAsO_{0.85}$ [Aiura et al. (2008)] compounds have observed isotropic superconducting gaps in the ab plane for both the inner and outer hole pockets centered about the Γ point as well as the electron pocket centered about the X point of the Brillouin zone. Not all ARPES experiments on the Nd-1111 compounds observe all reported gaps stated previously, but the superconducting gap amplitude observed about the

inner Γ point has been reported to have values from 12 to 20 meV.

Measurements of the London penetration depth, λ, in the 1111 system originally reported claims of exponential behavior at low temperatures, indicative of a nodeless OP, but after many careful measurements have been done since then, the consensus of the community has changed. Initial measurements of Pr-1111 taken with a microwave cavity technique reported that the penetration depth was flat at low temperatures, which was interpreted as evidence for a nodeless OP, but later it was found that this flat dependence is likely from a very low signal to noise ratio [Hashimoto et al. (2009)]. Transverse field muon spin rotation measurements (TF-μSR) of λ in La-1111 [Luetkens et al. (2008)] and Sm-1111 [Drew et al. (2008)] initially reported that λ exhibited exponential behavior at low temperatures, but later after more careful studies were done it was found that the effects of magnetic order and/or random frozen disorder of the vortex lattice in iron-based superconductors introduce considerable uncertainty in their ability to determine λ from TF-μSR data [Sonier et al. (2010)]. Tunnel diode resonator (TDR) measurements of λ in the Sm-1111 [Malone et al. (2009)] and the Nd-1111 [Prozorov et al. (2009b)] originally reported exponential behavior at low temperatures, but later it was shown by comparison to TDR measurements of the non-magnetic La-1111 compound and also by fitting the Sm-1111 and Nd-1111 data to a function that accounts for the additional contribution from the local moments that this exponential dependence is most probably an effect arising from the localized magnetism from the rare earth ions [Martin et al. (2009b)], which was also found to be the case for the electron-doped cuprate NCCO [Prozorov et al. (2000c)].

As for the 122 system, the initial claims of the measured gap symmetry from different experiments seemed just as conflicting as they were in the 1111 system. PCAR measurements performed on the K-doped Ba-122 compound are consistent with two nodeless superconducting gaps in the ab plane, while ARPES experiments in the same series have found the existence of multiple superconducting gaps on various sheets with differing amplitudes [Ding et al. (2008); Evtushinsky et al. (2009a)]. Before much of the data to be reported here, there was little done on the 122 system in terms of the magnetic penetration depth, but works that were performed

later [Bobowski et al. (2010); Luan et al. (2011)] are consistent with the data that are to be shown later in this chapter. Thermal conductivity and specific heat measurements performed as a function of the doping level in the $Ba(Fe_{1-x}Co_x)_2As_2$ series have indicated that the superconductivity at optimal doping in this compound is nodeless [Reid et al. (2010); Gofryk et al. (2009)], but near the edges of the superconducting dome they suggest the development of a significant gap anisotropy or the development of nodes in the gap that are not imposed by symmetry (accidental nodes).

All of the samples measured in this study were large single crystals grown out of Fe-As flux using standard high temperature solution growth techniques [Ni et al. (2008a,b)]. They were selected from several different batches that have been characterized by various techniques, including resistivity, magnetization and heat capacity. The actual doping concentrations were determined by wavelength dispersive x-ray spectroscopy (WDS) in the electron probe micro-analyzer of a JEOL JXA-8200 Superprobe. Magneto-optical imaging was also used to insure that the Meissner screening in the samples was homogeneous down to a length scale of $\approx 1\mu$m, which can be seen in Fig. 4.1. The temperature-doping phase diagram for several different transition metal doped 122 compounds is shown in Fig. 1.1.

4.2 $\Delta\lambda_{ab}(T)$ at optimal doping in $Ba(Fe_{1-x}Co_x)_2As_2$

The first measurements to be discussed here were performed on three different samples, all near optimal doping, of the $Ba(Fe_{1-x}Co_x)_2As_2$ series [Gordon et al. (2009b)]. These samples were all thin slabs having rectangular cross sections and typical dimensions of $\approx 1\times1\times0.8$ mm^3. WDS analysis has shown that the actual cobalt concentration for these samples, averaged over six measurements, is Co/(Co+Fe)=7.4%$\pm$ 0.2%. Doping at this level completely suppresses the antiferromagnetic and structural transitions that exist in the parent compound. Powder x-ray diffraction on ground crystals has yielded tetragonal lattice constants of $a = 3.9609 \pm 0.0008$ Å and $c = 12.9763 \pm 0.004$ Å. As mentioned previously, single crystal x-ray diffraction measurements have found no evidence for a tetragonal-to-orthorhombic structural transition, as can be seen from panels (a) and (b) in Fig. 4.2. In particular, the orthorhombic splitting

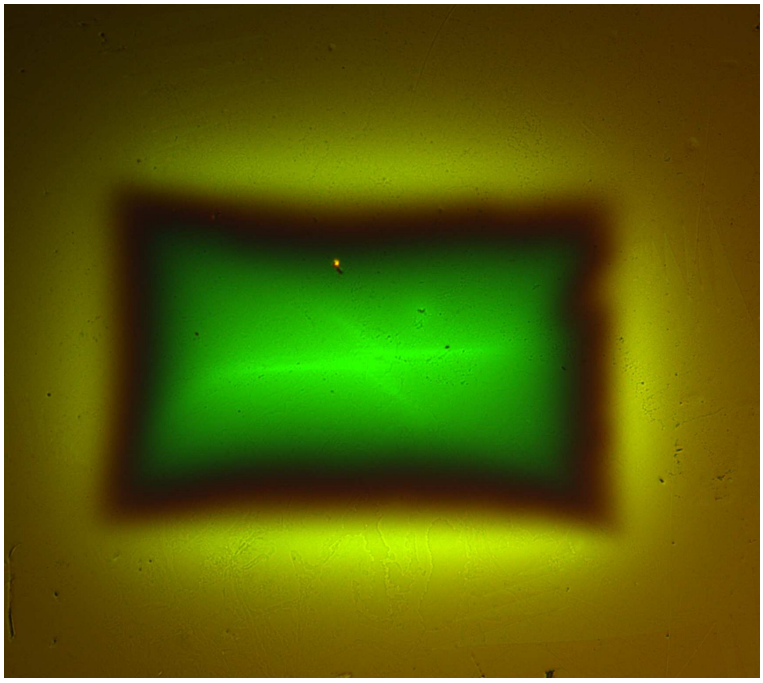

Figure 4.1 A magneto optical image of a $Ba(Fe_{1-x}Co_x)_2As_2$ sample showing that the trapped flux is uniformly distributed indicating homogeneous superconductivity.

observed in the (ν ν 0) scans for the parent compound [Ni et al. (2008a)] with a value of $\Delta\nu \approx 0.005$ at 10 K should be clearly observable as illustrated by the arrows in Fig. 4.2 (b). Furthermore, the similarity of the diffraction peak widths for the Co-doped and the parent $BaFe_2As_2$ compound indicates that the Co doping is homogeneous. Fig. 4.2 (c) shows the T-dependent in-plane resistivity, dc magnetization and penetration depth. The T_c, as defined by zero resistivity, coincides with the onset of diamagnetic magnetization and is close to the beginning of a sharp decrease in $\lambda(T)$.

The low-temperature behavior of the in-plane penetration depth, $\Delta\lambda_{ab}(T) = \lambda_{ab}(T) - \lambda_{ab}(0)$ and the superfluid density, $\rho_s(T) = [\lambda(0)/\lambda(T)]^2$, are commonly used to determine the symmetry of the superconducting pairing state [Prozorov and Giannetta (2006)]. In the case of a fully gapped Fermi surface for a clean, homogeneous superconductor that is in the local limit, $\Delta\lambda(T)/\lambda(0) \approx \sqrt{\pi\Delta(0)/2k_BT}\exp(-\Delta(0)/k_BT)$, which for the BCS (isotropic) case is applicable for $T \leqslant T_c/3$. This fully gapped form is also valid for the cases of an anisotropic gap and two-gap superconductivity if one allows $\Delta(0)/T_c$ to be a free parameter and $\Delta(0) = \Delta_{min}(0)$, the magnitude of the smaller gap. This behavior is consistent with our TDR measurements of the penetration depth in Nb, a well known, conventional BCS superconductor, as well as the multigap s-wave superconductor MgB_2, both shown in Fig. 4.3. For the case of a superconductor having $d_{x^2-y^2}$-wave pairing, as for the high-T_c cuprate superconductors [Harlingen (1995)], in the clean impurity scattering limit $\Delta\lambda(T)/\lambda(0) \approx [2ln(2)/\alpha\Delta(0)]T$, where $\alpha = \Delta^{-1}(0)|d\Delta(\phi)/d\phi|$ as $\phi \rightarrow \phi_{node}$. This linear T-dependence changes to a quadratic dependence from $T = 0$ K up to a characteristic temperature T^* if impurity scattering effects are non-negligible, where T^* depends on the concentration of impurity scatterers in the system [Hirschfeld and Goldenfeld (1993)]. The expected linear T-dependence for a clean $d_{x^2-y^2}$-wave superconductor has indeed been observed from TDR penetration depth measurements in the high-T_c cuprate superconductor Bi-2212 with a T_c of 90 K, also shown in Fig. 4.3. Non-magnetic impurity scattering does not affect the s-wave gap much, but it does suppress the $d_{x^2-y^2}$-wave gap. However, the superfluid density does change in both cases if non-magnetic impurity scattering is significant, as shown in Fig. 4.3. The functional form of the superfluid density

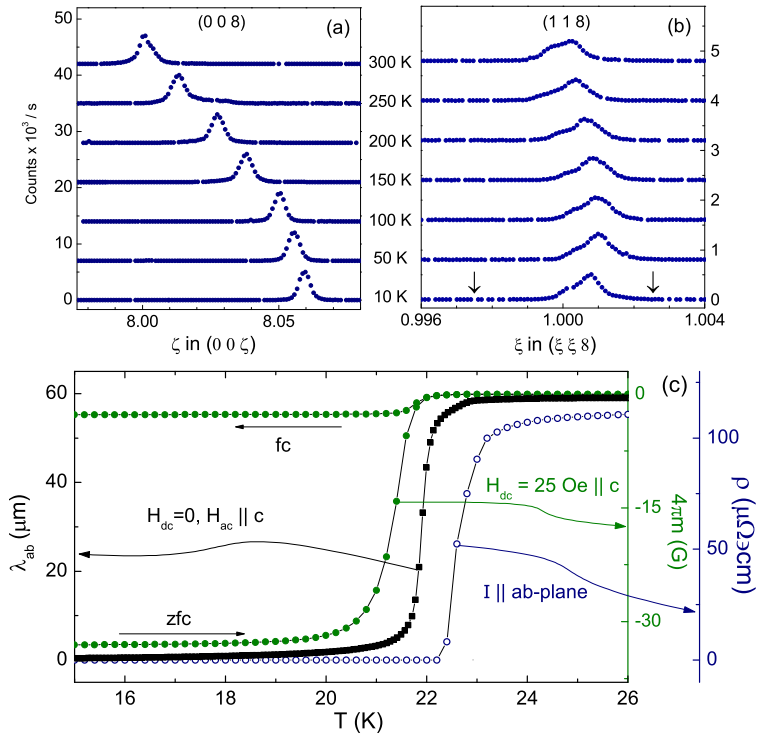

Figure 4.2 Characterization of $Ba(Fe_{0.93}Co_{0.07})_2As_2$ single crystals. (a) Longitudinal x-ray scans through the position of the (0 0 8) reflection for indicated temperatures. (b) Transverse (ξ ξ 0) scans through the position of the (1 1 8) reflection. Changes in the position of the peaks in (a) and (b) result from thermal expansion of the lattice. The asymmetric peak shape in the (ξ ξ 0) scan originates from a second grain with a slightly different orientation (sample mosaic) and is present at all temperatures. In (a) and (b) the horizontal axes depict the reciprocal lattice vectors relative to the alignment and lattice parameters at 300 K. The vertical arrows in (b) depict the positions of the split diffraction peaks at 10 K in the parent $BaFe_2As_2$ compound (after Ref. [Ni et al. (2008a)]). (c) In-plane resistivity (open circles), dc magnetization (filled circles) and in-plane penetration depth (squares).

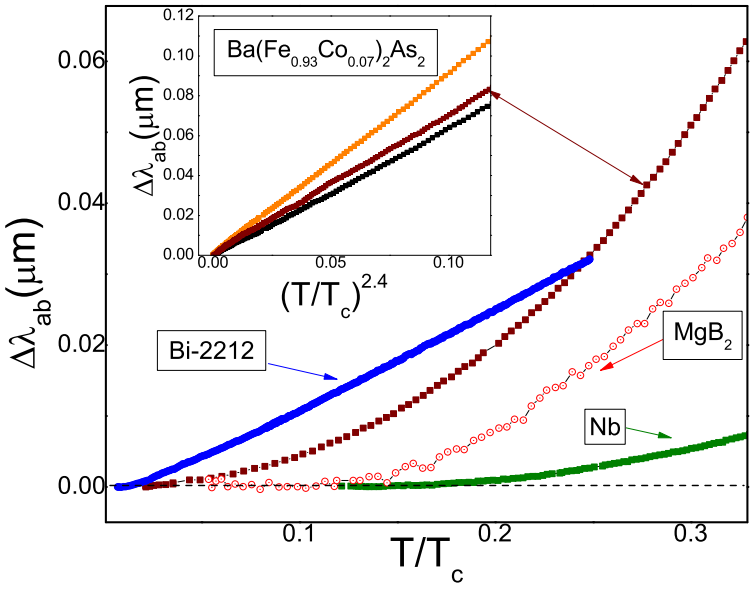

Figure 4.3 Comparison of the low temperature $\Delta\lambda_{ab}$(T) measured in $Ba(Fe_{0.93}Co_{0.07})_2As_2$ with known d-wave (Bi-2212), s-wave (Nb) and multi-gap s-wave (MgB_2) superconductors. Inset: $\Delta\lambda$ vs. $(T/T_c)^{2.4}$ for three different samples of $Ba(Fe_{0.93}Co_{0.07})_2As_2$ from different
batches.

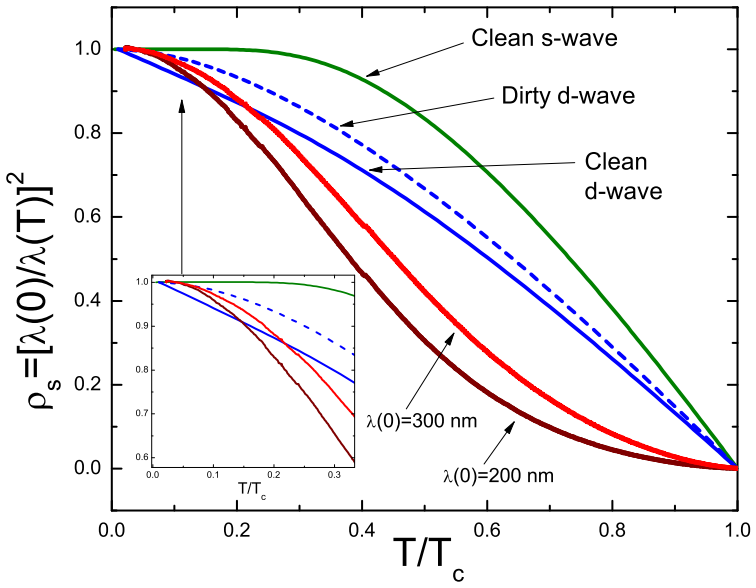

Figure 4.4 Superfluid density, ρ_s, as a function of normalized temperature for $Ba(Fe_{0.93}Co_{0.07})_2As_2$ using $\lambda(0) = 200$ nm and 300 nm. Also shown for comparison are calculated curves for clean s-wave, clean d-wave and dirty d-wave pairings.

for an s-wave superconductor in the dirty limit is $\rho_s(T) = \Delta(T)/\Delta(0)\tanh(\Delta(T)/2k_BT)$ [Tinkham (1996)].

The observed low-temperature behavior of the in-plane London penetration depth, $\lambda_{ab}(T)$, in $Ba(Fe_{0.93}Co_{0.07})_2As_2$ is clearly non-exponential, as can be observed in Fig. 4.3. The inset of Fig. 4.3 shows the data plotted as a function of $(T/T_c)^{2.4}$ for three samples at this doping level from different batches, all having unequal sizes and aspect ratios. The linear dependence shown in the inset indicates that the power law is close to 2.4 for each sample and the uncertainty in the penetration depth prefactor is reflected through the differences in the slopes of these curves. The bottom curve (orange triangles) corresponds to the smallest sample and therefore the smallest filling factor for the TDR coil, which explains why the data for that curve are noisier on average than the other two curves in the inset to Fig. 4.3.

The fitting function that was used to analyze the T-dependence of each $\Delta\lambda_{ab}$ curve had the general form of $\Delta\lambda_{ab}(T) = CT^n$. The low temperature end of the fitting interval was always fixed at the base temperature of the experiment, which corresponds to $T_{min}/T_c = 0.02$, and the fitting parameters C and n were determined by varying the high temperature end of the fitting interval up to as high as $T_{max}/T_c = 0.4$. This analysis has given values for the exponent n in the range of 2.15 to 2.42. To compare different curves, the maximum temperature of the fitting interval is always fixed at $T_c/3$. For these samples, this procedure yields $n = 2.4 \pm 0.1$, where the error reflects the scatter of the values of the exponents between different samples.

Fig. 4.4 shows $\rho_s(T)$ for one of the optimally doped $Ba(Fe_{0.93}Co_{0.07})_2As_2$ samples along with the known s-wave (clean case) and $d_{x^2-y^2}$-wave (both clean and dirty cases) calculated curves. The values of $\lambda(0)$ that were used to construct the $Ba(Fe_{0.93}Co_{0.07})_2As_2$ $\rho_s(T)$ curves shown in Fig. 4.4 are 200 nm and 300 nm. A value of $\lambda(0)$=208 nm was inferred from measurements of H_{c1}, obtained from M(H) loops taken using a Quantum Design (QD) magnetic property measurement system (MPMS). This was done by increasing the maximum field of the M(H) measurements until a non-linear region due to the penetration of vortices into the sample appeared to determine H_{c1} and by utilizing $H_{c1} = \Phi_0/[(4\pi\lambda^2)(ln(\lambda)/\xi + 0.05)]$ [Tinkham (1996)], with a value for the coherence length of ξ=2.76 nm at 6 K as measured by scanning

tunneling microscopy experiments [Yin et al. (2009)]. This value of $\lambda(0)$=208 nm is quite close to other reported measurements at the time [Luetkens et al. (2008); Drew et al. (2008)] and was before the $\lambda(0)$ values were measured in the $Ba(Fe_{1-x}Co_x)_2As_2$ series by using an aluminum coating procedure along with TDR frequency measurements [Gordon et al. (2010a)] that will be discussed later in this thesis, which also gave roughly 200±75 nm. The curve for $\lambda(0)$=300 nm produces $\rho_s(T)$ closer to the standard curves shown, but no value of $\lambda(0)$ can change the low-T dependence to an exponential one. The inset to Fig. 4.4 shows a zoomed-in view of the low-T region and clearly shows that the non-exponential behavior persists down to $\approx 0.02T_c$. At intermediate temperatures, the experimental $\rho_s(T)$ shows a significant departure from the $d_{x^2-y^2}$-wave and s-wave curves shown in the main panel of Fig. 4.4. Such behavior in $\rho_s(T)$ could be due to a significant anisotropy of the superconducting gap or multigap superconductivity.

Now let us turn to a discussion of the possible implications of the observed $\lambda \propto T^n$ dependence with $2.15 \leq n \leq 2.42$. If the upper temperature of the fitting interval is fixed at exactly $T_c/3$, then for these three samples it has been found that $n = 2.3$. For a BCS superconductor (single gap s-wave) in the clean limit and in the case where there are non-magnetic impurities, a power law fit to $\lambda(T)$ up to a maximum temperature of $T_c/3$ yields a value for the power of $n > 3$, which would correspond to the Nb data shown in Fig. 4.3. For a $d_{x^2-y^2}$-wave state, $n = 1$ in the clean case but for the dirty case the highest that can be found is $n = 2$. Point nodes can give $n = 2$, but probably the best explanation for the observed power law is a pair-breaking mechanism. For the clean case of the proposed $s_\pm$-wave state, an exponential T-dependence in the penetration depth is expected [Chubukov et al. (2008); Vorontsov et al. (2009); Mazin et al. (2008)], but non-magnetic impurity scattering for an $s_\pm$-wave OP acts as a pair-breaking mechanism, which we believe at this point is the best explanation for the observed power law behavior in the penetration depth.

Initially it was thought that the 1111 and 122 classes of the iron-based superconductors showed different temperature dependencies of the penetration depth, but later after a more careful analysis it was discovered that $\lambda(T)$ is likely to be qualitatively the same [Martin et al.

(2009b)]. The source of this initial confusion was a paramagnetic contribution to the measured penetration depth arising from the localized Nd ions in the lattice, which make a Curie-Weiss type of addition to the penetration depth. Both by accounting for this paramagnetism and by comparison to $\lambda(T)$ measurements of the non-magnetic La-1111 system, these suspicions were verified. After all, both classes share the Fe-As planes as key structural building blocks, electronic structure calculations have demonstrated that the states at the Fermi energy for both classes of compounds are dominated by the Fe-3d states and the resistivity values are similar for both classes. Therefore, the results discussed here will be examined with the premise that there is a common pairing mechanism and the same fundamental pairing symmetry in both classes of materials.

Previously, it has been argued that the inferred moderate anisotropy of the superconducting gap $\Delta(\phi)$ [Kondo et al. (2008); Prozorov et al. (2009b)] can be understood in terms of an OP that changes sign between Fermi surface sheets, which would be in line with the proposed $s_{\pm}$-wave superconducting gap Mazin et al. (2008) in which the OP passes through zero somewhere between the Γ and X points of the Brillouin zone [Chubukov et al. (2008)]. If the actual shape of the Fermi surface deviates much from being perfectly cylindrical, its equator may possibly reach the points where the OP changes sign and an accidental node is formed. This type of a node is not enforced by symmetry like in the cases of $d_{x^2-y^2}$-wave or p-wave superconductivity. Evidence for such accidental nodes has been found in recent measurements of the thermal conductivity [Reid et al. (2010)] in the $Ba(Fe_{1-x}Co_x)_2As_2$ series as a function of the doping level, x, and will be discussed in greater detail along with penetration depth measurements as a function of x later in this thesis.

To summarize this section, the low-temperature ($T < T_c/3$) in-plane London penetration depth, $\Delta\lambda_{ab} = \lambda_{ab}(T) - \lambda_{ab}(0)$, has been measured in three different single crystals of $Ba(Fe_{0.93}Co_{0.07})_2As_2$ and it has been found to exhibit a power law of the form $\Delta\lambda_{ab} \propto T^n$ with $n \approx 2.4 \pm 0.1$. This nonexponential behavior of $\Delta\lambda_{ab}(T)$ is indicative of the presence of normal state quasiparticles down to as low as $0.02T_c$, which could arise from either nodes in the superconducting gap function, $\Delta(\mathbf{k})$, or from some type of pair-breaking scattering mechanism,

which will be discussed in more detail later.

4.3 Doping dependence of $\Delta\lambda_{ab}(T)$ in the $Ba(Fe_{1-x}Co_x)_2As_2$ series

After the $\lambda_{ab}(T)$ measurements were performed on the three crystals near optimal doping in the $Ba(Fe_{1-x}Co_x)_2As_2$ series, a study was undertaken to determine the doping dependence of $\lambda_{ab}(T)$ in the same series [Gordon et al. (2009a)]. For this study of the concentration dependence, samples with doping levels of x=0.038, 0.047, 0.058, 0.074 and 0.10 were studied, which range from far underdoped to beyond optimal doping in this series, as can be seen in Fig. 4.5.

Microscopic, thermodynamic and transport measurements in the $Ba(Fe_{1-x}Co_x)_2As_2$ crystals used in this study have shown that superconductivity coexists with the orthorhombic phase in the underdoped regime of this particular system [Ni et al. (2008b); Pratt et al. (2009)]. Fig. 4.5 shows TDR frequency shifts as a function of temperature for scans running from below T_c to ≈120 K for two samples with x= 0.038 and 0.058. The data for the x=0.058 sample have been divided by a factor of 5 for clarity. In the normal state, the magnetic penetration depth is limited by the skin depth, which depends on the normal state resistivity. The overall variation of Δf through the transition region is about 20 Hz, which corresponds to a variation of about 45 nm in the skin depth. This should be compared to the 13300 Hz change corresponding to the superconducting transition of the sample. The temperature at which the structural transition, T_s, occurred was defined to be at the position of the minimum in $\Delta f(T)$, as illustrated in Fig. 4.5. The superconducting T_c was defined at the onset of the transition. Fig. 4.6 shows that by differentiating the TDR frequency shift data with respect to temperature, we are able to observed T_c, T_s and the magnetic transition, T_m, by using the same criteria used in [Pratt et al. (2009)]. Fig. 4.7 shows the *ac* susceptibility constructed from the TDR frequency shifts in $Ba(Fe_{1-x}Co_x)_2As_2$ for all measured concentrations. Optimal doping for this series occurs for a concentration between x=0.058 and 0.074.

The low-temperature variation of the penetration depth is examined in Fig. 4.8. For all superconducting samples, a power law T-dependence of the form $\Delta\lambda_{ab}(T) = CT^n$ has been

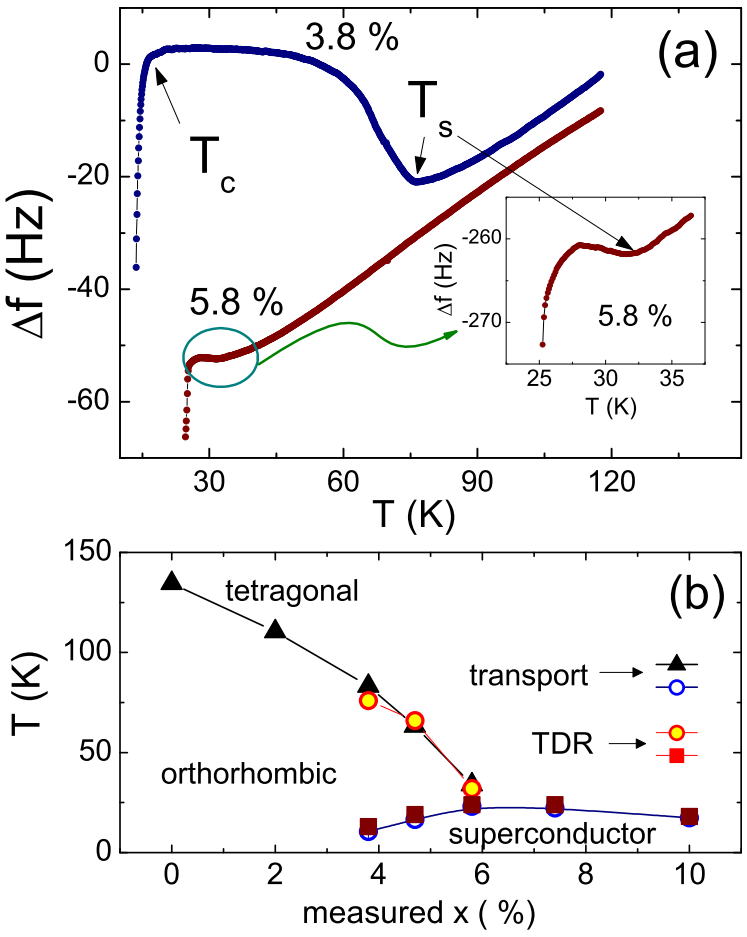

Figure 4.5 (a) Raw data for x=0.038 (underdoped) and x=0.058 (near optimal doping), where the data have been divided by a factor of five for the latter. The inset emphasizes the magnetic/structural transition for the sample with x=0.058. (b) Phase diagram showing the structural, T_s, and superconducting, T_c, transitions determined from transport [Ni et al. (2008b)] and TDR measurements.

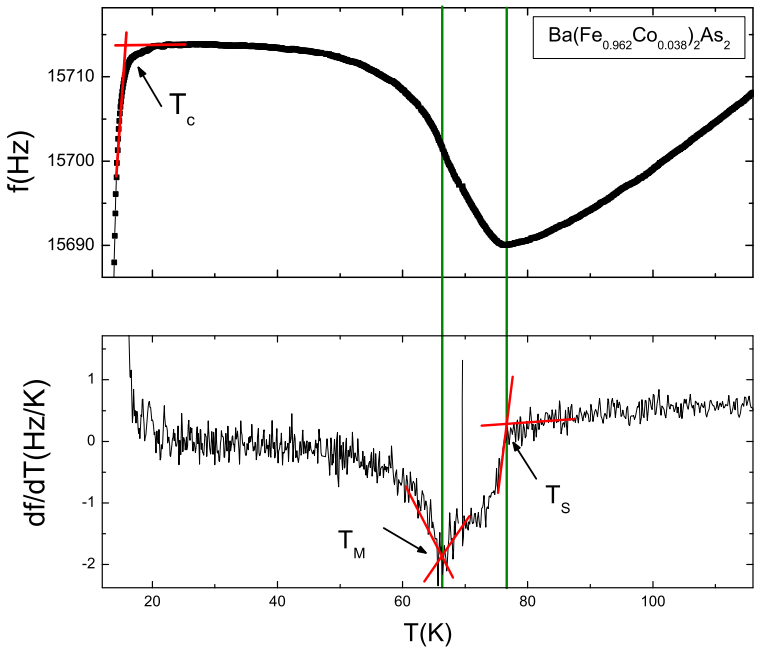

Figure 4.6 Top panel: raw frequency shift data for the x=0.038 sample shown in Fig. 4.5. Bottom panel: the derivative with respect to temperature shows that the TDR technique is able to detect the superconducting transition, T_c, the structural transition, T_s, and the magnetic transition, T_m, by using the same criteria outlined in [Pratt et al. (2009)].

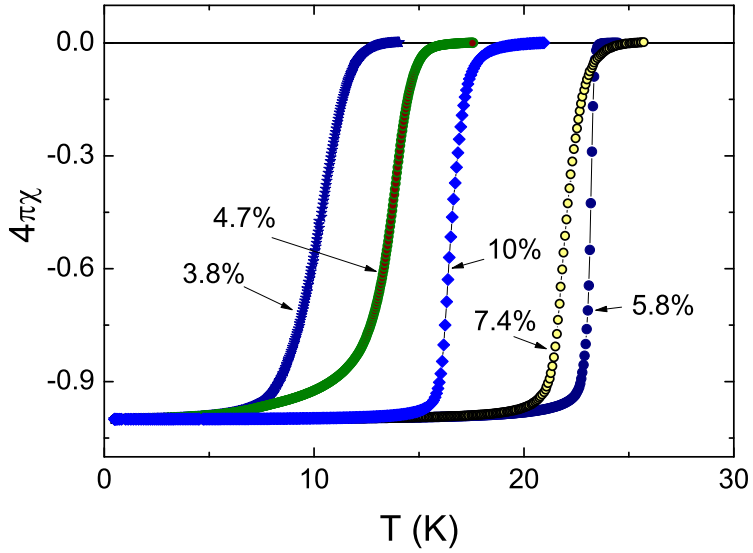

Figure 4.7 $4\pi\chi(T)$ constructed from TDR frequency shifts for $H_{ac}||c$-axis in single crystals of $Ba(Fe_{1-x}Co_x)_2As_2$ for different x.

observed. All of the fits to be discussed have been performed over the temperature range from the minimum temperature of the experiment up to $T_c/3$ unless stated otherwise. For these samples, it has been found that the power law exponent varies from $n = 2 \pm 0.1$ for underdoped samples to $n = 2.5 \pm 0.1$ for the overdoped samples. To examine how close the overall power law behavior is to quadratic, the fitting function $\Delta\lambda_{ab} = AT^2$ has been used to fit all data curves for these samples up to $T_c/3$, with A being the only free parameter. In Fig. 4.9, $\Delta\lambda_{ab}(T)$ has been scaled by the prefactor A and plotted as a function of reduced temperature squared, $(T/T_c)^2$. At a gross level, all samples follow the $\lambda_{ab}(T) \propto T^2$ dependence remarkably well.

To summarize the observed power law behavior, the upper panel of Fig. 4.10 shows the exponent n that was obtained from the best fit with two free parameters, $\Delta\lambda_{ab}(T) = CT^n$. The lower panel of Fig. 4.10 shows the doping dependencies of the prefactor C obtained by using the above fit, as well as the prefactor A, which was obtained by fitting to a function with purely quadratic behavior, $\Delta\lambda_{ab}(T) = AT^2$. There is a clear change of regime at $x \approx 0.06$ for n, C and A. One possible explanation for this change of regime below $x \approx 0.06$ could be some type of interaction between the itinerant antiferromagnetic and superconducting phases,

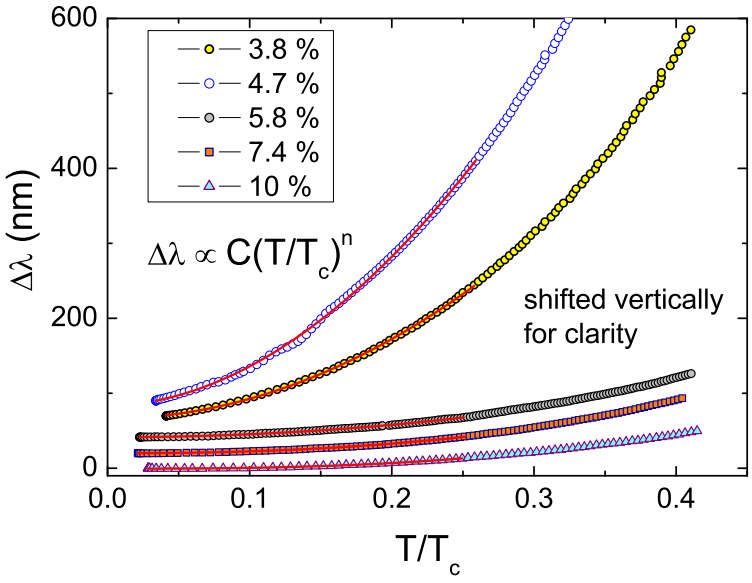

Figure 4.8 Low-temperature behavior of $\Delta\lambda_{ab}(T)$ for all studied concentrations. The solid lines are fits to $\Delta\lambda_{ab}(T) = C(T/T_c)^n$ with C and n as free parameters.

which have been shown to coexist homogeneously [Laplace et al. (2009); Ni et al. (2008b); Pratt et al. (2009); Gordon et al. (2010a)]. From Fig. 4.10, the upper panel shows that the power law exponent n changes from 2.0±0.1 to 2.5±0.1 as x changes from underdoped to overdoped concentrations, whereas the lower panel shows that from x=0.047 to 0.058, the prefactors suddenly drop by approximately one order of magnitude. The uncertainty of ±0.1 was determined from the difference in n obtained by measuring more than one sample with the same doping concentration.

In what follows, comments are given on the viability of various scenarios that could yield a power law behavior of $\lambda(T)$. If the impurity scattering rate in a superconductor is low and it is in the local limit, then anisotropic pairing with line or point nodes in the superconducting gap function give rise to a power law behavior in $\lambda(T)$, with $n = 1$ for line nodes and $n = 2$ for point nodes. Thus, the most direct interpretation of these results would be in terms of point nodes in the superconducting gap, as for example in $PrOs_4Sb_{12}$ [Einzel et al. (1986); Izawa et al. (2003)]. However, this conclusion would only make sense if these materials were

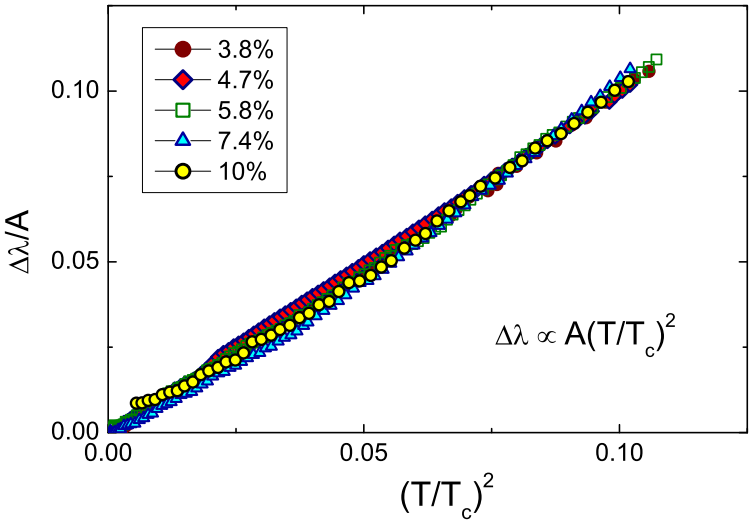

Figure 4.9 $\Delta\lambda_{ab}(T)$ scaled by the prefactor A, which was obtained from fits to the low-temperature region of the form $\Delta\lambda_{ab}(T) = A(T/T_c)^2$, plotted versus reduced temperature squared, $(T/T_c)^2$.

in the clean impurity scattering and local limits. A $\Delta\lambda_{ab}(T) \propto T^2$ dependence is consistent with line nodes in the gap if impurity scattering [Hirschfeld and Goldenfeld (1993)] is included or non-local corrections are made [Kosztin and Leggett (1997)]. In regard to the case of line nodes, unitary impurity scattering creates a state with a quadratic temperature dependence below some characteristic temperature T^*, such that $k_B T^* \propto \Gamma$, where Γ is the impurity scattering rate [Hirschfeld and Goldenfeld (1993)]. For these materials, the requirement would be $\Gamma \gtrsim k_B T_c/3$ since the power law dependence persists to such a high temperature, which would imply that the impurity scattering rate is high with a strong unitary component.

A power law temperature dependence of $\Delta\lambda$ could possibly be the result of strong impurity scattering in a superconductor that is fully gapped in the clean limit. The exponential behavior in the clean limit transforms to a quadratic one if the impurity scattering fills in the gap, causing a finite residual density of states for all energies [Abrikosov and Gor'kov (1960); Kogan (2009)]. As in Refs. [Chubukov et al. (2008); Parker et al. (2008)], such a power law dependence would require a scattering rate, Γ, on the order of the smallest gap, Δ_{min}, and a relatively fine balance between unitary and Born scattering. Another problem with this explanation is that there is

not a dependence of $\Delta\lambda(T)$ on the concentration of impurities, but rather an abrupt change of regime as the structural/magnetic region is crossed into Fig. 4.10.

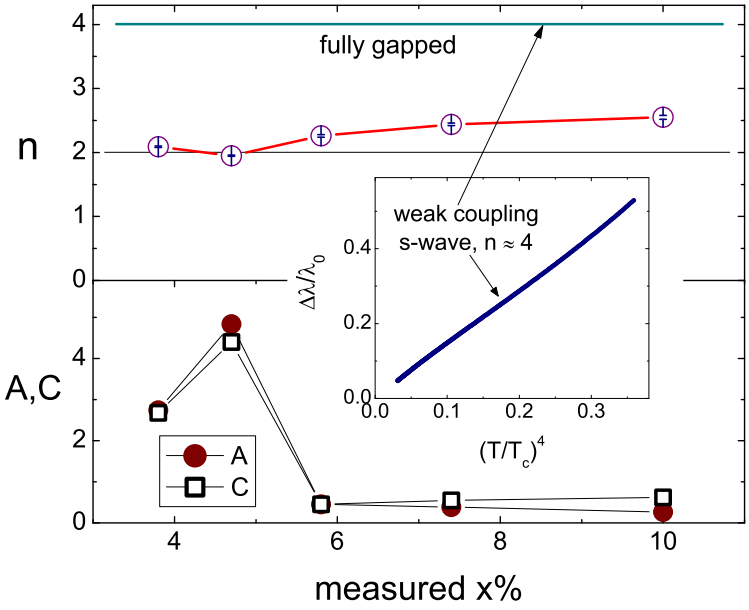

Figure 4.10 Doping dependence of the exponent n (upper panel) and of the fitting prefactors A and C, as defined in the text (lower panel). The inset shows that the expected exponential behavior for a single-gap BCS superconductor is well described by a power law function with exponent $n \approx 4$.

It should also be mentioned that another mechanism that can transform the linear temperature dependence of $\Delta\lambda(T)$ in the case of line nodes in the OP to a quadratic dependence for $T < T^* \simeq \Delta(0)\xi_0/\lambda(0)$ could be based on nonlocal effects [Kosztin and Leggett (1997)], where ξ_0 is the coherence length. In these materials, however, T^* would be less than 1 K.

The observed power law behavior in $\lambda(T)$ could also be a consequence of inhomogeneities in the materials. While the observation of a smearing of the jump in the heat capacity at T_c in under- and overdoped samples [Ni et al. (2008b)] may be considered a hint for such a scenario, the jump in C_p is doping dependent [Bud'ko et al. (2009)] and it is unlikely that any inhomogeneity can explain the universal behavior shown in Fig. 4.8 for all concentrations. Also, if these materials were homogeneous, it is unlikely that the Meissner screening would be

as homogeneous as has been observed [Prozorov et al. (2009a)].

In view of this discussion, it is tempting to search for an explanation on the phenomenological level that would not rely on impurity scattering as a crucial element changing the functional dependence of $\lambda(T)$. Indeed, any excitation coupled to electrons with an energy larger than $2\pi k_B T$ is pairbreaking, including regular phonons. Moreover, for an $s_{\pm}$-wave or a $d_{x^2-y^2}$-wave state, even phonons with arbitrarily small energies can be pairbreaking. The same reasoning holds for coupling to other bosonic modes, such as antiferromagnetic spin fluctuations. Since thermally excited bosons are needed for pairbreaking, the scattering rate, Γ, is temperature dependent [Abanov et al. (2001)]. In the case of line nodes, where a T-dependent Γ yields an exponent $n = 2$, strong scattering off of the thermally excited bosons would always yield a smaller exponent. Given the special role that may be played by the antiferromagnetic critical point, the possibility exists that the pairbreaking fluctuations are associated with an intermediate range dynamic ordering, like the dynamic domains speculated in Ref. [Mazin and Johannes (2009)]. These will have very small energies and a potential to be strong scatterers. A clear derivation of the exponent n that results from such a picture is still missing.

To summarize, the temperature dependence of the in-plane London penetration depth, $\Delta\lambda_{ab}(T)$, has been measured in single crystals of $Ba(Fe_{1-x}Co_x)_2As_2$ for concentrations of x=0.038, 0.047, 0.058, 0.074 and 0.1, which range from the underdoped to overdoped regimes. A robust power law for all measured dopings of the form $\Delta\lambda_{ab}(T) \propto T^n$ has been observed, with n ranging from ≈ 2 for underdoped sample to ≈ 2.5 in overdoped samples. The penetration depth prefactors C and A, determined from low temperature fits to the functions $\Delta\lambda_{ab}(T) = CT^n$ and $\Delta\lambda_{ab}(T) = AT^2$, have been observed to increase by as much as an order of magnitude when passing into the region of the doping phase diagram where superconductivity and antiferromagnetism likely coexist.

It should be noted that the power law temperature dependence that has been observed in the $Ba(Fe_{1-x}Co_x)_2As_2$ series was later confirmed by at least two different measurement techniques, one of which was a surface probe method using a magnetic force microscope Luan et al. (2010) and the other was a microwave cavity resonator technique Bobowski et al. (2010).

4.4 Doping dependence of $\Delta\lambda_{ab}(T)$ and $\Delta\lambda_c(T)$ in the $Ba(Fe_{1-x}Ni_x)_2As_2$ series

The doping dependence of the variation with temperature of both the in-plane, $\Delta\lambda_{ab}$, as well as the out-of-plane, $\Delta\lambda_c$, London penetration depth components have been measured for several concentrations, x, in single crystals of the electron doped $Ba(Fe_{1-x}Ni_x)_2As_2$ material spanning the superconducting region of the doping phase diagram [Martin et al. (2010a)]. The measured concentrations had WDS values of x=0.033, 0.046, 0.054, 0.065 and 0.072. Since each Ni atom contributes two electrons to the charge environment, half as much is needed to completely suppress superconductivity than in the $Ba(Fe_{1-x}Co_x)_2As_2$ system, meaning that the Ni doped compounds should be less disordered

The single crystals of the $Ba(Fe_{1-x}Ni_x)_2As_2$ samples were all grown using the same procedure used in Ref. [Canfield et al. (2009)]. Each sample was prescreened before the penetration depth measurements to ensure that the superconducting transition widths were as sharp as possible, as seen in the inset of Fig. 4.11 (a). The overall quality of the samples studied was determined by using x-ray diffraction, resistivity, magnetization, magneto-optics and WDS analysis. The Ni content was found to have a small variation within each of the samples tested.

The temperature versus doping phase diagram for the $Ba(Fe_{1-x}Ni_x)_2As_2$ series is shown in the main panel of Fig. 4.11 (a) and the superconducting transitions for each of the samples from this study are visible from the $\Delta\lambda_{ab}(T)$ curves shown in the inset. The location of T_{sm} shows roughly where the structural and magnetic transitions are and were taken from resistivity data [Ni et al. (2010b)]. The low-temperature region, $T_{min} < T < T_c/3$, of each $\Delta\lambda_{ab}(T)$ curve was fit to a function of the form $\Delta\lambda_{ab}(T) = CT^n$ in order to extract the power law exponent n to study its evolution with the doping level, x. The low-temperature region of $\Delta\lambda_{ab}(T)$ is shown as a function of $(T/T_c)^2$ for all samples in Fig. 4.11 (b) and the fact that these curves are very close to being linear on this scale indicates that the power law exponent n is close to 2 over this range for these samples. The exact value of n obtained from the fits is shown as a function of the Ni doping level in the inset to Fig. 4.11 (b), where it has values from $\approx$2.3 for x=0.033

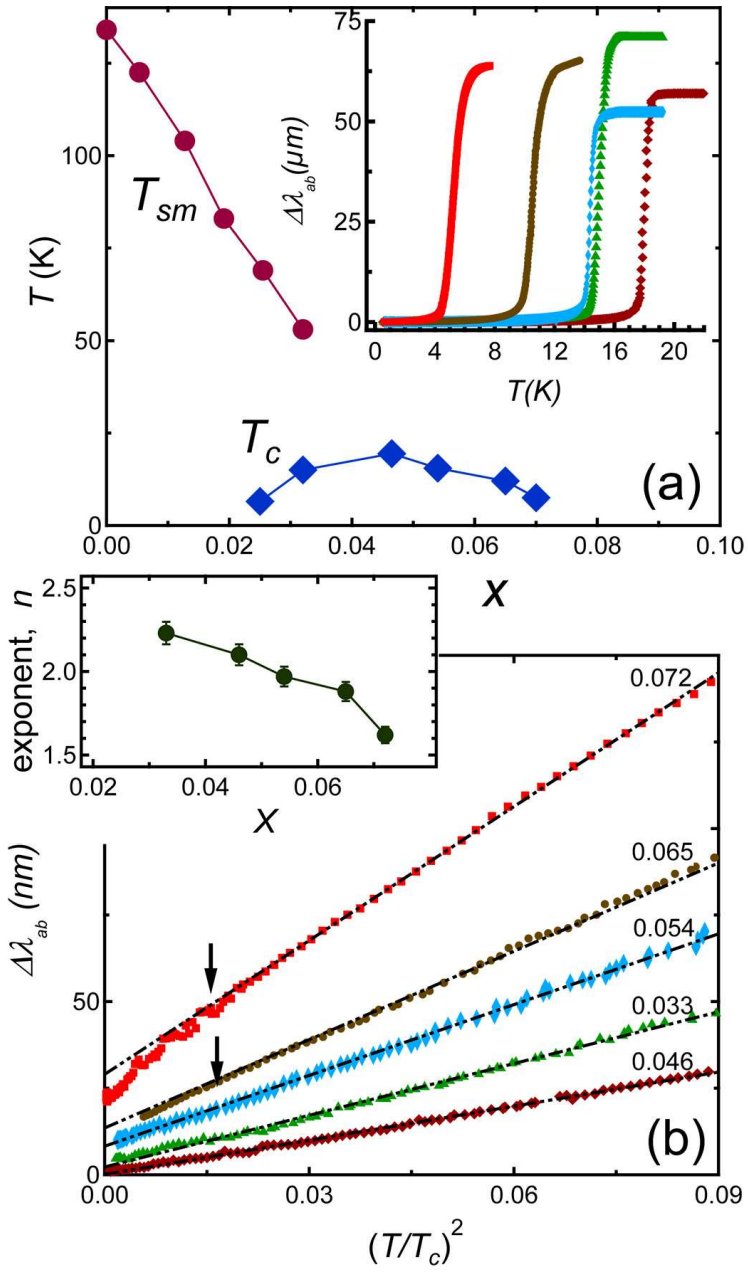

Figure 4.11 (a) Temperature-doping phase diagram for $Ba(Fe_{1-x}Ni_x)_2As_2$. The inset shows the full superconducting transition determined from in-plane penetration depth measurements. (b) $\Delta\lambda_{ab}(T)$ for different doping levels plotted versus $(T/T_c)^2$, where the curves are shifted vertically for clarity. The inset shows the doping dependence of the power law exponent n obtained from fits described in the text.

(underdoped) to ≈1.6 for x=0.072 (overdoped).

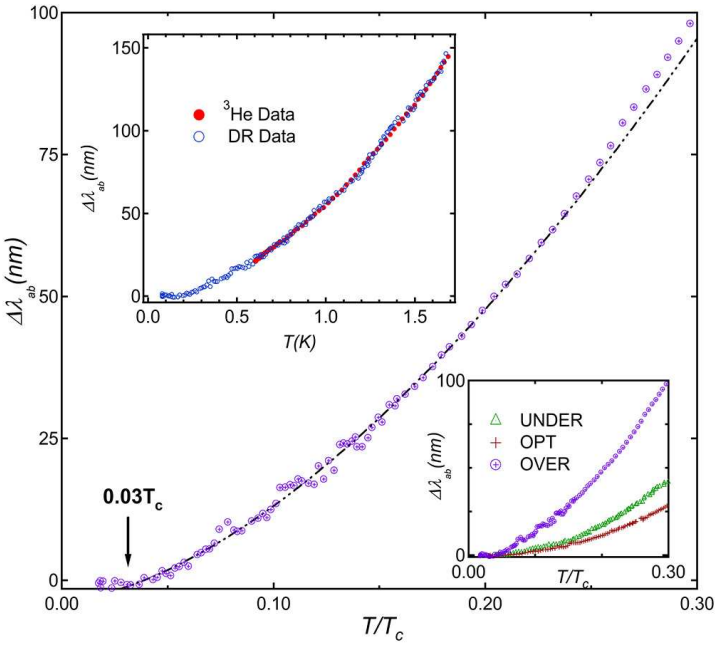

Figure 4.12 The main panel shows $\Delta\lambda_{ab}(T)$ for an overdoped sample with x=0.072 measured down to $T \approx 60$ mK in a dilution refrigerator. The upper inset shows the agreement between $\Delta\lambda_{ab}(T)$ for the same sample but with different TDR circuits, with one mounted in a ^3He cryostat and the other in a dilution refrigerator. The lower inset shows that the power law behavior in $\Delta\lambda_{ab}(T)$ persists down to 60 mK for underdoped, optimally doped and overdoped samples of $Ba(Fe_{1-x}Ni_x)_2As_2$.

To examine how far down in temperature the power law behavior persists in $\Delta\lambda_{ab}(T)$, three samples having x=0.033 (underdoped, T_c=15 K), 0.046 (optimally doped, T_c=19.4 K) and 0.072 (overdoped, T_c=7.5 K) were measured down to a temperature of $T_{min} \approx 60$ mK by using a TDR mounted inside of a dilution refrigerator. The main panel of Fig. 4.12 shows that the power law behavior persists in $\Delta\lambda_{ab}(T)$ for the overdoped sample down to $T < 0.03T_c$. Also shown in the main frame is a fit to the function $\Delta\lambda_{ab}(T) = CT^n$ (dashed line), which gives n=1.62. The upper inset to Fig. 4.12 shows very good agreement between $\Delta\lambda_{ab}(T)$ data taken with two different circuits, one in a ^3He cryostat and the other in a dilution refrigerator, for

the same sample. The lower inset to Fig. 4.12 shows that the power law behavior in $\Delta\lambda_{ab}(T)$ persists down to $T \approx$60 mK for all three samples measured in the dilution refrigerator.

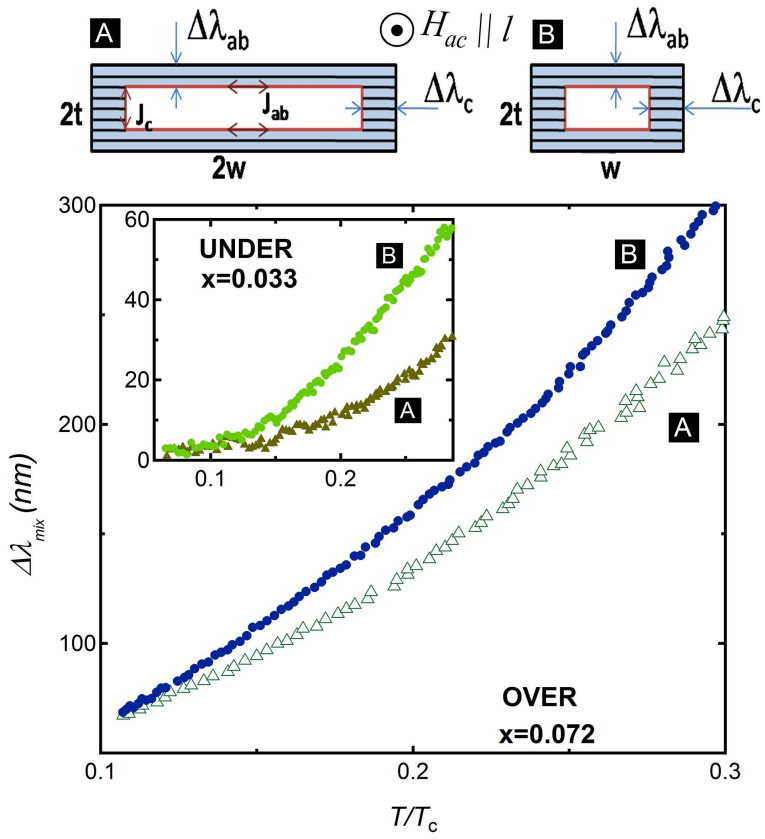

Figure 4.13 Main panel: $\Delta\lambda_{mix}$ obtained from measurements with $H_{ac}||l$ for an overdoped sample with x=0.072 and T_c=7.5 K before (A) and after (B) the sample was cut so that $2w \rightarrow w$. Inset: $\Delta\lambda_{mix}$ for an underdoped sample with x=0.033 and T_c= 15 K before (A) and after (B) cutting. Above: Schematics of the magnetic field penetration into the sample for H_{ac} applied along l before (A) and after (B) it is cut.

In addition to measuring the in-plane component of the penetration depth, $\Delta\lambda_{ab}(T)$, the out-of-plane component, $\Delta\lambda_c(T)$, has also been measured for three different $Ba(Fe_{1-x}Ni_x)_2As_2$ samples: one with x=0.033 (underdoped) and two having x=0.072 (overdoped). The following is a brief description of how $\Delta\lambda_c(T)$ was extracted from the TDR measurements.

Let us consider a plate-like sample having a rectangular cross section and dimensions $2t$

(thickness) x $2w$ (width) x l (length), with $l > 2w$. For the iron-based superconductors studied here, the c-axis of all samples points perpendicular to their largest flat face. The temperature dependence of the variation of the in-plane penetration depth, which arises only from supercurrents flowing in the ab-plane, is constructed from the TDR frequency shifts, $\Delta f_{ab}(T)$, by using the relation

$$\Delta f_{ab}(T) = \Big(\frac{\Delta f_{pullout}}{R_{eff}}\Big)\Delta\lambda_{ab}(T), \tag{4.1}$$

where R_{eff} is an effective radius for the sample constructed from its dimensions and $\Delta f_{pullout}$ is the shift in the TDR resonance frequency measured by extracting the sample from the primary coil at the base temperature of the experiment. This situation corresponds to the case where H_{ac} is aligned parallel to the c-axis of the sample, with H_{ac} being the excitation field generated in the TDR primary coil. If H_{ac} is oriented perpendicular to the c-axis, then not only in-plane supercurrents are excited, but out-of-plane supercurrents as well. For this case, the TDR frequency shifts, Δf_{mix}, contain components from $\Delta\lambda_{ab}$ as well as $\Delta\lambda_c$. More specifically,

$$\Delta f_{mix}(T) = \Big(\frac{G_{ab}}{2t}\Big)\Delta\lambda_{ab}(T) + \Big(\frac{G_c}{2w}\Big)\Delta\lambda_c(T) \tag{4.2}$$

with G_{ab} and G_c being geometrical calibration factors constructed from the sample dimensions. By only performing a single measurement with H_{ac} perpendicular to the c-axis, it is often impossible to extract $\Delta\lambda_c(T)$ from Eqn. 4.2 since for most samples $2t << 2w$ and hence the contribution to $\Delta f_{mix}(T)$ from $\Delta\lambda_c(T)$ is very weak. However, by measuring the sample once with $H_{ac}||l$ and then cutting it so that $2w \rightarrow w$ and all other dimensions remaining the same, $\Delta\lambda_c(T)$ can be obtained. After the cutting procedure, the TDR frequency shifts, $\Delta f^{cut}_{mix}(T)$, are given by

$$\Delta f^{cut}_{mix}(T) = \Big(\frac{G_{ab}}{2t}\Big)\Delta\lambda_{ab}(T) + \Big(\frac{G_c}{w}\Big)\Delta\lambda_c(T). \tag{4.3}$$

By subtracting Eqn. 4.2 from Eqn. 4.3, the difference of the frequencies allows one to access only the out-of-plane component of the penetration depth:

$$\Delta f_{mix}^{cut}(T) - \Delta f_{mix}(T) = \Big(\frac{G_c}{2w}\Big)\Delta\lambda_c(T). \tag{4.4}$$

The main panel of Fig. 4.13 shows the measured penetration depth, $\Delta\lambda_{mix} \propto \Delta f_{mix}$, for H_{ac} applied perpendicular to the c-axis along the longest sample side, l, both before (A) and after (B) an overdoped sample with x=0.072 (T_c=7.5 K) was cut so that $2w \rightarrow w$. The inset shows the same comparison for measurements before and after cutting for an underoped sample with x=0.033 (T_c=15 K). The schematics shown above the main panel of Fig. 4.13 are to help clarify the field orientation with respect to the crystal axes and show the contributions from $\Delta\lambda_{ab}$ and $\Delta\lambda_c$ to Δf_{mix} both before (A) and after (B) a sample is cut for these measurements. Notice that for both samples shown in Fig. 4.13, there is a clear change in $\Delta\lambda_{mix}$ after the sample is cut, indicating that the $\Delta\lambda_c$ contribution is strengthened after the cutting procedure.

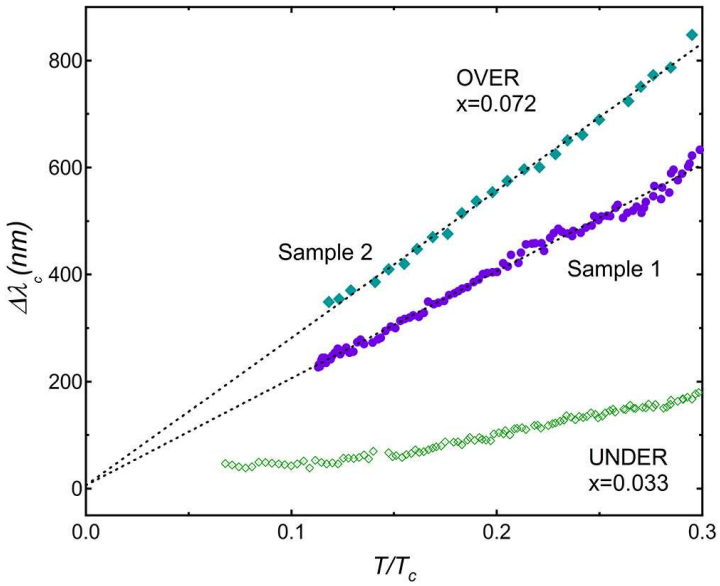

Figure 4.14 The c-axis component of the penetration depth, $\Delta\lambda_c$, plotted versus reduced temperature, T/T_c, for three different $Ba(Fe_{1-x}Ni_x)_2As_2$ samples. Two of them are overdoped with x=0.072 and one of them is underdoped with x=0.033.

By using the $\Delta f_{mix}(T)$ and $\Delta f_{mix}^{cut}(T)$ data obtained with $H_{ac}||l$ along with Eqn. 4.4, $\Delta\lambda_c(T)$ has been constructed for three different samples: one with x=0.033 and T_c=15 K (un-

derdoped) and two different samples with x=0.072 and T_c=7.5 K and 6.5 K (both overdoped). The resulting $\Delta\lambda_c(T)$ curves are shown in Fig. 4.14 for these samples. The two overdoped samples shown clearly exhibit a linear variation in $\Delta\lambda_c$ with temperature up to $T_c/3$, which strongly suggests the presence of line nodes in the superconducting gap on portions of the Fermi surface which contribute to c-axis conduction, consistent with the findings of thermal conductivity measurements for different dopings in the $Ba(Fe_{1-x}Co_x)_2As_2$ series for concentrations close to the edges of the superconducting dome of the temperature-doping phase diagram [Reid et al. (2010)].

To summarize, $\Delta\lambda_{ab}(T)$ has been measured for five different samples from the $Ba(Fe_{1-x}Ni_x)_2As_2$ series with doping levels ranging from x=0.033 (underdoped) to x=0.072 (overdoped). It has been found to exhibit a power law temperature dependence for all measured concentrations, where the power law decreases from $n \approx 2.3$ at x=0.033 to $n \approx 1.6$ at x=0.072. This doping dependence of n is different from what has been measured in the $Ba(Fe_{1-x}Co_x)_2As_2$ series, where it n has been found to increase from $\approx$2 for underdoped samples and increases to $\approx$2.5 beyond optimal doping. A possible explanation for the power law temperature dependence indicates that it arises from disorder effects, which will be elaborated on in more detail later in this thesis. In addition, the out of plane component, $\Delta\lambda_c(T)$, has been measured for two overdoped concentrations, both with x=0.072, and one underdoped concentration with x=0.033. For these samples near the edges of the superconducting dome, $\Delta\lambda_c$ has been found to have a linear temperature dependence, in agreement with the existence of line nodes in the superconducting gap of $Ba(Fe_{1-x}Ni_x)_2As_2$ on portions of the Fermi surface responsible for c-axis conduction.

4.5 $\Delta\lambda_{ab}(T)$ in $Ba(Fe_{1-x}T_x)_2As_2$ (T=Ru,Rh,Pd,Pt,Co+Cu)

The variation of the in-plane London penetration depth, $\Delta\lambda_{ab}$, has been measured as a function of temperature for various dopings in single crystals of $Ba(Fe_{1-x}T_x)_2As_2$ (T=Ru,Rh,Pd,Pt,Co+Cu). All samples show a non-exponential penetration depth, or more precisely a power law temperature dependence of the form $\Delta\lambda_{ab}(T) \propto T^n$, where n has been

found to be as small as ≈1.5 and as large as ≈2.5 for these samples. A collection of measurements such as this allows for one to study the effects of transition metal substitution for Fe on the superconducting properties of doped $BaFe_2As_2$. All of the samples for which data are shown in this section were obtained from the same source as in Ref. [Ni et al. (2008b)] with the exception of the $Ba(Fe_{1-x}Pt_x)_2As_2$, which came from the laboratory of Prof. H. H. Wen at the National Laboratory for Superconductivity, Institute of Physics and National Laboratory for Condensed Matter Physics, People's Republic of China.

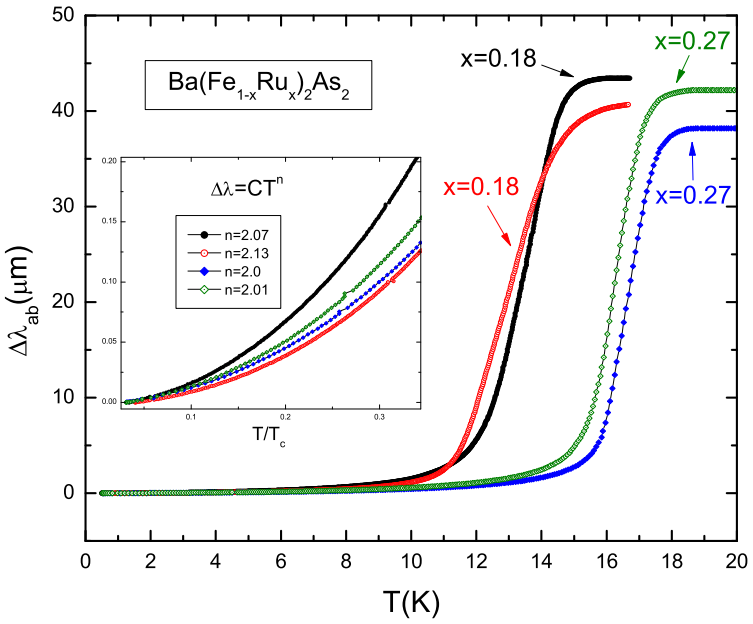

Figure 4.15 Main frame: the full superconducting transitions from the in-plane penetration depth for four $Ba(Fe_{1-x}Ru_x)_2As_2$ samples, two with x=0.18 and the other two have x=0.27. Inset: The low temperature region of the in-plane penetration depth for the same four samples. The legend shows the resulting power law exponent values for these samples.

The first material to be discussed is $Ba(Fe_{1-x}Ru_x)_2As_2$. Ru is an isovalent substitution for Fe, meaning that it nominally donates no extra electrons to the system. A temperature-doping phase diagram for this material can be seen in Fig. 1.1. The in-plane penetration depth was measured in four different samples, two with x=0.18 and the other two with x=0.27. The

in-plane penetration depth data can be seen from Fig. 4.15, where the inset shows a zoomed-in view of the low-temperature region. By fitting this region of the data for each sample to a power law function it has been determined that the power laws are n=2.13 and 2.07 for the x=0.18 samples and n=2.0 and 2.01 for the samples with x=0.27.

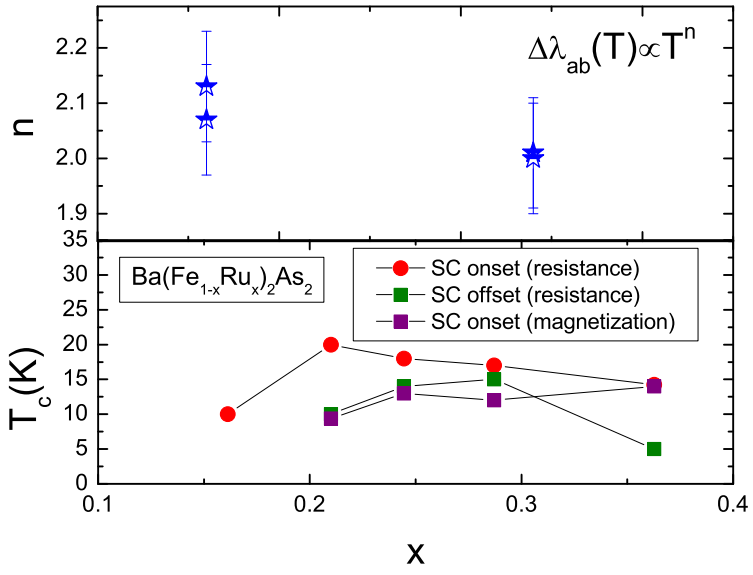

Figure 4.16 Top panel: power law exponent values, n, from low-T in-plane penetration depth fits plotted versus doping concentration, x, in the $Ba(Fe_{1-x}Ru_x)_2As_2$ series. Bottom panel: T_c versus x in the same series obtained from electrical resistivity data [Thaler et al. (2010)].

Fig. 4.17 shows the variation of the in-plane penetration depth for two $Ba(Fe_{1-x}Rh_x)_2As_2$ samples, x=0.057 and x=0.010, where the inset shows the low-temperature region along with the power law fits, which yielded n=2.5 and n=2.01. The superconducting portion of the phase diagram can be seen along with the resulting power law exponents in Fig. 4.18. The substitution of Rh for Fe donates the same number of carriers as the substitution of Co for Fe.

Two different samples, both overdoped with concentrations of x=0.053 (T_c ≈14 K) and x=0.067 (T_c ≈9 K), have been measured from the $Ba(Fe_{1-x}Pd_x)_2As_2$ series and can be seen in Fig. 4.19. The substitution of Pd for Fe donates the same number of electrons as the

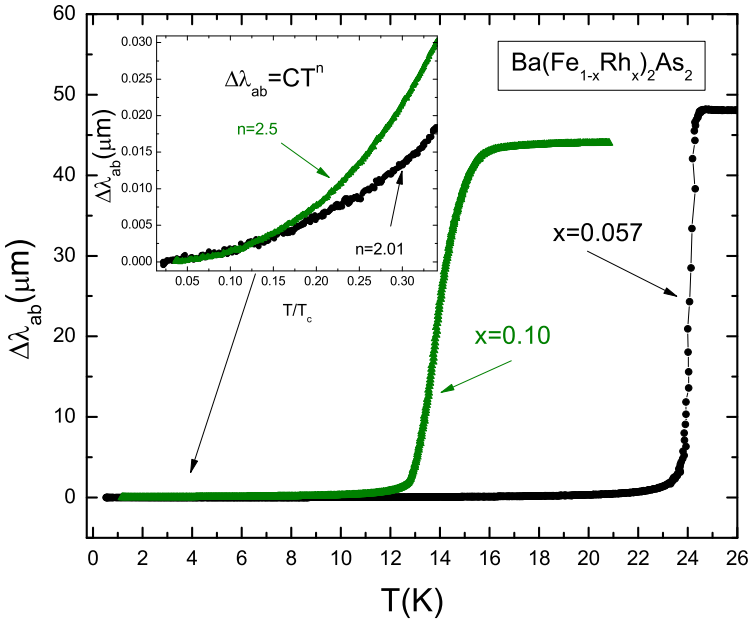

Figure 4.17 Main frame: the full superconducting transitions from the in-plane penetration depth for two $Ba(Fe_{1-x}Rh_x)_2As_2$ samples having x=0.057 and x=0.10. Inset: The low temperature region of the in-plane penetration depth for both samples along with the determined power law exponents.

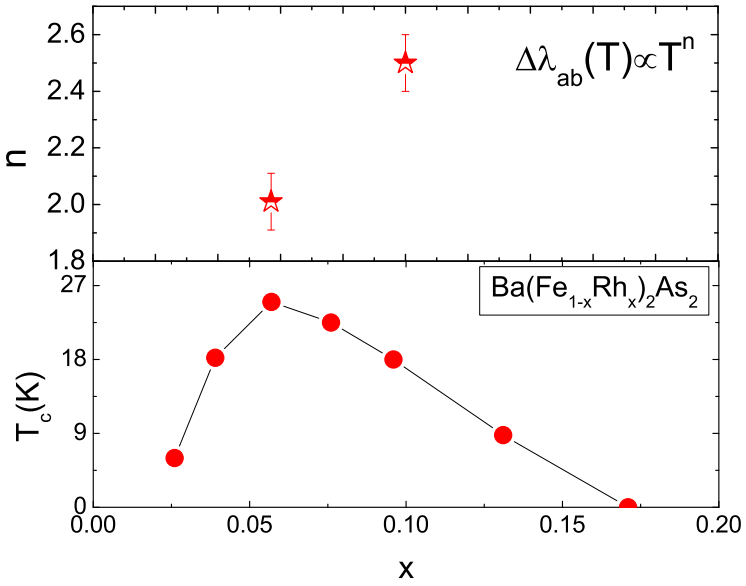

Figure 4.18 Top panel: power law exponent values, n, from low-T in-plane penetration depth fits plotted versus doping concentration, x, in the
$Ba(Fe_{1-x}Rh_x)_2As_2$ series. Bottom panel: T_c versus x in the same series obtained from electrical resistivity data [Ni et al. (2010a)]

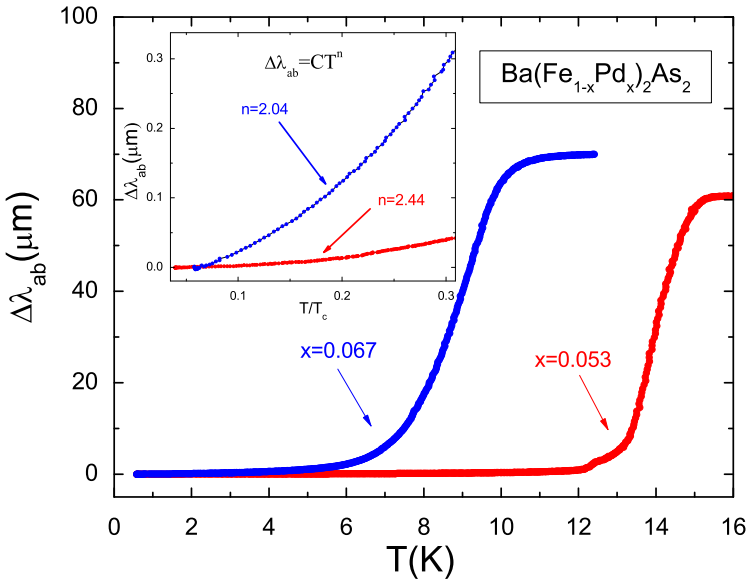

Figure 4.19 The main frame shows the superconducting transitions through $\Delta\lambda_{ab}(T)$ of two different Pd doped samples having x=0.053 (near optimal doping) and x=0.067 (overdoped). The inset shows a zoomed-in view of the low-temperature region of $\Delta\lambda_{ab}$ versus T/T_c for both samples.

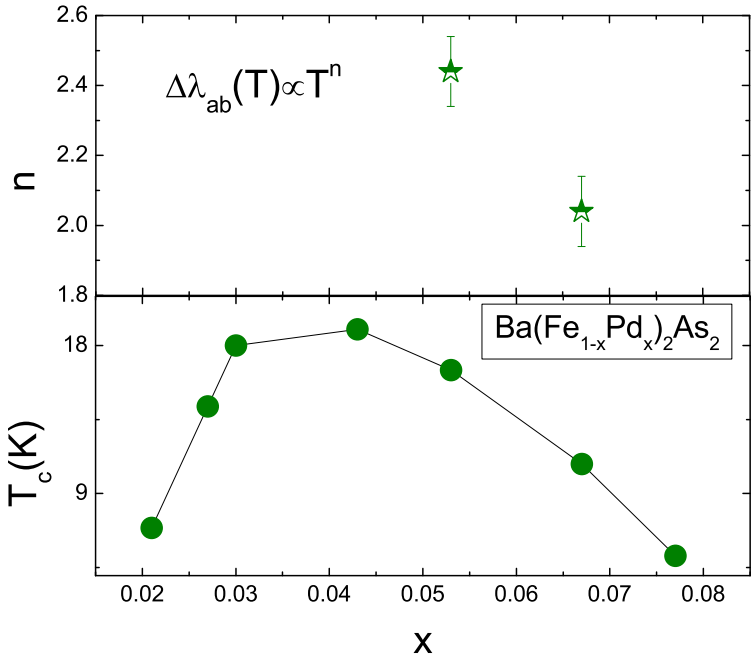

Figure 4.20 Top panel: power law exponent values, n, from low-T in-plane penetration depth fits plotted versus doping concentration, x, in the
$Ba(Fe_{1-x}Pd_x)_2As_2$ series. Bottom panel: T_c versus x in the same series obtained from electrical resistivity data [Ni et al. (2010a)]

substitution of Ni for Fe, but with a larger ionic radius. Fig. 4.19 shows the superconducting transitions of both samples measured in the main frame and the inset shows the power law fit of the form $\Delta\lambda_{ab} = CT^n$ that was used to extract the value of n. The superconducting portion of the phase diagram is shown in Fig. 4.20 along with the doping dependent power law exponent values.

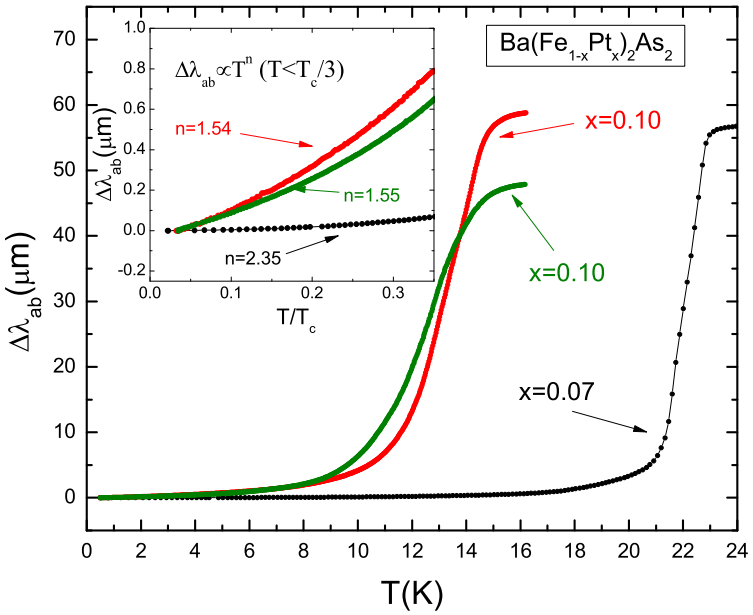

Figure 4.21 The main frame shows $\Delta\lambda_{ab}(T)$ for three different Pt doped samples, with the black curve being near optimal doping and the red and green curves both being overdoped concentrations. The inset shows a zoomed-in view of the low-temperature region of $\Delta\lambda_{ab}$ plotted versus the reduced temperature T/T_c.

Yet another isovalent substitution for Ni exists, with that being the substitution of Pt for Fe, which has an even larger ionic radius than Pd. The in-plane penetration depth of three different Pt doped samples has been measured, where one was near optimal doping (x=0.07 with T_c=23 K) and two of them were overdoped (x=0.10 with T_c=14 K) samples. The main frame of Fig. 4.21 shows the superconducting transitions of all three samples through the penetration depth and the inset shows the low-temperature region along with the power law exponents obtained from fits to $\Delta\lambda_{ab}(T) = CT^n$. Unfortunately, at the present time a phase

diagram for this material was not available to be shown.

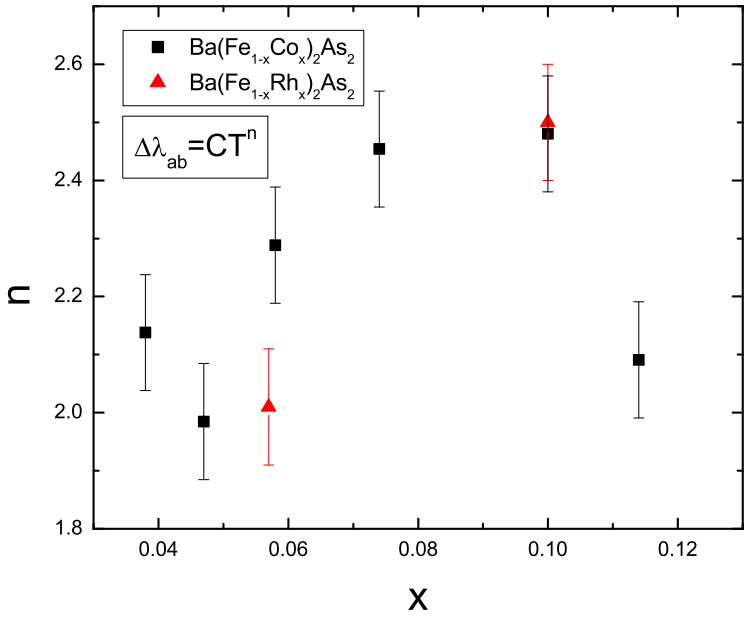

Figure 4.22 Comparison of the power law exponent versus doping level for the $Ba(Fe_{1-x}Co_x)_2As_2$ and $Ba(Fe_{1-x}Rh_x)_2As_2$ series, where Co and Rh are nominally isovalent substitutions for Fe.

By comparing the doping dependence of the power law exponent from the $Ba(Fe_{1-x}Co_x)_2As_2$ an $Ba(Fe_{1-x}Rh_x)_2As_2$ series, as shown in Fig. 4.22, we can see that there is some agreement. The substitution of Co or Rh for Fe are nominally isovalent ones, so it is natural to search for similarities between the two series. In fact, it is worth noting that these are the only two 122 systems reported here that do not show a decrease of n with increasing x.

Also, a plot of n versus x is shown to compare the $Ba(Fe_{1-x}Ni_x)_2As_2$ and $Ba(Fe_{1-x}Pd_x)_2As_2$ compounds in Fig. 4.23, with Ni and Pd being nominally isovalent substitutions for Fe. For these two materials, n decreases with increasing doping level, as it does for several of the other transition metal doped $BaFe_2As_2$ superconductors reported here. Also shown is a global phase diagram in Fig. 4.24 of the power law exponent versus the electron count, e, for the $Ba(Fe_{1-x}T_x)_2As_2$ (T=Co,Rh,Ni,Pd) superconductors. Although there are no immediate visible trends, it is worth noting such a comparison.

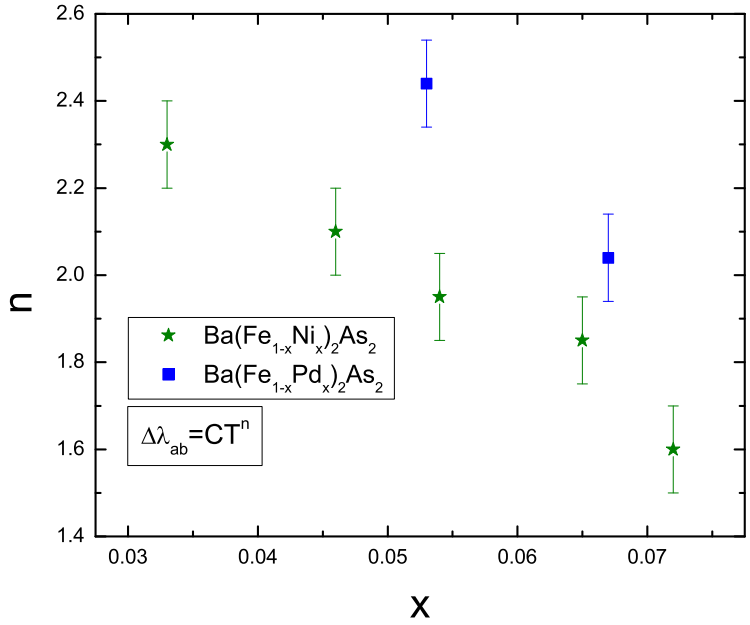

Figure 4.23 Comparison of the power law exponent versus doping level for the $Ba(Fe_{1-x}Ni_x)_2As_2$ and $Ba(Fe_{1-x}Pd_x)_2As_2$ series, where Ni and Pd are nominally isovalent substitutions for Fe.

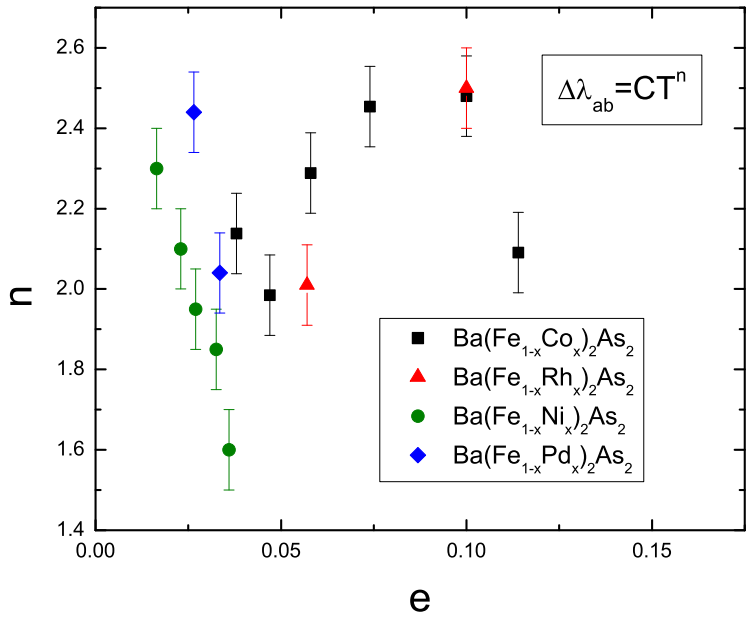

Figure 4.24 The power law exponent plotted versus e, which is the electron count, for the $Ba(Fe_{1-x}T_x)_2As_2$ (T=Co,Rh,Ni,Pd) series.

The last series for which data will be shown in this section is $Ba(Fe_{1-x-y}Co_xCu_y)_2As_2$. The in-plane penetration depth has been measured for two samples, one with x=0.02 and y=0.026 (T_c=11 K) and another with x=0.02 and y=0.033 (T_c=9 K). The full superconducting transitions are shown for these samples through the penetration depth in Fig. 4.25. The inset of this figure shows the low-T region along with the power law exponent values for each sample obtained from fitting. Doping with Cu alone in this series does not produce superconductivity for any concentration, but by also including Co superconductivity can be induced. By fixing the Co concentration at x=0.02 and increasing the Cu concentration y from 0.026 to 0.033, the power law exponent decreases from n=2.04 to 1.91.

A power law temperature dependence of the penetration implies the existence of low-temperature normal state quasiparticles, which can arise either from nodes in the superconducting gap or from pair-breaking impurity scattering mechanisms. A doping dependent power law exponent would be consistent either with a doping dependent modulation of the superconducting gap or from a pair-breaking impurity scattering mechanism that evolves

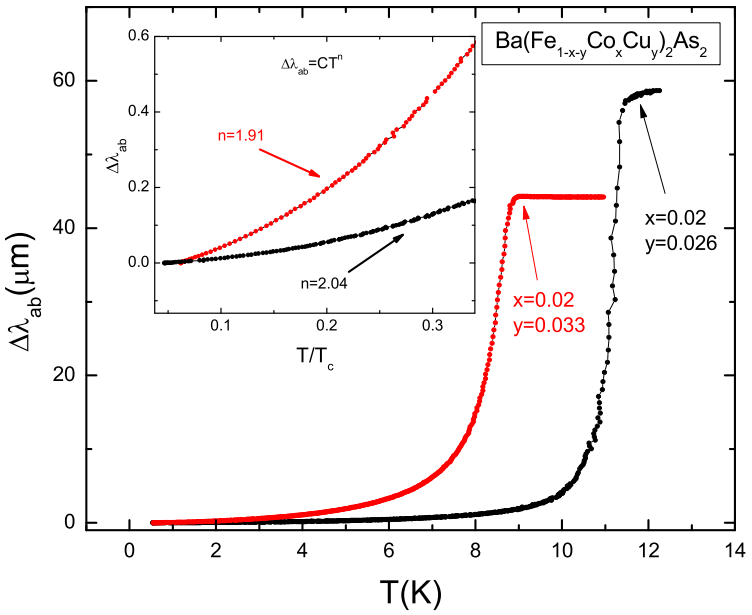

Figure 4.25 The main frame shows the superconducting transitions through $\Delta\lambda_{ab}(T)$ for two samples that are doped with both Co and Cu, but with different concentrations of Cu. The inset shows a zoomed-in view of $\Delta\lambda_{ab}$ versus T/T_c in the low-temperature regions for both samples

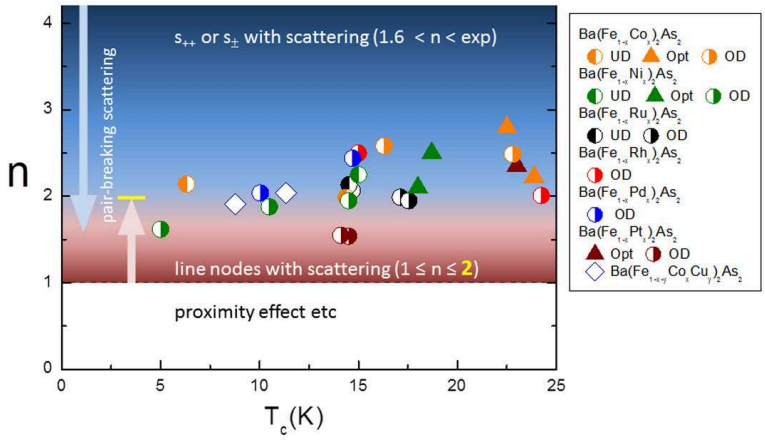

Figure 4.26 All power law exponent values, n, obtained from in–plane penetration depth measurements in $Ba(Fe_{1-x}T_x)_2As_2$ (T=Co,Ni,Ru,Rh,Pd,Pt,Co+Cu). The background colors indicate the ranges that n can have for different scenarios, including impurity scattering within the $s_{\pm}$-, s_{++}- and d-wave superconducting gap symmetries.

with the level of impurities in the material. Fig. 4.26 shows all of the resulting power law values obtained from the in-plane penetration depth measurements of $Ba(Fe_{1-x}T_x)_2As_2$ (T=Co,Ni,Ru,Rh,Pd,Pt,Co+Cu) plotted versus T_c. Also shown on this graph through the background colors are the ranges of the power law exponent that can be obtained for different scenarios, including the effects of scattering on $s_{\pm}$-, s_{++}- and d-wave superconducting gap symmetries.

In summary, the in-plane London penetration depth has been measured for several different transition metal doped $BaFe_2As_2$ compounds. The low-temperature region of the in-plane penetration depth for all studied compounds exhibits a power law temperature dependence of the form $\Delta\lambda_{ab} = CT^n$. Later in this thesis, it will be discussed that this power law temperature dependence likely arises from pair-breaking impurity scattering contributions to the penetration depth signal. For all studied samples, with the exception of the Rh doped compound, the doping dependence of the power law exponent decreases with increasing dopant concentration, in contrast to the observed behavior in the $Ba(Fe_{1-x}Co_x)_2As_2$ series.This may

suggest that by doping with Co and Rh, the superconductivity responds differently than for other transition metal substitutions.

4.6 Pair-breaking effects and the penetration depth prefactor

The variation of the in-plane London penetration depth, $\Delta\lambda_{ab}(T)$, has been measured over the low-temperature region, i.e. $T < T_c/3$, for several different classes of the iron-based superconductors by using the standard TDR technique [Gordon et al. (2010b)]. The main intentions of this study were to measure the prefactor β, extracted from fits to the low temperature penetration depth of the form $\Delta\lambda_{ab}(T) = \beta T^2$, for different classes of the iron-based superconductors. The materials measured for this study were $Ba(Fe_{1-x}Co_x)_2As_2$ (6 concentrations), $Ba(Fe_{1-x}Ni_x)_2As_2$ (5 concentrations), $(Ba_{0.7}K_{0.3})Fe_2As_2$, $Fe_{1.001}(Se_{0.367}Te_{0.632})$, $LaFeAs(O_{0.9}F_{0.1})$ and $NdFeAs(O_{0.9}F_{0.1})$.

The superconducting transitions of four of the the samples studied are visible through the in-plane penetration depth data shown in the inset to Fig. 4.27 (a). The numbered curves in Fig. 4.27 (a) correspond to: (1) $Ba(Fe_{0.942}Co_{0.058})_2As_2$, (2) $Ba(Fe_{0.941}Ni_{0.059})_2As_2$, (3) $Fe_{1.001}(Se_{0.367}Te_{0.632})$ and (4) $LaFeAs(O_{0.9}F_{0.1})$. The low-temperature functional form of the in-plane penetration depth for all of the samples has been fit to $\Delta\lambda_{ab}(T) = \beta T^2$ in order to extract the prefactor, β, and $\Delta\lambda_{ab}(T) = CT^n$ to determine the power law exponent, n, for each sample measured. The main frame of Fig. 4.27 (a) shows $\Delta\lambda_{ab}$ plotted versus the square of the reduced temperature, $(T/T_c)^2$, and the resulting linear behavior on this scale illustrates that the temperature dependence of the low-T penetration depth is very close to being purely quadratic for these samples.

The resulting power law exponent, n, obtained from fits to the low-T region of $\Delta\lambda_{ab}$, is shown for all samples and plotted versus the associated onset superconducting transition temperature, T_c, for each sample in Fig. 4.27 (b). The criteria that was used to determine the onset of the superconducting transition temperature can be seen in the inset to Fig. 4.28. From Fig. 4.27 (b) one can see that the power law functional form of $\Delta\lambda_{ab}(T) \propto T^n$ with $n \approx 2$ holds for superconductors from both the electron and hole doped 122 classes, two different members

of the 1111 class as well as the 11 class of iron-based superconductors.

The penetration depth prefactor can offer valuable information about the zero temperature value of the superconducting gap magnitude, $\Delta(0)$, the zero temperature value of the penetration depth, $\lambda(0)$, or even the slope of the gap near a node, $\alpha \equiv (d\Delta/d\phi)$ as $\phi \rightarrow \phi_{node}$, as in the case of a $d_{x^2-y^2}$-wave superconductor [Prozorov and Giannetta (2006); Poole et al. (2007)]. This can be understood by considering the functional forms of the penetration depth for the cases of an s-wave or a $d_{x^2-y^2}$-wave superconductor, which in the clean limit take the respective forms of

$$\Delta\lambda(T) \approx \lambda(0)\sqrt{\frac{\pi\Delta(0)}{2k_BT}}exp(-\frac{\Delta(0)}{k_BT}) \tag{4.5}$$

and

$$\Delta\lambda(T) \approx \frac{\lambda(0)2ln(2)}{d\Delta/d\phi|_{\phi\rightarrow\phi_{node}}}T \equiv \frac{\lambda(0)2ln(2)}{\alpha\Delta(0)}T. \tag{4.6}$$

In addition to this information, the penetration depth prefactor can also provide clues to the role played by pair-breaking scattering inside of a superconductor [Gordon et al. (2010b)].

The main source of motivation for looking at the penetration depth prefactor in the iron-based superconductors came from a prediction about its dependence on T_c which arises from pair-breaking scattering. This predicted dependence came about from a theoretical model based on the quasiclassical version of the weak-coupling Gor'kov theory that holds for a general anisotropic Fermi surface and for any superconducting gap symmetry [Eilenberger (1964)], which assumes a strong pairbreaking mechanism is present and has proven to be quite successful for describing the specific heat jump, $\Delta C \propto T_c^3$, as well as the slopes of the upper critical field, $dH_{c2}/dT \propto T_c$, in these materials [Bud'ko et al. (2009); Kogan (2009)]. According to this model, if the penetration depth is written in the form of $\Delta\lambda_{ab}(T) = \beta T^2$, then the prefactor β should take the form

$$\beta = \Big(\frac{1}{T_c^3}\Big)\frac{c\hbar}{8\pi k_B\tau_{\pm}}\sqrt{\frac{3<\Omega^4>-2}{\pi e^2N(0)<v_a^2\Omega^2>}} \tag{4.7}$$

where Ω describes the variation of the superconducting gap, Δ, along the Fermi surface, v_a is the Fermi velocity and $\tau_\pm$ are the two scattering times that characterize scattering within the Born approximation:

$$\frac{1}{\tau_\pm} = \frac{1}{\tau} \pm \frac{1}{\tau_m} \tag{4.8}$$

with τ being the transport scattering time associated with normal conductivity and τ_m is for processes that break time-reversal symmetry (e.g. spin flip). Commonly, two dimensionless parameters are used:

$$\rho = \frac{1}{2\pi T_c \tau} \tag{4.9}$$

and

$$\rho_m = \frac{1}{2\pi T_c \tau_m}, \tag{4.10}$$

or equivalently, $\rho_\pm = \rho \pm \rho_m$. Eqn. 4.7 was calculated assuming $< \Omega > \approx 0$, corresponding to a superconducting order parameter that has an amplitude that averages to zero about the Fermi surface.

Fig. 4.28 shows the penetration depth prefactor, β, obtained from low-T fits to $\Delta\lambda_{ab} = \beta T^2$, plotted as a function of T_c for all studied samples. Both axes are shown on a logarithmic scale for clarity. The horizontal error bars on the values of β represent the fact that not all samples had the same superonducting transition widths, so both the onset and the base of the transition were used for the fitting procedures. The solid black line is a fit to the data of the form $\beta = \eta/T_c^3$ and $\eta = 8.8 \pm 1.0$ μmK. For an additional check, by substituting $v_a \approx 10^7$ cm/s and $N(0) \approx 10^{33}$ erg^{-1}cm^{-3}, this gives a rough estimate of $\tau_+ \approx 3\text{x}10^{-14}$ s. This value corresponds to $\rho_+ \approx 5$ for T_c=40 K and to larger values for lower values of T_c, an observation consistent with the major model assumption of $\rho_+ \gg 1$.

The degree to which the experimental values follow the theory is remarkable, a substantial scatter of the data points notwithstanding. It is worth noting that the $1/T_c^3$ scaling in β is a result of strong pair-breaking scattering and does not follow from any other model to

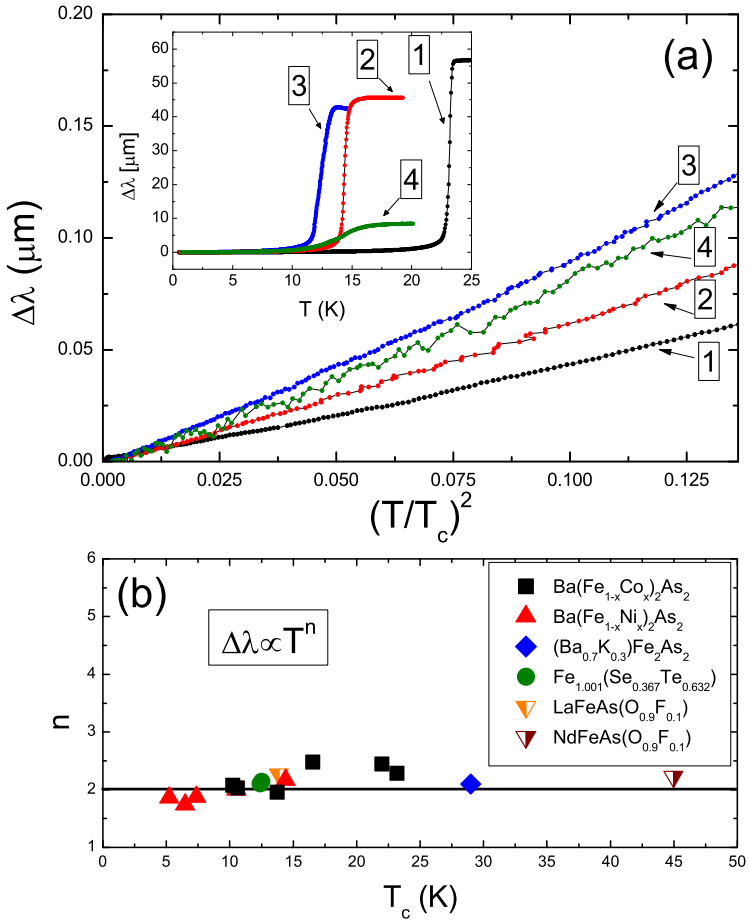

Figure 4.27 (a) Main frame: the low-T in-plane penetration depth for four different iron-based superconductors plotted versus $(T/T_c)^2$ to illustrate their nearly quadratic dependencies. The numbers correspond to: (1) $Ba(Fe_{0.942}Co_{0.058})_2As_2$, (2) $Ba(Fe_{0.941}Ni_{0.059})_2As_2$, (3) $Fe_{1.001}(Se_{0.367}Te_{0.632})$ and (4) $LaFeAs(O_{0.9}F_{0.1})$. Inset: the full superconducting transitions for these four samples as made visible by in-plane penetration depth measurements. (b) The power law exponent, n, resulting from low-T fits to $\Delta\lambda_{ab}$ and plotted versus the superconducting transition temperature, T_c, for each sample.

the author's knowledge. On the other hand, a larger data set is required to verify that this scaling holds for every class of iron-based superconductor. It should be stressed that the penetration depth scalings discussed here and in Ref. [Gordon et al. (2010b)] as well as the scalings for the specific heat jump [Bud'ko et al. (2009)] and for the slopes of $H_{c2}(T)$ [Kogan (2009)] are approximate by design since their derivation involves a number of simplifying assumptions. Still they are robust in showing that pair-breaking scattering is an important factor for superconductivity in the iron-based superconductors.

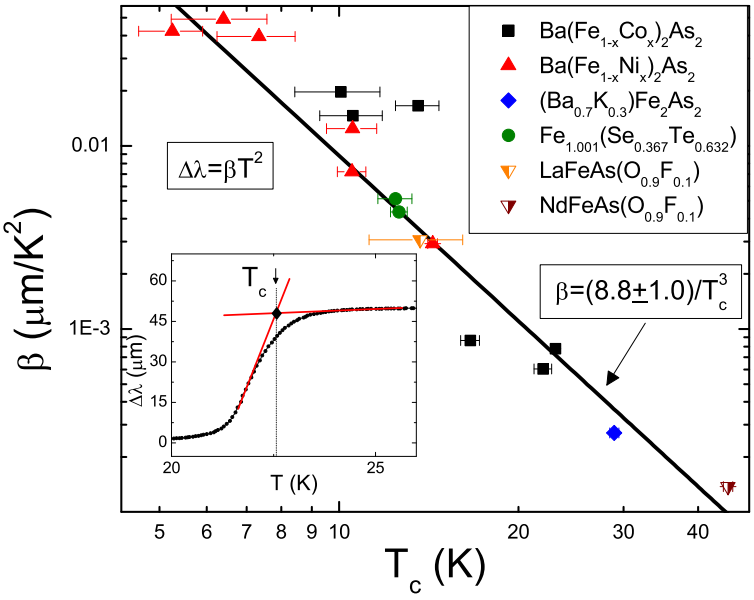

Figure 4.28 The penetration depth prefactor, β, obtained from low-T fits of the form $\Delta\lambda_{ab}(T) = \beta T^2$, plotted as a function of the superconducting critical temperature, T_c, on a log-log scale for many different members of the iron-based superconductor family. The solid black line is a fit of the form $\beta = \eta/T_c^3$ motivated by the pair-breaking theory described in the text.

Still there are other questions to be addressed, like why do the $Ba(Fe_{1-x}Co_x)_2As_2$ samples deviate on average more than any of the other compounds shown in Fig. 4.28? Another problem to address is how to reconcile the strong pair-breaking, which in the isotropic case leads to gapless superconductivity [Abrikosov and Gor'kov (1960)], with the in-plane thermal conductivity data showing $\kappa/T \to 0$ as $T \to 0$ [Luo et al. (2009); Tanatar et al. (2010)]?

The question arises whether or not one can have an iron-based superconductor free of any pair-breaking scattering. If possible, these materials would have much higher critical temperatures. For examples, if $\rho_+ \approx 5$ and $T_c \approx 20$ K, the clean material would have a critical temperature given by $T_{c0} = T_c \exp \psi(\rho_+ + 1/2) - \psi(1/2)$, which would be on the order of room temperature. Obviously, the formalism used to derive the $\beta \propto 1/T_c^3$ dependence does not capture all of the physics at hand in the iron-based superconductors, but it is possible that the same interactions responsible for pairing in these materials, presumably spin fluctuations, may also lead to strong pair-breaking scattering contributions and a more successful theory probably should account for both of these effects.

CHAPTER 5. Doping dependence of $\lambda_{ab}(0)$ and $\rho_s(T)$ in $Ba(Fe_{1-x}Co_x)_2As_2$

5.1 Introduction

The zero temperature value of the London penetration depth is directly related to the superfluid density in the ground state of a superconductor according to the relation $\lambda(0) \propto 1/\sqrt{n_s(0)}$ [Tinkham (1996)]. In the clean, low scattering limit, $n_s(0)$ is equal to the total density of conduction electrons, n_N. There are cases in which other phases, for example, itinerant magnetism, can compete with superconductivity for the same conduction electrons, thus reducing the overall number of carriers in the superconducting state at $T = 0$. Given the rich doping phase diagram of the newly discovered iron-based superconductors, in which a long-range magnetically ordered state with itinerant character coexists with a superconducting state, questions are raised regarding the effects of the competition between these states for the same electrons [Canfield and Bud'ko (2010); Ni et al. (2008b); Drew et al. (2009); Pratt et al. (2009); Christianson et al. (2004); Laplace et al. (2009); Goko et al. (2004); Fernandes et al. (2010)]. One way to approach this matter is to study the doping evolution of $\lambda_{ab}(0)$ across the phase diagram of these materials and use it to infer the corresponding change in the superfluid density, especially in the regime of the phase diagram where these two phases coexist. Determination of the absolute value of the London penetration depth is also important for the correct evaluation of the normalized, temperature-dependent superfluid density, $\rho_s(T) = [\lambda(0)/\lambda(T)]^2$. This quantity can be calculated from various models for different superconducting gap structures and provide insight into the pairing mechanism.

For these experiments [Gordon et al. (2010a)], we focus on $\lambda_{ab}(T = 0)$, which is the ground state screening length associated with supercurrent flowing in the crystallographic ab plane as a result of an external magnetic field applied along the c-axis. For $x \gtrsim 0.047$, the measured

values of $\lambda_{ab}(0)$ have been found between 120±50 and 300±50 nm. A pronounced increase in $\lambda_{ab}(0)$ to a value as high as 950±50 nm for $x \lesssim 0.047$ has been observed. The increase in $\lambda_{ab}(0)$ for samples with $x \lesssim 0.047$ has been interpreted as being due to the competition between the superconducting and itinerant antiferromagnetic states for the same conduction electrons.

The experimental determination of $\lambda(0)$ is a rather challenging task since only finite temperatures can be reached in the laboratory. There are techniques that are capable of obtaining an estimate of its value by taking advantage of the small variation of $\lambda(T)$ at low temperatures, which can be on the order of 1 nm/K, along with precision measurements. One such technique is muon-spin rotation (μSR) [Sonier (2007)], which has produced estimates for $\lambda_{ab}(0)$ of 320 nm in $(Ba_{1-x}K_x)Fe_2As_2$ ($T_c \simeq 32$ K) [Khasanov et al. (2009); Evtushinsky et al. (2009b)], 470 nm in $(Ba_{0.55}K_{0.45})Fe_2As_2$ ($T_c \simeq 30$ K) [Aczel et al. (2008)], 230 nm in $(Ba_{0.6}K_{0.4})Fe_2As_2$ ($T_c \simeq 38$ K) [Hiraishi et al. (2009)], 250 nm in $La(O_{1-x}F_x)FeAs$ [Luetkens et al. (2009)], and values ranging from 189 to 438 nm in the $Ba(Fe_{1-x}Co_x)_2As_2$ series [Williams et al. (2009, 2010)].

Another technique, magnetic force microscopy (MFM), has reported $\lambda_{ab}(0)$=325±50 nm in $Ba(Fe_{0.95}Co_{0.05})_2As_2$ [Luan et al. (2010)]. In addition, optical reflectivity measurements have been used to estimate $\lambda_{ab}(0)$ in $Ba(Fe_{1-x}Co_x)_2As_2$ and have reported values of 277±25 nm for x=0.06 and 315±30 nm for x=0.08 [Nakajima et al. (2010)]. It is important to compare the values of $\lambda(0)$ obtained from as many different techniques as possible because each experiment requires its own set of assumptions and modeling procedures.

Given the overall disparity between the measured values of $\lambda(0)$ from these different experimental techniques, it is valuable to perform a systematic study of $\lambda(0)$ as a function of doping in the series of which large, high quality single crystals having homogeneous doping levels are available, namely, the $Ba(Fe_{1-x}Co_x)_2As_2$ series. In this study, we utilized TDR frequency shift measurements to extract the full temperature dependence of the London penetration depth in these samples. The absolute values have been determined by using a technique in which samples from this series were coated with aluminum in order to provide a reference point for the penetration depth measurements. Having the absolute values, the normalized superfluid density has been constructed as a function of temperature for various cobalt dopings in order

to study the evolution of the superconducting gap structure across the phase diagram of this series.

5.2 Aluminum coating procedure for determining $\lambda_{ab}(0)$ in $Ba(Fe_{1-x}Co_x)_2As_2$

The TDR technique that is normally used to measure $\Delta\lambda(T)$ in superconductors is quite well suited for measuring the variation of the penetration depth with respect to its value at the minimum temperature of the experiment, but under usual circumstances it is insensitive to the absolute value of the penetration depth, $\lambda(T)$ [Prozorov et al. (2000b)]. However, as proposed in Ref. [Prozorov et al. (2000b)], the TDR technique can be extended to obtain the absolute value by coating the entire surface of the superconductor to be measured with a thin film of a conventional superconductor having a lower critical temperature and a known value of $\lambda(0)$. For this study, aluminum films were deposited onto the $Ba(Fe_{1-x}Co_x)_2As_2$, where $T_c^{Al} \approx 1.2$ K and thicknesses of 100 nm, as shown in Fig. 5.1.

While the Al film is superconducting, it participates with the coated superconductor to screen the magnetic field generated by the TDR coil. However, when it becomes normal it does effectively no screening because its thickness, t, is much less than the normal state skin depth at the TDR operating frequency of 14 MHz, where $\delta_{Al} \approx 75\mu$m for ρ_0^{Al}=10 $\mu\Omega$-cm [Hauser (1972)]. By measuring the frequency shift upon warming from T_{min}, which was the base temperature of the sample, to $T > T_c^{Al}$, the quantity $L \equiv \lambda_{eff}(T_c^{Al}) - \lambda_{eff}(T_{min})$ can be obtained, as can be seen in Fig. 5.2. This quantity can be used to calculate $\lambda(0)$ for the $Ba(Fe_{1-x}Co_x)_2As_2$ series by utilizing the previously determined power law relation $\Delta\lambda(T) = CT^n$ [Gordon et al. (2009a,b)] along with the formula for the effective magnetic penetration depth into both the Al film and the coated superconductor for $T < T_c^{Al}$, which is given by

$$\lambda_{eff}(T) = \lambda_{Al}(T)\frac{\lambda_{ab}(T) + \lambda_{Al}(T)\tanh\frac{t}{\lambda_{Al}(T)}}{\lambda_{Al} + \lambda_{ab}(T)\tanh\frac{t}{\lambda_{Al}(T)}}, \tag{5.1}$$

where $\lambda_{ab}(T)$ is the penetration depth of the coated superconductor and $\lambda_{Al}(T)$ is the penetration depth of the Al film. As usual with the TDR technique, the variation in the penetration

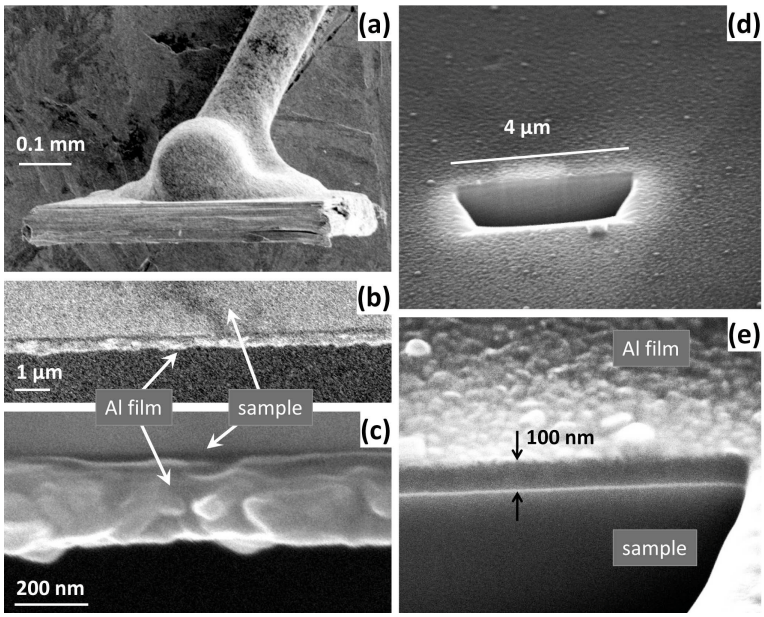

Figure 5.1 Scanning electron microscope images of the Al coated samples. (a) Large scale view of the sample where the exposed top was the broken edge. (b) and (c) Zoomed-in regions of the Al film exposed after the sample was broken. (d) Close-up view of the FIB trench showing the Al film and its thickness.

depth with temperature, $\Delta\lambda_{eff}(T) = \lambda_{eff}(T) - \lambda_{eff}(T_{min})$, is measured. This method has been successfully demonstrated on several high-T_c cuprate superconductors [Prozorov et al. (2000b)] and has shown agreement with measurements of $\lambda(0)$ in $Fe_{1+y}(Te_{1-x}Se_x)$ crystals obtained by different techniques [Kim et al. (2010b)]. Here we use an extended analysis obtained by solving the appropriate boundary value problem.

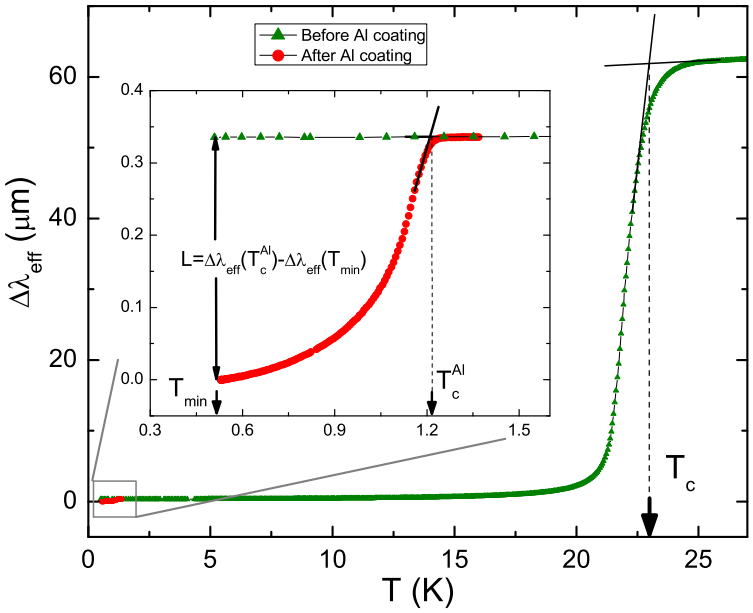

Figure 5.2 Main frame: the full superconducting transition of an optimally doped $Ba(Fe_{0.93}Co_{0.07})_2As_2$ crystal before and after coating. Inset: zoomed-in view of the low-temperature region, $T_{min} < T < T_c^{Al}$, before (green triangles) and after (red circles) the Al coating on the same sample. The overall frequency shift through the Al transition, denoted as L, was used for the calculation of $\lambda_{ab}(0)$.

The aluminum film was deposited onto each sample while it was suspended from a rotating stage by a fine wire in an argon atmosphere of a magnetron sputtering system. The formation of nonuniform regions in the film was avoided by bonding the suspension wire to only a portion of the narrowest edge of each sample. Each film thickness was checked using a scanning electron microscope in two ways, both of which are shown in Fig. 5.1. The first method involved breaking a coated sample after all measurements had been performed to expose its

cross section. After this, it was mounted on a scanning electron microscope (SEM) sample holder using silver paste, as shown in Fig. 5.1 (a). The images of the broken edge are shown for two different zoom levels in Fig. 5.1 (b) and (c). The second method used a focused-ion beam (FIB) to make a trench on the surface of a coated sample, with the trench depth being much greater than the Al coating thickness, as shown in Fig. 5.1 (d). The sample was then tilted and imaged by the SEM that was built into the FIB system, as shown in Fig. 5.1 (e).

5.3 $Ba(Fe_{1-x}Co_x)_2As_2$ samples

The samples used for this study were all members of the $Ba(Fe_{1-x}Co_x)_2As_2$ series, many of which were the same samples measured in previous penetration depth studies [Gordon et al. (2009a,b)], and were obtained from the same source as Ref. [Ni et al. (2008b)] using the same growth procedure. The samples from these batches were characterized by magnetization and resistivity measurements, which showed a robust superconducting response with sharp transitions. In addition, magneto-optical imaging was used to probe the mesoscopic (in)homogeneity of the samples, at least down to a length scale of 1 μm [Prozorov et al. (2009a)].

The Co concentrations were all determined by WDS analysis and the uncertainty within each batch can be as high as ± 0.0015. At the edges of the superconducting dome, where T_c changes quickly with x, this uncertainty is not negligible and brings about sizable variations in T_c, as can be seen in Table I, for concentrations that are nominally the same. Many samples were prescreened in order to select the best ones to be coated with aluminum. A distribution of different Co doping levels, x, within a given sample would lead to a broadening of the superconducting transition, so all samples were prescreened to ensure the sharpest possible T_c. The T_c of a sample is an excellent way of determining the actual doping level by using the previously determined doping phase diagram [Ni et al. (2008b)]. For highly overdoped samples, the superconducting transitions were quite broad and none could be found with transition widths comparable to that of the optimally doped compounds, which is why highly overdoped samples were not included in this study. Table I summarizes the relevant properties of all of the samples used in this study.

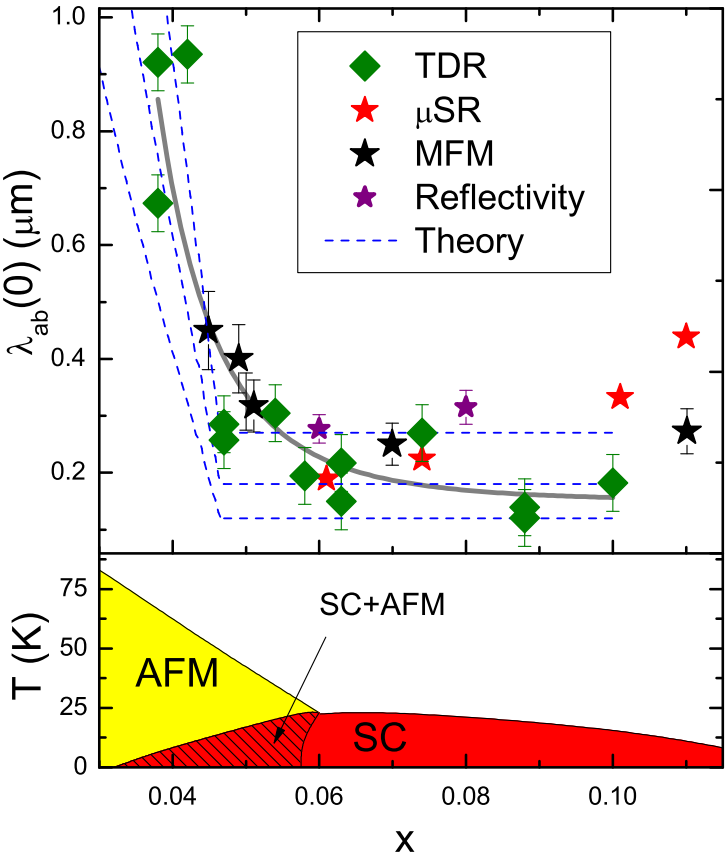

Figure 5.3 Top panel: the zero-temperature in-plane London penetration depth, $\lambda_{ab}(0)$, as a function of the Co concentration, x. The three dashed blue lines are theoretical curves obtained using a model accounting for competition between $s_{\pm}$-wave superconductivity and itinerant antierromagnetism representing three different values of $\lambda_{ab}(0)$ in the pure superconducting state. The solid gray line is a fit to the TDR data only of the form $A + B/x^n$. Also shown are values of $\lambda_{ab}(0)$ obtained by other experiments for comparison. Bottom panel: phase diagram for $Ba(Fe_{1-x}Co_x)_2As_2$.

Table 5.1 Summary of the parameters for individual samples. The actual error bar on the values of $\lambda(0)$ should consider the scatter between different samples, see Fig. 5.3.

Sample	x_{WDS}	T_c (K)	$\lambda(0)$ (nm)
1	0.038	7.4	673
2	0.038	11.6	921
3	0.042	15.5	935
4	0.047	18.5	258
5	0.047	18.3	285
6	0.054	20.5	305
7	0.058	23.3	195
8	0.063	23.4	150
9	0.063	23.5	217
10	0.074	22.8	270
11	0.088	21.1	121
12	0.088	21.0	140
13	0.100	17.2	182

5.4 Results and discussion

The values of $\lambda_{ab}(0)$ that were obtained using the procedure described above for the $Ba(Fe_{1-x}Co_x)_2As_2$ system are shown in the top panel of Fig. 5.3 for doping levels, x, across the superconducting region of the phase diagram, shown schematically in the bottom panel of Fig. 5.3. The size of the error bars for the $\lambda_{ab}(0)$ points was determined by considering the film thickness to be t=100±10 nm and $\lambda_{Al}(0)$=50±10 nm. The discrepancy for the two samples having x=0.038 is clearly beyond these error bars and this may possibly be due to cracks or inhomogeneities in the Al film, even though great care was taken to eliminate them during the coating process. Thus, the error bars represent the uncertainty of the known parameters and the scatter in the data may arise from uncontrolled effects such as cracks or inhomogeneities in the Al film. The discrepancy for the two x=0.038 samples could also arise from the uncertainty in knowing the actual Co concentrations, which is supported by the sizable variation in T_c, shown in Table I. The scatter in the λ_{ab} values shown in the upper panel of Fig. 5.3 has an approximately constant value of ±0.075 μm for all values of x, which probably indicates that the source of the scatter is the same for all doping levels. For comparison, Fig. 5.3 also shows

$\lambda_{ab}(0)$ obtained from μSR measurements (red stars) [Williams et al. (2009, 2010)], the MFM technique (black stars) [Luan et al. (2010, 2011)], which later confirmed the TDR values, and optical reflectivity (purple stars) [Nakajima et al. (2010)], all in the $Ba(Fe_{1-x}Co_x)_2As_2$ system, most of which are consistent with the TDR results within the scatter. It may also be important to note that the $\lambda_{ab}(0)$ values from other experiments are all on the high side of the scatter that exists within the TDR $\lambda_{ab}(0)$ data set. This is probably because any cracks or voids in the Al film will lead to underestimated values of $\lambda_{ab}(0)$. It should also be noted that the TDR measurements did not show an increase in $\lambda_{ab}(0)$ toward the overdoped regime that has been reported by μSR measurements [Williams et al. (2010)], although the values at optimal doping do agree quite reasonably.

Specifically, an increase in $\lambda_{ab}(0)$ on the underdoped side below $x \approx 0.047$ has been observed, which is in the region where the itinerant antiferromagnetic and superconducting phases coexist, as is shown in the bottom panel of Fig. 5.3. The dependence of $\lambda_{ab}(0)$ on carrier concentration is $\lambda_{ab}(0) \propto 1/\sqrt{n_s(0)}$, where $n_s(0)$ is the superfluid density at T=0, which is equal to the normal state carrier concentration in the clean impurity scattering limit. The relationship between $\lambda_{ab}(0)$ and $n_s(0)$ still holds if impurity scattering effects are included, but n_s is reduced due to a residual density of normal states within the gap. Overall, an increase in $\lambda_{ab}(0)$ is consistent with a decrease in the superfluid carrier concentration. There is compelling evidence which suggests that the itinerant antiferromagnetic spin density wave state in these materials acts to gap away a portion of the Fermi surface [Canfield and Bud'ko (2010); Ni et al. (2008b); Drew et al. (2009); Pratt et al. (2009); Christianson et al. (2004); Laplace et al. (2009); Goko et al. (2004); Fernandes et al. (2010)], which would remove mobile charge carriers and this qualitative idea is consistent with our experimental observations of the doping dependence of $\lambda_{ab}(0)$. Changes in the Hall coefficient for these materials, moving from doping levels that correspond to the pure superconducting region to the coexistence region, have also been interpreted as being due to the interaction between these phases [Mun et al. (2009); Fang et al. (2009)]. It has been shown that the opening of a superconducting gap in the antiferromagnetic state transfers optical spectral weight from a mid-infrared Drude peak,

even when the reconstructed Fermi surface would be fully gapped [Fernandes and Schmalian (2010)]. As a result, the coexistence state has a finite n_s, although smaller than in the pure superconducting state.

In order to provide a more quantitative explanation for the observed increase in $\lambda_{ab}(0)$ as x decreases in the underdoped region, we have considered the case of $s_{\pm}$-wave superconductivity coexisting with itinerant antiferromagnetism [Fernandes et al. (2010)]. For the case of particle-hole symmetry (nested bands), the zero temperature value of the in-plane penetration depth in the region where the two phases coexist is

$$\lambda_{ab}^{SC+SDW}(0) = \lambda_{ab}^{0}(0)\sqrt{1+\frac{\Delta_{AFM}^2}{\Delta_0^2}}, \tag{5.2}$$

where $\lambda_{ab}^{0}(0)$ is the value for a pure superconducting system with no magnetism present, and Δ_{AFM} and Δ_0 are the zero-temperature values of the antiferromagnetic and superconducting gaps, respectively. Deviations from particle-hole symmetry lead to a smaller increase in $\lambda_{ab}^{SC+SDW}(0)$, making the result in Eqn. 5.2 an upper estimate. For more information on the details of the calculation and the values of Δ_{AFM} and Δ_0 used, see Refs. [Fernandes et al. (2010); Fernandes and Schmalian (2010)].

The three blue dashed lines shown in the top panel of Fig. 5.3, which were produced using Eqn. 5.2, show the expected increase in $\lambda_{ab}(0)$ in the region of coexisting phases below $x \approx 0.047$ by normalizing to three different values of $\lambda_{ab}(0)$ in the pure superconducting state, with those being 120, 180 and 270 nm. This theory does not take into account changes in the pure superconducting state, so for $x > 0.047$ the dashed blue lines are horizontal. These theoretical curves were produced using parameters that agree with the phase diagram in the bottom panel of Fig. 5.3 [Fernandes et al. (2010); Nandi et al. (2010)], which includes a shift of the coexistence region to lower values of x by an amount of 0.012, and given the simplifications of the model, the agreement with the experimental observations is quite reasonable. A possible reason for the required shift of 0.012 in the theoretical curves could be that the scatter in the measured values of $\lambda_{ab}(0)$ is too large.

While the exact functional form was not provided by any physical motivation and merely

serves as a guide to the eye, the solid gray line in Fig. 5.3 is a fit of the TDR $\lambda_{ab}(0)$ data to a function of the form $A + B/x^n$, which does indeed show a dramatic increase in $\lambda_{ab}(0)$ in the coexistence region and also a relatively slight change in the pure superconducting phase. It should be noted that a dramatic increase in $\lambda_{ab}(0)$ below $x \approx 0.047$ cannot be explained by impurity scattering, which would only lead to relatively small corrections to the penetration depth.

Values of $\lambda_{ab}(0)$ obtained in this experiment can be used to calculate the actual penetration depth, $\lambda_{ab}(T) = \Delta\lambda_{ab}(T) + \lambda_{ab}(0)$, where $\Delta\lambda_{ab}(T)$ has been measured for most of the $Ba(Fe_{1-x}Co_x)_2As_2$ crystals used in this study before Al coating [Gordon et al. (2009a,b)]. In the top panel of Fig. 5.4, we examine $\lambda_{ab}^{-2}(T) \propto n_s(T)/m^*$ as a function of temperature in underdoped, optimally doped and overdoped samples, where the values of $\lambda_{ab}(0)$ used are the corresponding values shown in Fig. 5.3 and Table I. Shown in the top panel of Fig. 5.4 are an underdoped sample with T_c =7.4 K (x=0.038, sample no. 1), a sample close to optimal doping with T_c=22.8 K (x=0.074, sample no. 10) and an overdoped sample with T_c=17.2 K (x=0.1, sample no. 13). There is a clear evolution toward higher superfluid density approaching optimal doping.

Using the same penetration depth data that was used in the top panel of Fig. 5.4, the normalized superfluid density (phase stiffness), $\rho_s(T) = [\lambda(0)/\lambda(T)]^2$, has been constructed. The bottom panel of Fig. 5.4 shows $\rho_s(T)$ for the same samples shown in the top panel. Also shown for comparison are the $\rho_s(T)$ curves for a single band s-wave superconductor (dotted blue line) and a $d_{x^2-y^2}$-wave superconductor (dotted gray line), both in the clean limit. From Fig. 5.4, $\rho_s(T \to 0)$ and $\rho_s(T \to T_c)$ behave quite differently for the members of the $Ba(Fe_{1-x}Co_x)_2As_2$ series compared to the standard, single gap s-wave and $d_{x^2-y^2}$-wave clean limit cases. Impurity scattering would turn the $d_{x^2-y^2}$-wave curve quadratic at low temperatures, but would leave the s-wave curve nearly the same.

The data for all doping levels show an overall similar trend of the evolution of $\rho_s(T)$ across the doping phase diagram. A special feature of these curves is the region of upward concavity just below T_c. This behavior suggests that below T_c the superconducting gap develops more

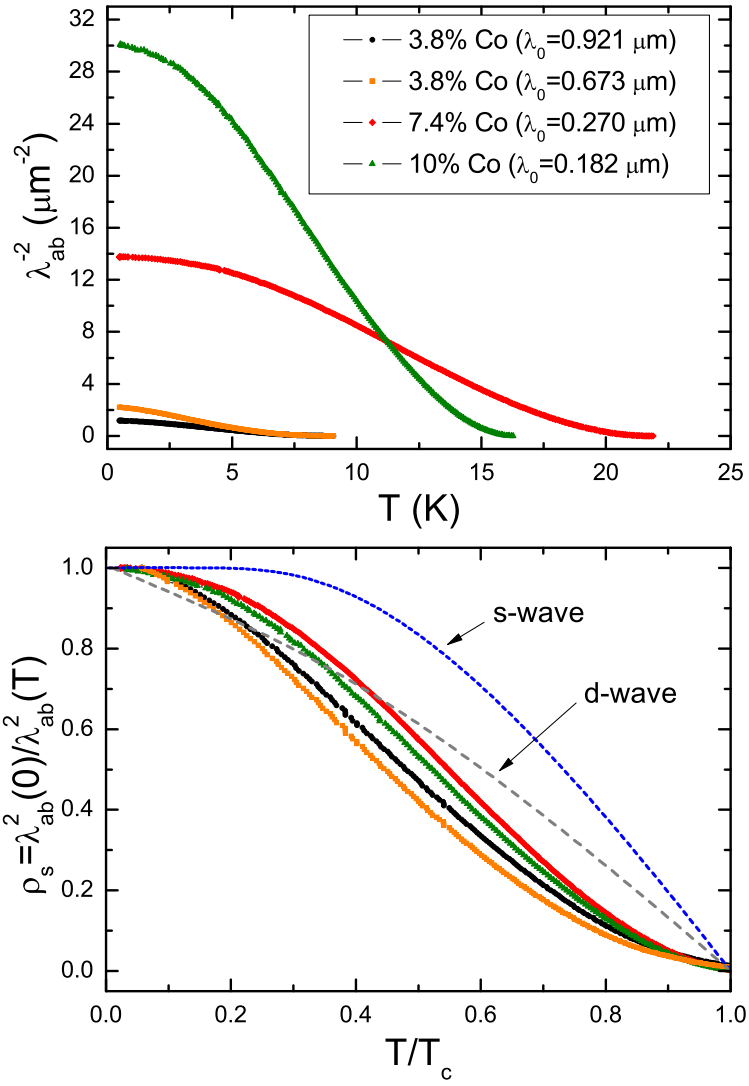

Figure 5.4 Top panel: $\lambda_{ab}^{-2}(T)$ for samples representing different doping regimes of the $Ba(Fe_{1-x}Co_x)_2As_2$ series. These curves were constructed from previous measurements of $\Delta\lambda_{ab}(T)$ with the measured values of $\lambda_{ab}(0)$ using the relationship $\lambda_{ab}(T) = \Delta\lambda_{ab}(T) + \lambda_{ab}(0)$. Bottom panel: the normalized superfluid density, $\rho_s(T) = [\lambda_{ab}(0)/\lambda_{ab}(T)]^2$, for the same samples shown in the top panel along with the standard clean s-wave and clean d-wave curves.

slowly than it does in the case of a single superconducting gap, implying that there is likely more than one gap [Kogan et al. (2009)]. Furthermore, the normalized $\rho_s(T)$ curve for the optimally doped sample over the entire temperature range stays above the curves for the heavily underdoped and overdoped samples, though in the latter case the difference is on the order of the statistical error in the measured values of $\lambda_{ab}(0)$ (Fig. 5.3). The distinction between the measurements on samples with different Co concentrations suggests that the gap anisotropy, which is generally considered as being either the actual angular variation in k-space and/or the development of an imbalance between the gaps on different sheets of the Fermi surface, increases as x moves away from optimal doping in either direction. Although these measurements do no go into the far overdoped regime, these results are consistent with the measurements of the specific heat jump [Bud'ko et al. (2009)] and the residual density of states [Gofryk et al. (2009)], as well as with measurements of the thermal conductivity in the same series [Tanatar et al. (2010); Reid et al. (2010)]. In particular, thermal conductivity measurements with heat flow along the c-axis actually suggest that nodal regions in the superconducting gap develop for heavily underdoped and heavily overdoped compositions. This is also consistent with measurements of $\lambda_c(T)$ performed in the closely related $Ba(Fe_{1-x}Ni_x)_2As_2$ series, where c-axis nodes have been suggested by the linear temperature dependence of the c-axis component of the penetration depth [Martin et al. (2010a)].

5.5 Summary

To conclude this chapter, the zero temperature value of the in-plane London penetration depth, $\lambda_{ab}(0)$, has been measured for the $Ba(Fe_{1-x}Co_x)_2As_2$ series across the superconducting dome of the phase diagram using an aluminum coating technique along with TDR frequency measurements [Gordon et al. (2010a)]. There is a clear increase in $\lambda_{ab}(0)$ below $x \approx 0.047$, which is consistent with a reduction in the superfluid density, $n_s(T)$, due to the competition between itinerant antiferromagnetism and superconductivity for the same conduction electrons [Fernandes et al. (2010); Fernandes and Schmalian (2010)]. The measured values of $\lambda_{ab}(0)$ were used to construct the normalized superfluid density, $\rho_s(T)$, and study its evolution with

doping. The region of upward concavity in $\rho_s(T)$ just below T_c for concentrations ranging across the phase diagram suggests the importance of two-gap superconductivity for all doping levels [Kogan et al. (2009)]. A notable suppression of $\rho_s(T)$ for heavily underdoped samples and a minor suppression for overdoped samples suggests an evolution of the anisotropy of the superconducting gaps as the doping level moves away from its optimal value, which is consistent with the behavior found in specific heat [Bud'ko et al. (2009); Gofryk et al. (2009)] and thermal conductivity [Tanatar et al. (2010); Reid et al. (2010)] studies.

CHAPTER 6. Conclusion

6.1 Initial remarks

Up to this point, much of this thesis has been intended to show penetration depth data taken on several different iron-based superconductors in an organized way, but this has not facilitated a general discussion of all of the penetration depth results. The intention of this chapter is not only to summarize what has already been shown, but also to provide a place for a general, organized discussion of the penetration depth data and also to allow for results from new experiments that have not yet been shown in this thesis to be introduced and included in the discussion.

6.2 Penetration depth power laws from pair-breaking impurity scattering in iron-based superconductors

At the present date the community has agreed upon the general idea that the power law temperature dependence observed in the penetration depth at low temperatures in the iron-based superconductors arises from pair-breaking impurity scattering effects. This claim has gained substantial support from penetration depth measurements performed on $Ba(Fe_{1-x}Co_x)_2As_2$ and $Ba(Fe_{1-x}Ni_x)_2As_2$ samples that were irradiated with heavy ions [Kim et al. (2010a)], so that contributions to the penetration depth from impurity scattering could be separated in the best way possible. It has also gained support from measurements of an exponential temperature dependence of the penetration depth in LiFeAs, which is believed to be be an intrinsically clean iron-based superconductor having $T_c \approx 18$ K [Kim et al. (2010c)]. In the clean impurity scattering limit of the proposed $s_{\pm}$-wave superconducting gap structure

one expects to recover an exponential dependence of the penetration depth [Vorontsov et al. (2009)].

In order to study the contribution to the measured in-plane London penetration depth in the iron-based superconductors from pair-breaking impurity scattering, optimally doped single crystals of $Ba(Fe_{1-x}Co_x)_2As_2$ ($T_c \approx 22.5$ K) and $Ba(Fe_{1-x}Ni_x)_2As_2$ ($T_c \approx 18.9$ K) were irradiated with $^{208}Pb^{56+}$ ions at the Argonne Tandem Linear Accelerator System (ATLAS) with an ion flux of $\approx 5 \times 10^{11}$ ions s^{-1} m^{-2} [Kim et al. (2010a)]. The Pb ions passed through the samples parallel to the c-axis and created tracks in the form of columnar defects. These defects act to increase impurity scattering in the crystals and their density can be monitored in a very controlled way. For each series, large single crystals were selected and then cut into several pieces preserving the widths and thicknesses. One piece from each series was left unirradiated and all other pieces were irradiated with different dosages.

The in-plane London penetration depth was measured for each sample to observe the effect of the heavy ion irradiation on the low-temperature behavior. For both series it has been found that an increase of the irradiation dose results in a monotonic decrease of T_c without affecting much the transition width. For all 122 samples measured, a power law temperature dependence of the low-T in-plane penetration depth has been observed of the form $\Delta\lambda_{ab}(T) \propto T^n$ with $2.2 < n < 2.8$. As the irradiation dosage increases, it has been found for both series that the power law exponent n decreases. This decrease in n as the concentration of impurities increases is at qualitative odds with the expectations for both an s-wave and a $d_{x^2-y^2}$-wave superconductor. Both the decrease in T_c and the decrease in n as the irradiation dosage increases can be explained by considering a model for $s_{\pm}$-wave superconductivity which takes into account both intra- and inter-band impurity scattering effects through the t-matrix approximation [Kim et al. (2010a)]. The superfluid density was constructed for this model by considering two isotropic gaps and it has been shown to evolve from exponential at low temperatures in the clean case to a power law dependence for samples in the dirty scattering limit, which describes the penetration depth data quite well. The best agreement between the theory and the experiment was for two isotropic gaps with $\Delta_2 \approx -0.6\Delta_1$, a strong interband

scattering component and a phase shift of $\delta = 60°$ between the born ($\delta \rightarrow 0°$) and unitary ($\delta \rightarrow 90°$) scattering limits.

Since the $Ba(Fe_{1-x}Co_x)_2As_2$ and $Ba(Fe_{1-x}Ni_x)_2As_2$ systems are naturally impure because they must be doped to achieve superconductivity, the predicted exponential temperature dependence of the penetration depth, corresponding to the clean impurity scattering limit, has not been observed. However, the stoiciometric LiFeAs compound has allowed for the hypothesis that the iron-based superconductors show an exponential penetration depth in the clean limit to be tested because it is an undoped superconductor with $T_c \approx 18$ K. The statement that LiFeAs is in the intrinsically clean limit is further supported by its relatively large residual resistivity ratio (RRR), which is a way of determining the purity level of a sample by comparing the amount of scattering in the high and low temperature states. A large RRR value usually corresponds to a very small resistivity at low temperatures, indicating that the crystal has few imperfections. The RRR of LiFeAs has been found to be ≈50 for the measured samples, compared to RRR≈3 in the $Ba(Fe_{1-x}Co_x)_2As_2$ series [Ni et al. (2008b)], indicating that LiFeAs has fewer imperfections that can contribute to scattering at low temperatures.

The in-plane London penetration depth has been measured in three different samples of LiFeAs and the out-of-plane penetration depth was also measured for one of the samples [Kim et al. (2010c)]. Remarkably, the low-temperature region of the in-plane penetration depth for the LiFeAs samples exhibits an exponential temperature dependence, which is expected for an $s_{\pm}$-wave superconductor in the clean impurity scattering limit. By performing a power law fit of the form $\Delta\lambda_{ab}(T) = CT^n$, the resulting power law is $n \approx 3.1$, which is larger than any other value obtained previously for an iron-based superconductor and would be consistent with an exponential behavior. The out-of-plane penetration depth, which was measured with H_{ac} perpendicular to the c-axis, also shows evidence for saturation at low temperatures, although the data are much noiser for that experiment.

A single gap BCS fit to the low-T region of the in-plane penetration depth for LiFeAs yields values for the fit residuals that are as good as the previously mentioned power law fit. The single gap BCS fit gives $\lambda(0) \approx 280$ nm and a gap ratio of $\Delta(0)/T_c$=1.09. This value of $\lambda(0)$

is comparable to values obtained in other iron-based superconductors [Gordon et al. (2010a)], but the gap ratio is smaller than the expected weak coupling value of 1.76 for a single fully-gapped s-wave superconductor. Such a small gap ratio has also been found by using a single gap BCS fit on data from superconductors that are known to have multiple superconducting gaps, like MgB_2, V_3Si and $Lu_2Fe_3Si_5$ [Kogan et al. (2009); Martin et al. (2008)]. To see how well the data may be described by a model accounting for multiple gaps, the two gap γ-model [Kogan et al. (2009)] was used to fit the LiFeAs superfluid density data, where both gaps were computed self-consistently and both intra and inter-band impurtiy scattering effects were taken into account. The best fit gave $\Delta_1(0)/T_c$=1.885 and $\Delta_2(0)/T_c$=1.111, which is in agreement with the observation that the penetration depth data of all two gap superconductors, when fit to the two gap self-consistent γ model, produce one gap ratio that is larger than the weak coupling BCS value and one that is smaller.

To summarize, heavy ion irradiation experiments on single crystals of $Ba(Fe_{1-x}Co_x)_2As_2$ and $Ba(Fe_{1-x}Ni_x)_2As_2$ superconductors have indicated that as the concentration of impurity scatterers inside of the material increases, the power law exponent of the London penetration depth decreases as does the T_c of the material without changing the width by much. These observations are very well described by a model for $s_{\pm}$-wave superconductivity which accounts for both intra- and inter-band impurity scattering, implying that in the clean impurity scattering limit, the iron-based superconductors should display an exponential saturation of the in-plane penetration depth at low temperatures. This hypothesis has been tested by measuring the penetration depth in single crystals of clean and stoichiometric LiFeAs ($T_c \approx$18 K), which indeed do show an exponential saturation of the in-plane penetration depth at low temperatures and the superfluid density data are well fit by the self-consistent two gap γ-model.

6.3 The doping dependence of $\Delta\lambda_{ab}$ in $Ba(Fe_{1-x}T_x)As_2$ (T=Co,Ni)

Let us now turn to a discussion of the doping dependence of the power law exponent, n, of the low-temperature region of the in-plane London penetration depth in the $Ba(Fe_{1-x}Co_x)_2As_2$ [Gordon et al. (2009b,a)] and $Ba(Fe_{1-x}Ni_x)_2As_2$ [Martin et al. (2010a)] compounds. For all

concentrations a power law temperature dependence of the form $\Delta\lambda_{ab} \propto T^n$ has been observed. As explained previously, the power law exponent, n, was obtained by fitting the low-T region of the penetration depth ($T < T_c/3$) data to a function of the form $\Delta\lambda_{ab}(T) = CT^n$. By measuring several different doping concentrations, x, of both series, n has been studied as a function of the doping level across different regions of their respective temperature-doping phase diagrams. There is supporting evidence to suggest that the observed power law temperature dependence of the penetration depth in the Ba-based 122 iron-based superconductors arises from pair-breaking impurity scattering [Kim et al. (2010a)] and that in the clean scattering limit these materials would exhibit an exponential temperature dependence in the penetration depth, which is expected for a superconductor having an $s_{\pm}$-wave order parameter symmetry and has actually been observed in the intrinsically clean LiFeAs [Kim et al. (2010c)]. In what follows, possible explanations for the observed doping dependence of the power law exponent in the $Ba(Fe_{1-x}Co_x)_2As_2$ and $Ba(Fe_{1-x}Ni_x)_2As_2$ compounds are discussed. Penetration depth data do exist for other transition metal dopings of the $BaFe_2As_2$ series, but none have been studied as extensively as the Ni and Co doped members from a penetration depth perspective.

Recall that for the $Ba(Fe_{1-x}Co_x)_2As_2$ series, the in-plane penetration depth has been measured for samples with x=0.038,0.047, 0.058,0.074 and 0.10, with optimal doping being between 0.058 and 0.074. The x=0.10 sample is only slightly overdoped and higher concentrations were not studied because large single crystals were not available at the time of these measurements. A power law temperature dependence of the low-T in-plane penetration depth has been observed for all concentrations, with n being as low as 2 for underdoped samples and climbing as high as 2.5 for the highest measured overdoped concentration of x=0.10. There is a clear change of regime at $x \approx$0.06 where the power law, n, increases rapidly and the penetration depth prefactor, C from $\Delta\lambda_{ab}(T) = CT^n$, jumps by an order of magnitude, which both happen while moving toward higher concentrations.

One possible reason for the change of regime that occurs at $x \approx$0.06, where there are clear signatures in the power law exponent n and the prefactor C, could be associated with the fact that this is the portion of the phase diagram where the antiferromagnetic/structural phase

transition lines intersect the superconducting dome. On the underdoped side of the dome, the formation of structural domains may be able to account for why the external magnetic field is being screened differently with respect to all other measured concentrations. Alternatively, the change of regime at $x \approx 0.06$ could be explained by an interaction between the superconducting and itinerant antiferromagnetic phases on the underdoped side of the dome. There have been reports of evidence confirming that these two phases coexist in this region of the phase diagram [Canfield and Bud'ko (2010); Ni et al. (2008b); Drew et al. (2009); Pratt et al. (2009); Christianson et al. (2004); Laplace et al. (2009); Goko et al. (2004); Fernandes et al. (2010)] and also measurements of the zero temperature value of the penetration depth, $\lambda_{ab}(0)$, have shown that it increases by an order of magnitude upon passing into the region of coexistence in this series [Gordon et al. (2010a)], which has been shown to be in quantitative agreement with a theoretical model accounting for competition between $s_{\pm}$-wave superconductivity and itinerant antiferromagnetism for the same charge carriers [Fernandes et al. (2010); Fernandes and Schmalian (2010)].

A different possible explanation for the change in regime at $x \approx 0.06$ in the $Ba(Fe_{1-x}Co_x)_2As_2$ series could be a modulation of the superconducting gap with Co doping. Thermal conductivity measurements [Tanatar et al. (2010)] performed as a function of doping in this series have found that the superconductivity is fully gapped in the ab-plane for all doping levels, but the application of a magnetic field indicates that quasiparticles are excited easitly. Because they are excited easily by a magnetic field, it has been proposed that this is due to a significant anisotropy in the superconducting gap.

Other measurements of the thermal conductivity in this series have been performed with heat current applied both parallel and perpendicular to the c-axis for seven different Co concentrations ranging from x=0.038 (underdoped) to x=0.127 (overdoped) [Reid et al. (2010)]. In zero applied magnetic field, the resulting thermal conductivity for heat current applied perpendicular to the c-axis, more specifically along the a-direction, shows no residual linear term across the entire superconducting phase diagram. The residual linear term is the electronic contribution to the thermal conductivity in the low-temperature limit and if it is a negligible

fraction of the normal state value, then there are no normal state quasiparticles available to transport heat along the measured direction. The situation for heat current applied along the c-axis tells a different story though. Along the c-axis, in zero applied magnetic field, a negligible linear term has been found at optimal doping, but as one moves toward either edge of the superconducting dome, the linear term in the thermal conductivity rises to a significant fraction of the normal state thermal conductivity. This implies that at optimal doping there are no nodes in the gap anywhere on the Fermi surface, but as one moves away from optimal doping, nodes in the gap are present on portions of the Fermi surface that are responsible for c-axis conduction.

The thermal conductivity data taken in applied magnetic fields gives very useful information because the magnetic field acts as another way to excite quasiparticles. For the thermal conductivity measured along the a-axis it has been found that the application of a moderate magnetic field, $H_{c2}/4$, excites quasiparticles along the a-direction just as well as nodal quasiparticles are excited along the c-axis in zero applied magnetic field. This would imply that along portions of the Fermi surface that contribute to in-plane conductance the superconducting gap magnitude is small, but nonzero. Altogether, the thermal conductivity study as a function of doping in $Ba(Fe_{1-x}Co_x)_2As_2$ has been interpreted in terms of a strong $\mathbf{k}$ dependence of the gap $\Delta(\mathbf{k})$ which produces nodes on a Fermi surface sheet with pronounced c-axis dispersion and deep minima on the remaining, quasi two-dimensional sheets. Since the proposed c-axis nodes disappear at optimal doping, it is most likely that they are accidental, meaning that they are not enforced by symmetry, in contrast to the symmetry enforced line nodes in a $d_{x^2-y^2}$-wave superconductor.

The proposed modulation of the superconducting gap with doping in the $Ba(Fe_{1-x}Co_x)_2As_2$ series from thermal conductivity data could explain the doping dependence of the power law exponent from penetration depth measurements in the same series. Since $\Delta\lambda_{ab}(T)$ mainly gives information about the in-plane superconducting gap, it is likely that the decrease near the underdoped edge of the superconducting dome is due to the development of a significant in-plane gap anisotropy. Another question that can arise when comparing the thermal con-

ductivity and penetration depth data in the $Ba(Fe_{1-x}Co_x)_2As_2$ series is if there are no nodes on the Fermi surface at optimal doping, then why isn't the penetration depth exponential? The most probable answer to this question is that penetration depth measurements seem to be more susceptible to impurity scattering than thermal conductivity measurements. The heavy ion irradiation penetration depth study provides very strong evidence for a large contribution to the 122 data from pair-breaking impurity scattering, but a negligible linear term in the thermal conductivity for heat current applied both parallel and perpendicular to the c-axis is very compelling evidence for fully gapped superconductivity at optimal doping in $Ba(Fe_{1-x}Co_x)_2As_2$.

Now let us turn to a discussion of the doping dependence of the penetration depth in the $Ba(Fe_{1-x}Ni_x)_2As_2$ series. Recall that $\Delta\lambda_{ab}(T)$ was measured for five different concentrations ranging from x=0.033 (underdoped) to x=0.072 (overdoped). A power law temperature dependence has been observed for all samples measured and it decreases monotonically from $n \approx$2.2 at x=0.033 to $n \approx$1.6 at x=0.072. Measurements performed in a dilution refrigerator have indicated that this power law temperature dependence persists down to as low as $T = T_c/100$. In addition, for this series $\Delta\lambda_c(T)$ has been measured for two overdoped samples (both x=0.072) and one underdoped sample (x=0.033) and it has been found that for these concentrations near both edges of the superconducting dome the penetration depth exhibits a linear temperature dependence.

First, let us consider the doping dependence of the in-plane penetration depth power law exponent in the $Ba(Fe_{1-x}Ni_x)_2As_2$ series. Compared to the $Ba(Fe_{1-x}Co_x)_2As_2$ series the relative change in n with doping for superconducting concentrations across the phase diagram is quite different. This may seem surprising because both materials share many similar features in their respective temperature-doping phase diagrams and both are the result of transition metal substitutions in the same parent compound. For the Ni doped series, n decreases monotonically from 2.2 for very far underdoped concentrations to 1.6 for very far overdoped ones, while for the Co doped series n is roughly 2 near the underdoped edge and increases toward optimal doping to a value as high as 2.5 for x=0.10. One major difference that exists between the

$Ba(Fe_{1-x}Ni_x)_2As_2$ and $Ba(Fe_{1-x}Co_x)_2As_2$ compounds is the amount of the dopant ion that is needed to completely suppress superconductivity. Since Ni donates two electrons per ion and Co donates only one per ion, roughly half as much Ni is needed to completely suppress superconductivity in this system compared to Co doping [Canfield et al. (2009)]. Since we know that doping in the Ba-based 122 series does induce pair-breaking scattering [Kim et al. (2010a)], the fact that the Co doped crystals require more disorder to achieve superconductivity may imply that the pair-breaking scattering in these two series is not playing exactly the same role. If the doping dependence of the power law exponent is strongly influenced by pair-breaking scattering in these materials, then one viable explanation for the observed difference in the behavior of $n(x)$ for the Co and Ni doped systems is that these two series lie in different regimes of pair-breaking impurity scattering.

As for why the power law exponent n *decreases* as the Ni concentration is increased, perhaps the best understanding of this can come from the result of the heavy ion irradiation study done on the Ni and Co doped 122 systems. From this study it was found that as the impurity concentration increases, the resulting power law exponent decreases for these materials. This could explain why the power law exponent decreases as the Ni concentration increases for those $Ba(Fe_{1-x}Ni_x)_2As_2$ samples on which the penetration depth measurements were performed. However, applying this same logic to the $Ba(Fe_{1-x}Co_x)_2As_2$ series does not work, but arguments may be invoked related to the fact that these materials may be in different impurity scattering regimes. Another possible explanation, but albeit much more complicated, is that the doping dependence of the superconducting gaps in Ni and Co doped 122 systems is not the same, but before such complicated assertions are made it is perhaps wiser to search for a simpler explanation where the superconductivity in these two very similar systems is fundamentally the same.

The observed linear temperature dependence of $\Delta\lambda_c(T)$ in the $Ba(Fe_{1-x}Ni_x)_2As_2$ series for two samples near the overdoped edge of the phase diagram and one sample near its underdoped edge has been interpreted as the formation of line nodes in the superconducting gap on portions of the Fermi surface that contribute to c-axis conduction. This is consistent with

the previously mentioned thermal conductivity data in $Ba(Fe_{1-x}Co_x)_2As_2$, where their data has been interpreted in terms of a full superconducting gap at optimal doping that is doping dependent with the formation of c-axis nodes in concentrations that are near both edges of the superconducting dome [Reid et al. (2010)]. Naturally, for this hypothesis to be tested further $\Delta\lambda_c(T)$ measurements should be performed on many different doping levels spanning the entire superconducting region of the phase diagrams for both Ba-based 122 systems to confirm that indeed there is not a linear temperature dependence at optimal doping, indicating that these c-axis nodes are accidental and they disappear at optimal doping.

To conclude the discussion of the doping dependence of the London penetration depth in $Ba(Fe_{1-x}T_x)_2As_2$ (T=Co,Ni) superconductors, a power law temperature dependence of the form $\Delta\lambda_{ab}(T) \propto T^n$ has been observed for all samples and the power n has been found to change with the doping level x in the material. It is known that the origin of the power law temperature dependence is pair-breaking impurity scattering, which is supported by heavy ion irradiation measurements in $Ba(Fe_{1-x}T_x)_2As_2$ (T=Co,Ni) and the observation of an exponential temperature dependence in the intrinsically clean LiFeAs superconductor. The doping dependence of the power law exponent could arise from a doping-dependent pair-breaking impurity scattering mechanism or from a modulation of the superconducting gap with doping, which is supported by thermal conductivity measurements in $Ba(Fe_{1-x}Co_x)_2As_2$ and consistent with the linear temperature dependence of $\Delta\lambda_c(T)$ for concentrations near both edges of the superconducting dome in $Ba(Fe_{1-x}Ni_x)_2As_2$.

6.4 The doping dependence of $\Delta\lambda_{ab}(T)$ in $Ba(Fe_{1-x}T_x)_2As_2$ (T=Ru,Rh,Pd,Pt,Co+Cu)

The in-plane London penetration depth has been measured in single crystals at various doping levels from the $Ba(Fe_{1-x}T_x)_2As_2$ series with T=Ru,Rh,Pd,Pt,Co+Cu. For all measured concentrations, the variation of the in-plane penetration depth from its zero temperature value has been found to follow a power law behavior of the form $\Delta\lambda_{ab}(T) \propto T^n$ with n taking values that range from 1.5 to 2.5. The power law exponent, n, for each sample was determined by

fitting the penetration depth below $T_c/3$, which is usually referred to as the low-temperature region of the data. Although the measurements done on the $Ba(Fe_{1-x}T_x)_2As_2$ compounds are less complete in terms of doping levels studied than those done on the Co and Ni doped materials discussed in the previous section, they are still useful for studying the effect of transition metal doping on the Fe site of $BaFe_2As_2$.

In general, it has been found for $Ba(Fe_{1-x}T_x)_2As_2$ (T=Ni,Ru,Pd,Pt,Co+Cu) superconductors that as x increase, the power law exponent n decreases, which is at least qualitatively consistent with the conclusions derived from the heavy ion irradiation penetration depth experiment [Kim et al. (2010a)]. This is in contrast to the doping dependence of the power law exponent in the $Ba(Fe_{1-x}Co_x)_2As_2$ and $Ba(Fe_{1-x}Rh_x)_2As_2$ series. It is interesting to note that both systems that do not show a decrease of n with increaseing x, namely the Co and Rh systems, both donate the same nominal number of carriers to the charge environment of the crystal.

Most probably, the origin of the power law exponent in all transition metal substituted Ba-based 122 iron-based superconductors is the same, with that being pair-breaking impurity scattering [Kim et al. (2010a)]. It is believed that this power law dependence evolves into an exponential one for an iron-based superconductor in the intrinsically clean limit [Kim et al. (2010c)]. However, the doping dependence of the power law exponent for $Ba(Fe_{1-x}T_x)_2As_2$ (T=Co,Ni,Ru,Rh,Pd,Pt,Co+Cu) superconductors has not yet been understood. For T=Co and Rh, the power law exponent has been found to display a different doping dependence than all other transition metal substitutions and future measurements should be poised to address why this is so.

6.5 The evolution of $\lambda_{ab}(0)$ and $\rho_s(T)$ in $Ba(Fe_{1-x}Co_x)_2As_2$

The ability to measure the absolute value of the London penetration depth in a superconductor is valuable because not only does it allow one to construct the normalized superfluid density, but also it can be used to study the effects arising from interactions between the superconductivity and other nearby phases. A novel procedure has been developed to allow

for TDR frequency shift measurements to be calibrated to obtain the absolute value of the penetration depth in a superconductor that takes advantage of the calibration point supplied by a thin film of aluminum deposited onto the surface of the sample to be studied.

By using the aforementioned calibration procedure, the zero temperature value of the in-plane London penetration depth has been measured as a function of Co doping level, x, in $Ba(Fe_{1-x}Co_x)_2As_2$ for 13 samples with concentrations ranging from very underdoped (x=0.038) to beyond optimally doped (x=0.10) [Gordon et al. (2010a)]. Far overdoped samples were not measured because at the time of these experiments, high quality single crystals were not yet available in that range of the phase diagram. For $x \geq 0.047$, $\lambda_{ab}(0)$ has been found to have values in the range of roughly 200±75 nm, but for $x < 0.047$, $\lambda_{ab}(0)$ statistically increases by almost a factor of 5 to values as high as 935 nm, which was later verified by a different type of measurement that is sensitive to the penetration depth [Luan et al. (2011)]. There appears to be a constant scatter in the data points of approximately ±75 nm for all concentrations, which probably means that the source of the scatter is the same for all samples. Most likely, it arises due to inhomogeneities or imperfections in the Al film. Along with previous measurements in this same series [Gordon et al. (2009b,a)] of the variation of the in-plane penetration depth with respect to its low-temperature value, $\Delta\lambda_{ab}(T)$, these values of $\lambda_{ab}(0)$ have been used to properly normalize the superfluid density, $\rho_s(T) = (1 + \Delta\lambda(T)/\lambda(0))^{-2}$, in order to study the doping evolution of the superconducting gap, $\Delta(\mathbf{k})$.

The most likely explanation for the observed statistical increase in $\lambda_{ab}(0)$ by a factor of 5 upon moving into the far underdoped region of the phase diagram is a competition between the superconducting and itinerant antiferromagnetic phases for the same charge carriers. In support of this hypothesis is the fact that many different experiments have shown that it is very likely that these two phases coexist in $Ba(Fe_{1-x}Co_x)_2As_2$ [Canfield and Bud'ko (2010); Ni et al. (2008b); Drew et al. (2009); Pratt et al. (2009); Christianson et al. (2004); Laplace et al. (2009); Goko et al. (2004); Fernandes et al. (2010)]. In addition, a theoretical model [Fernandes and Schmalian (2010)] has been developed in order to calculate the expected increase in $\lambda_{ab}(0)$ in the coexistence region based on a competition between an $s_{\pm}$-wave superconducting state

and an itinerant antiferromagnetic phase for the same charge carriers. This theory has used actual neutron scattering data to produce curves for the doping dependence of $\lambda_{ab}(0)$, which fit the experimental data quite well after considering the simplicity of the model.

Nearly all of the samples that were used in this study already had $\Delta\lambda_{ab}(T)$ measurements performed on them [Gordon et al. (2009b,a)], so the measured values of $\lambda_{ab}(0)$ allowed for the construction of the normalized superfluid density by using $\rho_s(T) = (1 + \Delta\lambda(T)/\lambda(0))^{-2}$ for various superconducting concentrations across the phase diagram of $Ba(Fe_{1-x}Co_x)_2As_2$. The superfluid density curves for all measured concentrations do share some common features, mainly that there is a reduction of the superfluid density at all temperatures, especially intermediate ones, with respect to the standard curve for the single gapped, isotropic case and there is a region of upward concavity just below T_c. This behavior of the normalized superfluid density with temperature is qualitatively the same as what has been measured for two gap superconductors like MgB_2 or V_3Si [Kogan et al. (2009)]. The optimally doped superfluid density curve remains above the superfluid density curves for underdoped samples as well as for the sample that is beyond optimal doping. This could be explained by a modulation of the superconducting gap with doping that is full at optimal doping, even though pair-breaking scattering still produces a power law temperature dependence there, and the formation of nodes for concentrations moving away from optimal doping. This picture would be consistent with recent measurements of the in-plane and c-axis thermal conductivity in this same series [Reid et al. (2010)].

6.6 Pair-breaking scattering effects from the penetration depth prefactor

Understanding the role of pair-breaking impurity scattering effects in superconductors is vital to discovering the true superconducting gap symmetry in materials where these contributions are not negligible. By measuring the prefactor of the penetration depth for various iron-based superconductors [Gordon et al. (2010b)], a theoretical prediction was able to be tested and it has been found to describe the data quite successfully. This result supports the hypothesis that pair-breaking impurity scattering effects are important for understanding and

interpreting the penetration depth data in iron-based superconductors.

The samples used in this study were six concentrations from the $Ba(Fe_{1-x}Co_x)_2As_2$ series, five concentrations from the $Ba(Fe_{1-x}Ni_x)_2As_2$ series, the hole doped $(Ba_{0.07}K_{0.30})Fe_2As_2$ compound, $Fe_{1.001}(Se_{0.367}Te_{0.632})$, $LaFeAs(O_{0.9}F_{0.1})$ and $NdFeAs(O_{0.9}F_{0.1})$. With such a diverse collection of iron-based superconductors, the results have been interpreted as being general to all classes of these materials.

The variation of the in-plane penetration depth with temperature, $\Delta\lambda_{ab}(T)$, was measured for all of the previously mentioned samples. The low-temperature region of each data curve was fit to a function of the form $\Delta\lambda_{ab} = \beta T^2$ in order to extract the prefactor β for each sample, in contrast to fits of the form $\Delta\lambda_{ab}(T) = CT^n$ where the units on C depend on the power law value n. The prefactor β was determined for these samples in order to test a theoretical prediction stating $\beta \propto 1/T_c^3$, which was derived from a quasiclassical version of the weak-coupling Gor'kov theorgy that holds for a general Fermi surface geometry and requires that the average value of the superconducting gap about the Fermi surface is very small. According to this model, the previously stated dependence of β on T_c arises only from pair-breaking impurity scattering, making this an excellent way through which the pair-breaking impurity scattering in these superconductors can be studied. This same model has been successful in describing the specific heat jump versus T_c and the slopes of the upper critical fields in these materials [Kogan (2009); Bud'ko et al. (2009)].

The fact that the prefactors determined from the low-T fits are so well described by the $\beta \propto 1/T_c^3$ relationship is strongly in support of a non-negligible contribution to the penetration depth data from pair-breaking impurity scattering, but no model is perfect and the weak points of this theory should be reviewed. First of all, the assumption that the average value of the order parameter is very small would be consistent with the proposed $s_{\pm}$-wave symmetry, but it is still not clear if this is the true superconducting gap symmetry in the iron-based superconductors. There are some who believe that many different ground states are close to each other for these materials [Maier et al. (2011); Wang et al. (2011); Das and Balatsky (2011)], i.e. $s_{\pm}$-wave and nodeless d-wave states, and more than one has actually been realized in these

materials, which could explain the reported experimental discrepancies. Another concern is that the $\beta \propto 1/T_c^3$ dependence was derived under the assumption that the material is in the strongly disordered limit. The problem with this assumption is that a rough calculation of the T_c that would correspond to the clean limit of the material would be on the order of room temperature, which most people believe is highly unlikely.

Although this model has been scrutinized by many, it is still the result of a wonderful effort to attempt to describe the physics of these materials. There are obvious problems that arise when considering the simplifying assumptions of this model, but the ability for it to describe the penetration depth prefactor versus T_c [Gordon et al. (2010b)], the specific heat jump versus T_c [Bud'ko et al. (2009)] and the slopes of the upper critical fields [Kogan (2009)] is actually quite amazing.

6.7 Closing remarks

Superconductivity has come a long way since its initial discovery in low T_c materials that are now considered to be "conventional" [Onnes (1911)]. Many researchers hoped that the discovery of high-T_c superconductivity in the iron-based superconductors [Kamihara et al. (2008)] would shed enough light to solve the perplexing puzzle that was put before us in 1986 with the discovery of the high-T_c cuprates [Müller and Bednorz (1987)], but to no avail this hope has not yet been realized.

One major drawback for experimentalists after the discovery of the cuprates was the lack of availability of large, high quality single crystals from which trustworthy experimental results could be obtained. In fact, many people believed that the low-temperature penetration depth in the cuprates was $\Delta\lambda \propto T^2$ until it was shown that this observation was an artifact of impurity scattering in samples of poor quality nearly seven years after their discovery [Hardy et al. (1993)]. Fortunately for the iron-based superconductors, the sample quality for some compounds became quite good just months after their initial discovery, making it a little easier to trust experimental reports than it was for the case of the cuprates.

Just as it was the case for the cuprates, the initial reports of the temperature dependence

of the low-T penetration depth in the iron-based superconductors were spurious [Malone et al. (2009)]. These claims stated that an exponential saturation of the penetration depth at low-temperatures had been observed in $SmFeAs(O_{1-x}F_x)$, which was taken as evidence for fully gapped superconductivity. According to our present understanding, the exponential temperature dependence was actually a power law temperature dependence plus a low-T upturn arising from contributions to the penetration depth from the rare earth ions. This has been confirmed by performing a careful analysis on $NdFeAs(O_{0.9}F_{0.1})$, where the rare earth ordering temperature and moment size were both known, to account for the Nd magnetism and also by measuring the non-magnetic $LaFeAs(O_{0.9}F_{0.1})$, which indeed does show a power law behavior with no upturn in the penetration depth at low temperatures. [Martin et al. (2009b)].

As for other iron-based superconductors, most measurements have indicated that the low-temperature form of the in-plane penetration depth follows a power law relation of the form $\Delta\lambda_{ab} \propto T^n$ [Gordon et al. (2009b,a, 2010b); Kim et al. (2010b,a)]. This power law dependence was initially interpreted as arising from point nodes in the superconducting gap [Gordon et al. (2009b)], but after more careful measurements were performed it is currently accepted that it arises from pair-breaking impurity scattering effects. This claim has gained support from penetration depth measurements done on samples that were irradiated with heavy ions in order to study the effects of disorder in a very controlled way [Kim et al. (2010a)]. A decrease of the power law exponent with increasing disorder was observed, in line with predictions for the popular $s_{\pm}$-wave symmetry of the superconducting gap [Mazin et al. (2008)] if impurity scattering effects are included [Chubukov et al. (2008)], which predicts that in the clean limit it should saturate with temperature exponentially. In fact, the claim that pair-breaking effects have a significant effect on the behavior of the penetration depth is further supported by an exponential saturation of the penetration depth that has been observed in LiFeAs [Kim et al. (2010c)], which is believed to be an iron-based superconductor in the intrinsically clean limit. One last piece of supporting evidence for strong pair-breaking effects in the iron-based superconductors comes from measuring the penetration depth prefactor, β from $\Delta\lambda(T) = \beta T^2$, which has been found to follow $\beta \propto 1/T_c^3$, consistent with a theoretical result derived assuming

a strong pair-breaking contribution [Kogan (2009)]. This behavior has been found to hold for samples from the $Ba(Fe_{1-x}Co_x)_2As_2$, $Ba(Fe_{1-x}Ni_x)_2As_2$, $(Ba_{1-x}K_x)Fe_2As_2$, $Fe_{1+y}(Se_{1-x}Te_x)$, $LaFeAs(O_{1-x}F_x)$ and $NdFeAs(O_{1-x}F_x)$ classes of iron based superconductors [Gordon et al. (2010b)]. Perhaps future measurements should focus on understanding the exact nature of the pair-breaking scattering and how it can change between different classes of the iron-based superconductor family.

Careful studies have also been done to measure the doping dependence of the power law exponent, n, in the $Ba(Fe_{1-x}Co_x)_2As_2$ [Gordon et al. (2009b,a)] and $Ba(Fe_{1-x}Ni_x)_2As_2$ [Martin et al. (2010a)] series. For the $Ba(Fe_{1-x}Co_x)_2As_2$ series, it has been found that n is a maximum near optimal doping and decreases to a value as low as 2 for very underdoped concentrations. This has been interpreted as being consistent with thermal conductivity studies that have found evidence for the formation of c-axis accidental nodes that appear upon departure from optimal doping [Reid et al. (2010)]. A linear temperature dependence of the out-of-plane component of the penetration depth, $\Delta\lambda_c$, in samples of $Ba(Fe_{1-x}Ni_x)_2As_2$ that have dopings near the edges of the superconducting dome has also been taken to be in support of this claim [Martin et al. (2010a)]. However, for all other transition metal dopings studied, including Ni, the power law has been found to decrease with increasing disorder, consistent with the observations made during the heavy ion irradiation study [Kim et al. (2010a)]. From a penetration depth standpoint, one major question to be answered is the exact role of pair-breaking impurity scattering effects in these superconductors, which future measurements should be planned to address.

Another question to be answered with respect to superconductivity in the iron-based superconductors pertains to the exact role played by magnetism. One popular idea is that the cuprates and the iron-based superconductors are both examples of superconductors mediated by spin fluctuations, analagous to phonon-mediated pairing in BCS superconductors [Taillefer (2010); Monthoux et al. (2007)]. From penetration depth measurements in $Ba(Fe_{1-x}Co_x)_2As_2$, it has been found that $\lambda_{ab}(0)$ increases upon moving from the pure superconducting state to the region of coexistence by a factor of 5 in the temperature-doping phase diagram. Since

$\lambda_{ab}^2(0)$ is inversely proportional to the density of superconducting electrons [Tinkham (1996)], the most natural explanation for the increase in the coexistence region is a competition between the superconducting state and the itinerant antiferromagnetic state for the same charge carriers, which has been well described by a theoretical model to account for such a competition [Fernandes and Schmalian (2010)]. Whether superconductivity and antiferromagnetism are competing or not, it is still not clear what the role played by the magnetism is and this is one question that future measurements should definitely address.

The same calibration procedure that allowed for the measurement of $\lambda_{ab}(0)$ in $Ba(Fe_{1-x}Co_x)_2As_2$ has also allowed for the construction of the normalized superfluid density by using, $\rho_s(T) = [\lambda(0)/\lambda(T)]^2$, which has allowed for the study of the evolution of the superconducting gap with doping. This procedure was recently developed to allow for the measurement of the absolute value of the London penetration depth in superconductors by using an aluminum coating procedure for the sample along with usual TDR frequency shift measurements. For the $Ba(Fe_{1-x}Co_x)_2As_2$ series, the $\rho_s(T)$ curves for all dopings show a suppression over the entire temperature range from base to T_c, consistent with the behavior for multigap superconductors like MgB_2 and V_3Si [Kogan et al. (2009)]. In addition, the optimally doped $\rho_s(T)$ curve is larger over the whole temperature range than underdoped and overdoped samples. This would be consistent with the formation of nodal regions in the gap for concentrations moving away from optimal doping. These results are in support of multigap superconductivity in the iron-based superconductors, as do many others, but still much is to be learned about the gap structure possessed by these superconductors, so future measurements should also pay close attention to these details.

To conclude, measurements of the London penetration depth have been performed on several different materials from the family of iron-based superconductors with the hope of elucidating the structure of the momentum-dependent superconducting gap to shed light on the pairing mechanism in these materials. A strong pair-breaking impurity scattering contribution to the penetration depth has been uncovered, which likely arise from effects associated with multigap superconductivity. In addition, there is evidence to suggest that in the clean limit

these materials display an exponential temperature dependence of the penetration depth at low-temperatures. From doping dependent penetration depth measurements in the Ba-based 122 series, evidence has been found for the formation of c-axis accidental nodes in the superconducting gap for concentrations near the edges of the superconducting dome. Also evidence for a competition between the superconducting and itinerant antiferromagnetic phases has been found by measuring the doping dependence of $\lambda_{ab}(0)$. Future measurements should focus on understanding the exact structure of the superconducting gap in these materials and also to pinpoint the pairing mechanism. The hope is that eventually not only will a better understanding of superconductivity in the iron-based superconductors be achieved, but an understanding of the phenomenon of superconductivity in general.

Bibliography

Abanov, A., Chubukov, A. V., and Schmalian, J. (2001). Quantum-critical superconductivity in underdoped cuprates. *Europhys. Lett.*, 55:369.

Abrikosov, A. A. (1957). On the magnetic properties of superconductors of the second group. *Soviet Phyics JETP*, 5:1174.

Abrikosov, A. A. (2004). Nobel lecture: Type-II superconductors and the vortex lattice. *Rev. Mod. Phys.*, 76:975.

Abrikosov, A. A. and Gor'kov, L. P. (1960). *Zh. Eksp. Teor. Fiz.*, 39:1781.

Aczel, A., Baggio-Saitovitch, E., Bud'ko, S. L., Canfield, P. C., Carlo, J. P., Chen, G. F., Dai, P., Goko, T., Hu, W. Z., Luke, G. M., Luo, J. L., Ni, N., Sanchez-Candela, D. R., Tafti, F. F., Wang, N. L., Williams, T. J., Yu, W., and Uemura, Y. J. (2008). Muon-spin-relaxation studies of magnetic order and superfluid density in antiferromagnetic NdFeAsO, $BaFe_2As_2$, and superconducting $Ba_{1-x}K_xFe_2As_2$. *Phys. Rev. B*, 78:214503.

Aguilar, R. V., Bilbro, L. S., Lee, S., Bark, C. W., Jiang, J., Weiss, J. D., Hellstrom, E. E., Larbalestier, D. C., Eom, C. B., and Armitage, N. P. (2010). Pair-breaking effects and coherence peak in the terahertz conductivity of superconducting $BaFe_{2-2x}Co_{2x}As_2$. *Phys. Rev. B*, 82:180514(R).

Aiura, Y., Sato, K., Iwasawa, H., Nakashima, Y., Anzai, H., Ino, A., Arita, M., Shimada, K., an M. Taniguchi, H. N., Hase, I., Miyazawa, K., Shirage, P., Eisaki, H., Kito, H., and Iyo, A. (2008). Sheet dependence on superconducting gap in oxygen-deficient iron-based oxypnictide superconductors $NdFeAsO_{0.85}$. *J. Phys. Soc. Jpn.*, 77:103712.

Anderson, P. W. (1959). Theory of dirty superconductors. *J. Phys. Chem. Solids*, 11:26.

Annett, J., Goldenfeld, N., and Renn, S. R. (1991). Interpretation of the temperature dependence of the electromagnetic penetration depth in $YBa_2Cu_3O_{7-\delta}$. *Phys. Rev. B*, 43:2778.

Ashcroft, N. W. and Mermin, N. D. (1976). *Solid State Physics*. Thomson Learning, Inc.

Bardeen, J., Cooper, L. N., and Schrieffer, J. R. (1957). Theory of superconductivity. *Phys. Rev.*, 108:1175.

Basov, D. N. and Timusk, T. (2005). Electrodynamics of high-T_c superconductors. *Rev. Mod. Phys.*, 77:721.

Bobowski, J. S., Baglo, J. C., Day, J., Dosanjh, P., Ofer, R., Ramshaw, B. J., Liang, R., Bonn, D. A., Hardy, W. N., Luo, H., Wang, Z.-S., Fang, L., and Wen, H.-H. (2010). Precision microwave electrodynamic measurements of K- and Co-doped $BaFe_2As_2$. *arXiv:1009.3941*.

Bouquet, F., Wang, Y., Fisher, R. A., Hinks, D. G., Jorgensen, J. D., Junod, A., and Phillips, N. E. (2001a). Phenomological two-gap model for the specific heat of MgB_2. *Europhys. Lett.*, 56:097005.

Bouquet, F., Wang, Y., Fisher, R. A., Hinks, D. G., Jorgensen, J. D., Junod, A., and Phillips, N. E. (2001b). Temperature-dependent anisotropy of the penetration depth and coherence lengt of MgB_2. *Europhys. Lett.*, 56:097005.

Buchanan, M. (2001). Mind the pseudogap. *Nature*, 409:8.

Bud'ko, S. L., Ni, N., and Canfield, P. C. (2009). Jump in specific heat at the superconducting transition temperature in $Ba(Fe_{1-x}Co_x)_2As_2$ and $Ba(Fe_{1-x}Ni_{1-x})_2As_2$. *Phys. Rev. B*, 79:220516.

Canfield, P. C. and Bud'ko, S. L. (2010). FeAs-based superconductivity: A case study of the effects of transition metal doping on $BaFe_2As_2$. *Annu. Rev. Condens. Matter Phys.*, 1:27–50.

Canfield, P. C., Bud'ko, S. L., Ni, N., Yan, J. Q., and Kracher, A. (2009). Decoupling of the superconducting and magnetic/structural phase transitions in electron-doped $BaFe_2As_2$. *Phys. Rev. B*, 80:060501.

Chandrasekhar, B. S. and Einzel, D. (1993). The superconducting penetration depth from the semiclassical model. *Ann. Physik*, 2:535.

Chen, T. Y., Tesanovic, Z., Liu, R. H., Chen, X. H., and Chien, C. L. (2008). A BCS-like gap in the superconductor $SmFeAsO_{0.85}F_{0.15}$. *Nature (London)*, 453:1224.

Christianson, A. D., Lumsden, M. D., Nagler, S. E., MacDougall, G. J., McGuire, M. A., Sefat, A. S., Jin, R., Sales, B. C., and Mandrus, D. (2004). Static and dynamic magnetism in underdoped superconductor $BaFe_{1.92}Co_{0.08}As_2$. *Phys. Rev. Lett.*, 103:087002.

Chubukov, A. V., Efremov, D. V., and Eremin, I. (2008). Magnetism, superconductivity, and pairing symmetry in iron-based superconductors. *Phys. Rev. B*, 78:134512.

Cooper, L. N. (1956). Bound electron pairs in a degenerate fermi gas. *Physical Review*, 104:1189.

Cvetkovic, V. and Tesanovic, Z. (2009). Multiband magnetism and superconductivity in Fe-based compounds. *Europhys. Lett.*, 85:37002.

Das, T. and Balatsky, A. V. (2011). Stripes, spin resonance and $d_{x^2-y^2}$-pairing symmetry in FeSe-based layered superconductors. *arXiv:1101.6056*.

Ding, H., Richard, P., Nakayama, K., Sugawara, K., Arakane, T., Sekiba, Y., Takayama, A., Souma, S., Sato, T., Takahashi, T., Wang, Z., Dai, X., Fang, Z., Chen, G. F., Luo, J. L., and Wang, N. L. (2008). Observation of fermi-surface-dependent nodeless superconducting gaps in $Ba_{0.6}K_{0.4}Fe_2As_2$. *Europhys. Lett.*, 83:47001.

Drew, A. J., Niedermayer, C., Baker, P. J., Pratt, F. L., Blundell, S. J., Lancaster, T., Liu, R. H., Wu, G., Chen, X. H., Watanabe, I., Malik, V. K., Dubroka, A., Rössle, M., Kim,

K. W., Baines, C., and Bernhard, C. (2009). Coexistence of static magnetism and superconductivity in $SmFeAsO_{1-x}F_x$ as revealed by muon spin rotation. *Nature Mater.*, 8:310.

Drew, A. J., Pratt, F. L., Lancaster, T., Blundell, S. J., Baker, P. J., Liu, R. H., Wu, G., Chen, X. H., Watanabe, I., Malik, V. K., Dubroka, A., Kim, K. W., Rössle, M., and Bernhard, C. (2008). Coexistence of magnetic fluctuations and superconductivity in the pnictide high temperature superconductor $SmFeAsO_{1-x}F_x$ measured by muon spin rotation. *Phys. Rev. Lett*, 101:097010.

Drude, P. (1900). *Annalen der Physik*, 1:566.

Eilenberger, G. (1964). *Z. Phys.*, 214:195.

Eilenberger, G. (1968). *Z. Phys. A*, 214:195.

Einzel, D., Hirschfeld, P. J., Gross, F., Chandrasekhar, B. S., Andres, K., Ott, H. R., Beuers, J., Fisk, Z., and Smith, J. L. (1986). Magnetic field penetration depth in the heavy-electron superconductor UBe_{13}. *Phys. Rev. Lett.*, 56:2513.

Evtushinsky, D. V., Inosov, D. S., Zabolotnyy, V. B., Koitzsch, A., Knupfer, M., Büchner, B., Viazovska, M. S., Sun, G. L., Hinkov, V., Boris, A. V., Lin, C. T., Keimer, B., Varykhalov, A., Kordyuk, A. A., and Borisenko, S. V. (2009a). Momentum dependence of the superconducting gap in $Ba_{1-x}K_xFe_2As_2$. *Phys. Rev. B*, 79:054517.

Evtushinsky, D. V., Inosov, D. S., Zabolotnyy, V. B., Viazovska, M. S., Khasanov, R., Amato, A., Klaus, H. H., Luetkens, H., Niedermayer, C., Sun, G. L., Hinkov, V., Lin, C. T., Varykhalov, A., Koitzsch, A., Knupfer, M., Büchner, B., Kordyuk, A. A., and Borisenko, S. V. (2009b). Momentum-resolved superconducting gap in the bulk of $Ba_{1-x}K_xFe_2As_2$ from combined ARPES and μSR measurements. *New. J. Phys.*, 11:055069.

Fang, L., Luo, H., Cheng, P., Wang, Z., Jia, Y., Mu, G., Shen, B., Mazin, I. I., Shan, L., Ren, C., and Wen, H. H. (2009). Roles of multiband effects and electron-hole asymmetry in the superconductivity and normal-state properties of $Ba(Fe_{1-x}Co_x)_2As_2$. *Phys. Rev. B*, 80:140508(R).

Fernandes, R. and Schmalian, J. (2010). Transfer of optical spectral weight in magnetically ordered superconductors. *Phys. Rev. B*, 82:014520.

Fernandes, R. M., Pratt, D. K., Tian, W., Zarestky, J., Kreyssig, A., Nandi, S., Kim, M. G., Thaler, A., Ni, N., Canfield, P. C., McQueeney, R. J., Schmalian, J., and Goldman, A. I. (2010). Unconventional pairing in the iron arsenide superconductors. *Phys. Rev. B*, 81:140501(R).

Ginsberg, D. M. (1994). *Physical Properties of High Temperature Superconductors III*. World Scientific Publishing Co.

Gofryk, K., Sefat, A. S., McGuire, M. A., Sales, B. C., Mandrus, D., Thompson, J. D., Bauer, E. D., and Ronning, F. (2009). Doping-dependent specific heat study of the superconducting gap in $Ba(Fe_{1-x}Co_x)_2As_2$. *Phys. Rev. B*, 81:184518.

Goko, T., Aczel, A. A., Baggio-Saitovitch, E., Bud'ko, S. L., Canfield, P. C., Carlo, J. P., Chen, G. F., Dai, P., Hamann, A. C., Hu, W. Z., Kageyama, H., Luke, G. M., Luo, J. L., Nachumi, B., N. Ni, D. R., Sanchez-Candela, D. R., Savici, A. T., Sikes, K. J., Wang, N. L., Wiebe, C. R., Williams, T. J., Yamamoto, T., Yu, W., and Uemura, Y. J. (2004). Superconducting state coexisting with a phase-separated static magnetic order in $(Ba,K)Fe_2As_2$, $(Sr,Na)Fe_2As_2$, and $CaFe_2As_2$. *Phys. Rev. Lett.*, 92:147201.

Golubov, A. A. and Mazin, I. I. (1997). Effect of magnetic and non-magnetic impurities on highly anisotropic superconductivity. *Phys. Rev. B*, 55:15146.

Gordon, R. T., Kim, H., Salovich, N., Giannetta, R. W., Fernandes, R. M., Kogan, V. G., Prozorov, T., Bud'ko, S. L., Canfield, P. C., Tanatar, M. A., and Prozorov, R. (2010a). Doping evolution of the absolute value of the London penetration depth and superfluid density in single crystals of $Ba(Fe_{1-x}Co_x)_2As_2$. *Phys. Rev. B*, 48:4219.

Gordon, R. T., Kim, H., Tanatar, M. A., Prozorov, R., and Kogan, V. G. (2010b). London penetration depth and strong pair breaking in iron-based superconductors. *Phys. Rev. B*, 81:180501(R).

Gordon, R. T., Martin, C., Kim, H., Ni, N., Tanatar, M. A., Schmalian, J., Mazin, I. I., Bud'ko, S. L., Canfield, P. C., and Prozorov, R. (2009a). London penetration depth in single crystals of $Ba(Fe_{1-x}Co_x)_2As_2$ spanning underdoped to overdoped compositions. *Phys. Rev. B*, 79:100506(R).

Gordon, R. T., Ni, N., Martin, C., Tanatar, M. A., Vannette, M. D., Kim, H., Samolyuk, G. D., Schmalian, J., Nandi, S., Kreyssig, A., Goldman, A. I., Yan, J. Q., Bud'ko, S. L., Canfield, P. C., and Prozorov, R. (2009b). Unconventional London penetration depth in single-crystal $Ba(Fe_{0.93}Co_{0.07})_2As_2$ superconductors. *Phys. Rev. Lett.*, 102:127004.

Gordon, R. T., Vannette, M. D., Martin, C., Nakajima, Y., Tamegai, T., and Prozorov, R. (2008). Two-gap superconductivity seen in penetration-depth measurements of $Lu_2Fe_3Si_5$. *Phys. Rev. B*, 78:024514.

Gorter, C. J. (1935). Notes on the supraconductivity of alloys. *Physica*, 2:449.

Gorter, C. J. and Casimir, H. B. G. (1934). *Phys. Z.*, 35:963.

Grafe, H.-J., Paar, D., Lang, G., Curro, N. J., Behr, G., Werner, J., Hamann-Borrero, J., Hess, C., Leps, N., Klingeler, R., and Büchner, B. (2008). ^{75}As nmr studies of superconducting $LaFeAsO_{0.9}F_{0.1}$. *Phys. Rev. Lett.*, 101:047003.

Hardy, W. N., Bonn, D. A., Morgan, D. C., Liang, R., and Zhang, K. (1993). Precision measurements of the temperature dependence of λ in $YBa_2Cu_3O_{6.95}$: Strong evidence for nodes in the gap function. *Phys. Rev. Lett.*, 70:3999.

Harlingen, D. J. V. (1995). Phase-sensitive tests of the symmetry of the pairing state in the high-temperature superconductors-Evidence for $d_{x^2-y^2}$ symmetry. *Rev. Mod. Phys.*, 67:515–535.

Hashimoto, K., Shibauchi, T., Kato, T., Ikada, K., Okazaki, R., Shishido, H., Ishikado, M., Kito, H., Iyo, A., Eisaki, H., Shamoto, S., and Matsuda, Y. (2009). Microwave penetration depth and quasiparticle conductivity of $PrFeAsO_{1-y}$ single crystals: Evidence for a full-gap superconductor. *Phys. Rev. Lett*, 102:017002.

Hauser, J. J. (1972). Penetration depth and related properties of Al films with enhanced superconductivity. *J. Low Temp. Phys.*, 7:335.

Hiebl, K. and Rogl, P. (1985). Magnetism and structural chemistry of ternary silicides (RE,Th,U)Pt_2Si_2 (RE=Rare Earth). *J. Magn. Magn. Mater.*, 50:39.

Hiraishi, M., Kadono, R., Takeshita, S., Miyazaki, M., Koda, A., Okabe, H., and Akimitsu, J. (2009). Full gap superconductivity in $Ba_{0.6}K_{0.4}Fe_2As_2$ probed by muon spin rotation. *J. Phys. Soc. Jpn.*, 78:023710.

Hirschfeld, P. J. and Goldenfeld, N. (1993). Effect of strong scattering on the low-temperature penetration depth of a *d*-wave superconductor. *Phys. Rev. B*, 48:4219.

Hosono, H. (2010). Layered iron pnictide superconductors: discovery and current status. *Annu. Rev. Condens. Matter Phys.*, 1:27–50.

Izawa, K., Nakajima, Y., Goryo, J., Matsuda, Y., Osaki, S., Sugawar, H., Sato, H., Thalmeier, P., and Maki, K. (2003). Multiple superconducting phases in new heavy fermion superconductor $PrOs_4Sb_{12}$. *Phys. Rev. Lett.*, 90:117001.

Johnston, D. (2010). The puzzle of high temperature superconductivity in layered iron pnictides and iron chalcogenides. *Advances in Physics*, 59:803–1061.

Kamihara, Y., Watanabe, T., Hirano, M., and Hosono, H. (2008). Iron-based layered superconductor La[$O_{1-x}F_x$]FeAs (x=0.05-0.12) with T_c=26 K. *J. Am. Chem. Soc.*, 130:3296.

Khasanov, R., Evtushinsky, D. V., Amato, A., Klaus, H. H., Luetkens, H., Niedermayer, C., Büchner, B., Sun, G. L., Lin, C. T., Park, J. T., Inosov, D. S., and Hinkov, V. (2009). Two-gap superconductivity in $Ba_{1-x}K_xFe_2As_2$: A complimentary study of the magnetic penetration depth by muon-spin rotation and angle-resolved photoemission. *Phys. Rev. Lett.*, 102:187005.

Kim, H., Gordon, R. T., Tanatar, M. A., Hua, J., Welp, U., Kwok, W. K., Ni, N., Bud'ko, S. L., Canfield, P. C., Vorontsov, A. B., and Prozorov, R. (2010a). London penetration

depth in $Ba(Fe_{1-x}T_x)_2As_2$ (T=Co,Ni) superconductors irradiated with heavy ions. *Phys. Rev. B*, 82:060518(R).

Kim, H., Martin, C., Gordon, R. T., Tanatar, M. A., Hu, J., Qian, B., Mao, Z. Q., Hu, R., Petrovic, C., Salovich, N., Giannetta, R., and Prozorov, R. (2010b). London penetration depth and superfluid density of single-crystalline $Fe_{1+y}(Te_{1-x}Se_x)$ and $Fe_{1+y}(Te_{1-x}S_x)$. *Phys. Rev. B*, 81:180503(R).

Kim, H., Tanatar, M. A., Song, Y. J., Kwon, Y. S., and Prozorov, R. (2010c). Exponential low-temperature London penetration depth and two-gap superconductivity in stoichiometric pnictide LiFeAs. *arXiv:1008.3251.*

Kogan, V. G. (1981). London approach to anisotropic type-ii superconductors. *Phys. Rev. B*, 24:3.

Kogan, V. G. (2009). Pair breaking in iron pnictides. *Phys. Rev. B*, 80:214532.

Kogan, V. G., Martin, C., and Prozorov, R. (2009). Superfluid density and specific heat within a self-consistent scheme for a two-band superconductor. *Phys. Rev. B*, 80:014507.

Kondo, T., Santander-Syro, A. F., Copie, O., Liu, C., Tillman, M. E., Mun, E. D., Schmalian, J., Bud'ko, S. L., Tanatar, M. A., Canfield, P. C., and Kaminski, A. (2008). Momentum dependence of the superconducting gap in $NdFeAsO_{1-x}F_x$ single crystals measured by angle resolved photoemission spectroscopy. *Phys. Rev. Lett.*, 101:147003.

Kosztin, I. and Leggett, A. J. (1997). Nonlocal effects on the magnetic penetration depth in *d*-wave superconductors. *Phys. Rev. Lett.*, 79:135.

Laplace, Y., Bobroff, J., Rullier-Albenque, F., Colson, D., and Forget, A. (2009). Atomic coeistence of superconductivity and incommensurate magnetic order in the pnictide $Ba(Fe_{1-x}Co_x)_2As_2$. *Phys. Rev. B*, 80:140501(R).

Lewis, H. W. (1956). Two-fluid model of an "energy-gap" superconductor. *Phys. Rev.*, 102:6.

Liu, C., Kondo, T., Palczewski, A. D., Samolyuk, G. D., Lee, Y., Tillman, M. E., Ni, N., Mun, E. D., Gordon, R., Santander-Syro, A. F., Bud'ko, S. L., McChesney, J. L., Rotenberg, E., Fedorov, A. V., Valla, T., Copie, O., Tanatar, M. A., Martin, C., Harmon, B. N., Canfield, P. C., Prozorov, R., Schmalian, J., and Kaminski, A. (2009). Electronic properties of iron arsenic high temperature superconductors revealed by angle resolved photoemission spectroscopy (ARPES). *Physica C*, 469:491.

Liu, C., Kondo, T., Tillman, M. E., Gordon, R., Samolyuk, G. D., Lee, Y., Martin, C., McChesney, J. L., Bud'ko, S., Tanatar, M. A., Rotenberg, E., Canfield, P. C., Prozorov, R., Harmon, B. N., and Kaminski, A. (2008). Fermi surface and strong coupling superconductivity in single crystal $NdFeAsO_{1-x}F_x$. *arXiv:0806.2147*.

London, F. (1950). *Superfluids, vol. I.* Wiley, New York.

London, F. and London, H. (1935). *Proc. Roy. Soc. (London)*, A149:71.

Luan, L., Auslaender, O. M., Lippman, T. M., Hicks, C. W., Kalisky, B., Chu, J.-H., Analytis, J. G., Fisher, I. R., Kirtley, J. R., and Moler, K. A. (2010). Local measurement of the penetration depth in the pnictide superconductor $Ba(Fe_{0.95}Co_{0.05})_2As_2$. *Phys. Rev. B*, 81:100501(R).

Luan, L., Lippman, T. M., Hicks, C. W., Bert, J. A., Auslaender, O. M., Chu, J.-H., Analytis, J. G., Fisher, I. R., and Moler, K. A. (2011). Local measurement of the superfluid density in the pnictide superconductor $Ba(Fe_{1-x}Co_x)_2As_2$ across the superconducting dome. *Phys. Rev. Lett.*, 106:067001.

Luetkens, H., Klaus, H. H., Fraken, M., Litterst, F. J., Dellmann, T., Klingeler, R., Hess, C., Khasanov, R., Amato, A., Baines, C., Kosmala, M., Schumann, O. J., Braden, M., Hamann-Borrero, J., Leps, N., Kondrat, A., Behr, G., Werner, J., and Büchner, B. (2009). The electronic phase diagram of the $LaO_{1-x}F_xFeAs$ superconductor. *Nature Mater.*, 8:305.

Luetkens, H., Klaus, H.-H., Khasanov, R., Amato, A., Klingeler, R., Hellmann, I., Leps, N., Kondrat, A., Hess, C., Koehler, A., Behr, G., Werner, J., and Büchner, B. (2008). Field

and temperature dependence of the superfluid density in $LaFeAsO_{1-x}F_x$ superconductors: A muon spin relaxation study. *Phys. Rev. Lett*, 101:097009.

Luo, X. G., Tanatar, M. A., Reid, J.-P., Shakeripour, H., Doiron-Leyraud, N., Ni, N., Bud'ko, S. L., Canfield, P. C., Luo, H., Wang, Z., Wen, H.-H., Prozorov, R., and Taillefer, L. (2009). Quasiparticle heat transport in single-crystalline $Ba_{1-x}K_xFe_2As_2$: Evidence for a k-dependent superconducting gap without nodes. *Phys. Rev. B*, 80:140503(R).

Maier, T. A., Graser, S., Hirschfeld, P. J., and Scalopino, D. J. (2011). d-wave pairing from spin fluctuations in the $K_xFe_{2-y}Se_2$ superconductors. *arXiv:1101.4988*.

Malone, L., Fletcher, J. D., Serafin, A., Carrington, A., Zhigadlo, N. D., Bukowski, Z., Katrych, S., and Karpinski, J. (2009). Magnetic penetration depth of single-crystalline $SmFeAsO_{1-x}F_y$. *Phys. Rev. B*, 79:140501(R).

Martin, C., Gordon, R. T., Tanatar, M. A., Kim, H., Ni, N., Bud'ko, S. L., Canfield, P. C., Luo, H., Wen, H. H., Wang, Z., Vorontsov, A. B., Kogan, V. G., and Prozorov, R. (2009a). Nonexponential London penetration depth of external magnetic fields in superconducting $Ba_{1-x}K_xFe_2As_2$ single crystals. *Phys. Rev. B*, 80:020501(R).

Martin, C., Kim, H., Gordon, R. T., Ni, N., Kogan, V. G., Bud'ko, S. L., Canfield, P. C., Tanatar, M. A., and Prozorov, R. (2010a). Evidence from anisotropic penetration depth for a three-dimensional nodal superconducting gap in single-crystalline $Ba(Fe_{1-x}Ni_x)_2As_2$. *Phys. Rev. B*, 81:060505.

Martin, C., Kim, H., Gordon, R. T., Ni, N., Thaler, A., Kogan, V. G., Bud'ko, S. L., Canfield, P. C., Tanatar, M. A., and Prozorov, R. (2010b). The London penetration depth in $BaFe_2As_2$ superconductors at high electron doping level. *Supercond. Sci. Technol.*, 23:065022.

Martin, C., Tillman, M. E., Kim, H., Tanatar, M. A., Kim, S. K., Kreyssig, A., Gordon, R. T., Vannette, M. D., Nandi, S., Kogan, V. G., Bud'ko, S. L., Canfield, P. C., Goldman,

A. I., and Prozorov, R. (2009b). Nonexponential London penetration depth of FeAs-based superconducting $RFeAsO_{0.9}F_{0.1}$ (R-La, Nd) single crystals. *Phys. Rev. Lett.*, 102:247002.

Martin, C., Vannette, M. D., Gordon, R. T., Prozorov, R., Karpinski, J., and Zhigadlo, N. D. (2008). Effects of C and Li doping on the rf magnetic susceptibility of MgB_2 single crystals. *Phys. Rev. B*, 78:144512.

Matthias, B. T., Geballe, T. H., and Compton, V. B. (1963). Superconductivity. *Rev. Mod. Phys.*, 35:1–22.

Mazin, I. I. and Johannes, M. D. (2009). A key role for unusual spin dynamics in ferropnictides. *Nat. Phys.*, 5:141.

Mazin, I. I. and Schmalian, J. (2009). Pairing symmetry and pairing state in ferropnictides: Theoretical overview. *Physica C*, 469:614.

Mazin, I. I., Singh, D. J., Johannes, M. D., and Du, M. H. (2008). Unconventional superconductivity with a sign reversal in the order parameter of $LaFeAsO_{1-x}F_x$. *Phys. Rev. Lett.*, 101:057003.

Meissner, W. and Ochsenfeld, R. (1933). Ein neuer effekt bei eintritt deer supraleitfähigkeit. *Naturwissenschaften*, 21:787.

Monthoux, P., Pines, D., and Lonzarich, G. G. (2007). Superconductivity without phonons. *Nature*, 450:1177.

Morris, R. C., Coleman, R. V., and Bhandari, R. (1972). Superconductivity and magnetoresistance in $NbSe_2$. *Phys. Rev. B*, 5:895.

Moskalenko, V. A. (1959). *Phys. Met. Metallogr.*, 8:503.

Muhlschlegel, B. (1959). *Z. Phys.*, 155:313.

Müller, K. A. and Bednorz, J. G. (1987). The discovery of a class of high-temperature superconductors. *Advances in Physics*, 237:1133–1139.

Mun, E. D., Bud'ko, S. L., Ni, N., Thaler, A. N., and Canfield, P. C. (2009). Thermoelectric power and Hall coefficient measurements on $Ba(Fe_{1-x}T_x)As_2$ (T=Co and Cu). *Phys. Rev. B*, 80:054517.

Nakai, Y., Ishida, K., Kamihara, Y., Hirano, M., and Hosono, H. (2008). Evolution from itinerant antiferromagnet to unconventional superconductor with fluorine doping in $LaFeAsO_{1-x}F_x$ revealed by ^{75}As and ^{139}La nuclear magnetic resonance. *J. Phys. Soc. Jpn.*, 77:073701.

Nakajima, M., Ishida, S., Kihou, K., Tomioka, Y., Ito, T., Yoshida, Y., Lee, C. H., Kito, H., Iyo, A., Eisaki, H., Kojima, K. M., Kojima, K. M., and Uchida, S. (2010). Evolution of the optical spectrum with doping in $Ba(Fe_{1-x}Co_x)_2As_2$. *Phys. Rev. B*, 81:104528.

Nandi, S., Kim, M. G., Kreyssig, A., Fernandes, R. M., Pratt, D. K., Thaler, A. N., Ni, N., Bud'ko, S. L., Canfield, P. C., Schmalian, J., McQueeney, R. J., and Goldman, A. I. (2010). Anomalous suppression of the orthorhombic lattice distortion in superconducting $Ba(Fe_{1-x}Co_x)_2As_2$. *Phys. Rev. Lett.*, 104:057006.

Ni, N., Bud'ko, S. L., Kreyssig, A., Nandi, S., Rustan, G. E., Goldman, A. I., Gupta, S., Corbett, J. D., Kracher, A., and Canfield, P. C. (2008a). Anisotropic thermodynamic and transport properties of $Ba_{1-x}K_xFe_2As_2$ (x=0 and 0.45). *Phys. Rev. B*, 78:014507.

Ni, N., Thaler, A., Kracher, A., Yan, J. Q., Bud'ko, S. L., and Canfield, P. C. (2010a). Phase diagrams of $Ba(Fe_{1-x}M_x)_2As_2$) single crystals (M=Rh and Pd). *Phys. Rev. B*, 80:024511.

Ni, N., Thaler, A., Kracher, J. Q. Y. A., Colombier, E., Bud'ko, S. L., Hannahs, S. T., and Canfield, P. C. (2010b). Temperature versus doping phase diagrams for $ba(fe_{1-x}tm_x)_2as_2$ (tm=ni,cu,cu/co) single crystals. *Phys. Rev. B*, 82:024519.

Ni, N., Tillman, M. E., Yan, J.-Q., Kracher, A., Hannahs, S. T., Bud'ko, S. L., and Canfield, P. C. (2008b). Effects of Co substitution on thermodynamic and transport properties and anisotropic H_{c2} in $Ba(Fe_{1-x}Co_x)_2As_2$ single crystals. *Phys. Rev. B*, 78:214515.

Nicol, E. J. and Carbotte, J. P. (2005). Properties of the superconduting state in a two-band model. *Phys. Rev. B*, 71:054501.

Onnes, H. K. (1911). The resistance of pure mercury at helium temperatures. *Commun. Phys. Lab. Univ. Leiden*, 12:120.

Ott, H. R., Rudigier, H., Fisk, Z., and Smith, J. L. (1983). UBe_{13}: An unconventional actinide superconductor. *Phys. Rev. Lett.*, 50:1595.

Paglione, J. and Greene, R. (2010). High-temperature superconductivity in iron-based materials. *Nat. Phys.*, 6:645–658.

Parker, D., Dolgov, O. V., Korshunov, M. M., Golubov, A. A., and Mazin, I. I. (2008). Extended $s_{\pm}$ scenario for the nuclear spin-lattice relaxation rate in superconducting pnictides. *Phys. Rev. B*, 78:134524.

Pippard, A. B. (1953). An experimental and theoretical study of the relation between magnetic field and current in a superconductor. *Proc. Roy. Soc. (London)*, A216:547.

Poole, C. P., Farach, H. A., Creswick, R. J., and Prozorov, R. (2007). *Superconductivity*. Elsevier.

Pratt, D. K., Tian, W., Kreyssig, A., Zarestky, J. L., Nandi, S., Ni, N., Bud'ko, S. L., Canfield, P. C., Goldman, A. I., and Mcqueeney, R. J. (2009). Coexistence of competing anitferromagnetic and superconducting phases in the underdoped $Ba(Fe_{0.953}Co_{0.047})_2As_2$ compound using X-ray and neutron scattering techniques. *Phys. Rev. Lett.*, 103:087001.

Prozorov, R. and Giannetta, R. W. (2006). Magnetic penetration depth in unconventional superconductors. *Supercond. Sci. Technol.*, 19:R41–R46.

Prozorov, R., Giannetta, R. W., Carrington, A., and Araujo-Moreira, F. M. (2000a). Meissner-London state in superconductors of rectangular cross section in a perpendicular magnetic field. *Phys. Rev. B*, 62:115.

Prozorov, R., Giannetta, R. W., Carrington, A., Fournier, P., Greene, R. L., Guptasarma, P., Hinks, D. G., and Banks, A. R. (2000b). Measurements of the absolute value of the penetration depth in high-T_c superconductors using a low-T_c superconductive coating. *Appl. Phys. Lett.*, 77:4202.

Prozorov, R., Giannetta, R. W., Fournier, P., and Greene, R. L. (2000c). Evidence for nodal quasiparticles in electron-doped cuprates from penetration depth measurements. *Phys. Rev. Lett.*, 85:3700.

Prozorov, R., Tanatar, M. A., Blomberg, E. C., Prommapan, P., Gordon, R. T., Ni, N., Bud'ko, S. L., and Canfield, P. C. (2009a). Doping-dependent irreversible magnetic properties of $Ba(Fe_{1-x}Co_x)_2As_2$ single crystals. *Physica C*, 469:667.

Prozorov, R., Tanatar, M. A., Gordon, R. T., Martin, C., Kim, H., Kogan, V. G., Ni, N., Tillman, M. E., Bud'ko, S. L., and Canfield, P. C. (2009b). Anisotropic London penetration depth and superfluid density in single crystals of iron-based pnictide superconductors. *Physica C*, 469:582–589.

Prozorov, R., Vannette, M. D., Gordon, R. T., Martin, C., Bud'ko, S. L., and Canfield, P. C. (2009c). Coexistence of long-range magnetic order and superconductivity from Campbell penetration depth measurements. *Supercond. Sci. Technol.*, 22:034008.

Reid, J.-P., Tanatar, M. A., Luo, X.-G., Shakeripour, H., Doiron-Leyraud, N., Ni, N., Bud'ko, S. L., Canfield, P. C., Prozorov, R., and Taillefer, L. (2010). Nodes in the gap structure of the iron arsenide superconductor $Ba(Fe_{1-x}Co_x)_2As_2$ from *c*-axis heat transport measurements. *Phys. Rev. B*, 82:064501.

Ren, Z.-A., Wei, L., Yang, J., Yi, W., Shen, X.-L., Zheng, C., Che, G.-C., Dong, X.-L., Sun, L.-L., Zhou, F., and Zhao, Z.-X. (2008). Superconductivity at 55 K in iron-based F-doped layered quaternary compound $Sm[O_{1-x}F_x]FeAs$. *Chin. Phys. Lett.*, 25:2215.

Rotter, M., Tegel, M., Schellenberg, I., Hermes, W., Pöttgen, R., and Johrendt, D. (2008). Superconductivity at 38 K in the iron arsenide $(Ba_{1-x}K_x)Fe_2As_2$. *Phys. Rev. Lett.*, 101:107006.

Samuely, P., Szabo, P., Pribulova, Z., Tillman, M. E., Bud'ko, S. L., and Canfield, P. C. (2009). Possible two-gap superconductivity in $NdFeAsO_{0.9}F_{0.1}$. *Supercond. Sci. Technol.*, 22:014003.

Sefat, A. S., Jin, R., McGuire, M. A., Sales, B. C., Singh, D. J., and Mandrus, D. (2008). Superconductivity at 22 K in Co-doped $Ba(Fe_{1-x}Co_x)_2As_2$. *Phys. Rev. Lett.*, 101:117004.

Shoenberg, D. (1940). Properties of superconducting colloids and emulsions. *Proc. Roy. Soc. (London)*, A175:49.

Sigrist, M. and Ueda, K. (1991). Phenomenological thoery of unconventional superconductivity. *Rev. Mod. Phys.*, 63:239.

Sonier, J. E. (2007). Muon spin rotation studies of electronic excitations and magnetism in the vortex cores of superconductors. *Rep. Prog. Phys.*, 70:1717.

Sonier, J. E., Huang, W., Kaiser, C. V., Cochrane, C., Pacradouni, V., Sabok-Sayr, S. A., Lumsden, M. D., Sales, B. C., McGuire, M. A., Sefat, A. S., and Mandrus, D. (2010). Magnetism and disorder effects on μSR measurements of the magnetic penetration depth in iron-based superconductors. *arXiv:1010.6046*.

Suhl, H., Matthias, B. T., and Walker, L. R. (1959). Bardeen-cooper-schrieffer theory of superconductivity in the case of overlapping bands. *Phys. Rev. Lett.*, 3:552.

Taillefer, L. (2010). Scattering and pairing in cuprate superconductors. *Ann. Rev. Condens. Matt. Phys.*, 1:51.

Tanatar, M. A., Ni, N., Samolyuk, G. G., Bud'ko, S. L., Canfield, P. C., and Prozorov, R. (2009). Resistivity anisotropy of AFe_2As_2 (A=Ca, Sr, Ba): Direct versus montgomery technique measurements. *Phys. Rev. B*, 79:134528.

Tanatar, M. A., Reid, J., Shakeripour, H., Luo, X. G., Doiron-Leyraud, N., Ni, N., Bud'ko, S. L., Canfield, P. C., Prozorov, R., and Taillefer, L. (2010). Doping dependence of heat transport in the iron-arsenide superconductor $Ba(Fe_{1-x}Co_x)_2As_2$. *Phys. Rev. Lett.*, 104:067002.

Thaler, A., Ni, N., Kracher, A., Yan, J. Q., Bud'ko, S. L., and Canfield, P. C. (2010). Physical and magnetic properties of $Ba(Fe_{1-x}Ru_x)_2As_2$ single crystals. *Phys. Rev. B*, 82:014534.

Tinkham, M. (1996). *Introduction to Superconductivity*. Dover.

Vannette, M. D. (2008). *Dynamic magnetic susceptibility of systems with long-range magnetic order*. PhD dissertation, Iowa State University.

VanDegrift, C. T. (1975a). *Tunnel diode oscillator for 0.001 ppm measurements at low temperatures*. PhD dissertation, Univeristy of California, Irvine.

VanDegrift, C. T. (1975b). Tunnel diode oscillator for 0.001 ppm measurements at low temperatures. *Rev. Sci. Instrum.*, 46:599.

Vorontsov, A. B., Vavilov, M. G., and Chubukov, A. V. (2009). Superfluid density and penetration depth in the iron pnictides. *Phys. Rev. B*, 79:140507(R).

Wang, F., Yang, F., Gao, M., Lu, Z.-Y., Xi-ang, T., and Lee, D.-H. (2011). The electron pairing of $K_xFe_{2-y}Se_2$. *arXiv:1101:4390*.

Wang, Y.-L., Shan, L., Fang, L., Cheng, P., Ren, C., and Wen, H.-H. (2009). Multiple gaps in $SmFeAsO_{0.9}F_{0.1}$ revealed by point-contact spectroscopy. *Supercond. Sci. Technol.*, 22:015018.

Wen, H.-H. and Li, S. (2011). Materials and noverl superconductivity in iron pnictide superconductors. *Annu. Rev. Condens. Matter Phys.*, 2:121–140.

Williams, T. J., Aczel, A. A., Baggio-Saitovitch, E., Bud'ko, S. L., Canfield, P. C., Carlo, J. P., Goko, T., Munevar, J., Ni, N., Uemura, Y. J., Yu, W., and Luke, G. M. (2009). Muon spin rotation measurement of the magnetic field penetration depth in $Ba(Fe_{1-x}Co_x)_2As_2$. *Phys. Rev. B*, 80:094501.

Williams, T. J., Aczel, A. A., Baggio-Saitovitch, E., S. L. Bud'ko, P. C. C., Carlo, J. P., Goko, T., Kageyama, H., Kitada, A., Munevar, J., Ni, N., Saha, S. R., Kirschenbaum, K., Paglione, J., Sanchez-Candela, D. R., Uemura, Y. J., and Luke, G. M. (2010). Superfluid density and

field-induced magnetism in $Ba(Fe_{1-x}Co_x)_2As_2$ and $Sr(Fe_{1-x}Co_x)_2As_2$ measured with muon spin relaxation. *Phys. Rev. B*, 82:094512.

Yin, Y., Zech, M., Williams, T. L., Wang, X. F., Wu, G., Chen, X. H., and Hoffman, J. E. (2009). Scanning tunneling spectroscopy and vortex imaging in the iron pnictide superconductor $BaFe_{1.8}Co_{0.2}As_2$. *Phys. Rev. B*, 48:4219.

BIBLIOGRAPHY

Allen, B. S. (1984). System-assigned learning strategies and CBI. *Journal of Instructional Computing Research*, *1*(1), 3–18.

Bruner, J. (1960). *The process of education*. New York: Random House.

Cox, S. R. (1974). Computer-assisted instruction and student performance in macroeconomic principles. *The Journal of Economic Education*, *6*(1), 29–37.